Cenozoic plate tectonic reconstructions and plate boundary processes in the Southwest Pacific

Thesis by

William R. Keller

In Partial Fulfillment of the Requirements

for the Degree of

Doctor of Philosophy

California Institute of Technology

Pasadena, California

2004

(Defended April 10, 2003)

Acknowledgements

I'd like to thank my wife, Hallie, for her patience and understanding. Completing this thesis would have never been possible without her loving support.

Abstract

The Australia-Pacific-Antarctic plate circuit has long been a weak link in global plate reconstruction models for Cenozoic time. The time period spanning chron 20 to chron 7 (43-25 Ma) is particularly problematic for global plate models because seafloor spreading was occurring in two poorly constrained regions in the Southwest Pacific - the Macquarie Basin southwest of New Zealand, and the Adare Basin north of the Ross Sea, Antarctica. I present a new shipboard dataset collected aboard several recent geophysical cruises which places important constraints on the tectonic evolution of these two regions. Utilizing multibeam bathymetry, magnetic, gravity, and seismic data in the Macquarie Basin, I am able to locate tectonic features and magnetic anomalies with greater accuracy than was previously possible. These tectonic features and magnetic anomalies are then used to calculate relative motion between the Australia and Pacific Plates for chrons 18-11 (40-30 Ma). I use revised locations of the rifted margins along the boundary of the Macquarie Basin to determine a best-fit pre-rift reconstruction for this region. During this same time period, seafloor spreading between East and West Antarctica was occurring along the Adare Trough, an extinct spreading center located north of the Ross Sea. Motion along the Adare Trough accounts for roughly 180 km of previously unrecognized motion between East and West Antarctica. I present multibeam and seismic data in the Adare Basin that place constraints on the timing and character of motion along this plate boundary.

Contents

List of Figures

List of Tables

Chapter 1

Introduction

The time period spanning chron 20 to chron 7 (43-25 Ma) has long been problematic for global plate models because seafloor spreading was occurring in two poorly constrained regions in the Southwest Pacific - the Macquarie Basin southwest of New Zealand, and the Adare Basin north of the Ross Sea, Antarctica (Figure 2.1). When put into context, understanding the complicated tectonic history of these two regions provides vital information for deciphering the Cenozoic tectonic evolution of the Southwest Pacific.

Seafloor spreading along the Tasman Ridge initiated at roughly 83 Ma (chron 34), opening the Tasman Sea ocean basin between Australia and the Lord Howe Rise-New Zealand continental block [*Weissel and Hayes*, 1972]. Continental extension between East Antarctica and Australia and subsequent slow spreading along the Southeast Indian Ridge (SEIR) was also occurring during this time period. As spreading along the SEIR became more established, the ridge lengthened eastward toward the Tasman and Pacific-Antarctic ridge systems. Spreading along the Tasman Ridge continued until roughly 52 Ma (chon 24) when spreading ceased and the Lord Howe Rise became part of the Australia Plate (e.g., *Hayes and Ringis* [1973]; *Weissel et al.* [1977]; *Gaina et al.* [1998]). Seafloor spreading between the Australia and Pacific plates was initiated along the Macquarie Spreading Center just prior to 40 Ma (chron 18), marking a 90 degree change in spreading direction relative to the previous Tasman Ridge spreading direction [*Weissel et al.*, 1977; *Gaina et al.*, 1998].

Seafloor spreading along the Macquarie Spreading Center in Eocene and Oligocene time formed new oceanic crust in the Emerald Basin and South Tasman Ocean Crust

(STOC), collectively referred to here as the Macquarie Basin. During the initial stages of rifting, extension propagated northward and stepped progressively eastward along zones of weakness parallel to fracture zones associated with an earlier stage of seafloor spreading along the Tasman Ridge [*Sutherland et al.*, 2000]. This pattern of rifting produced two distinctively shaped conjugate intra-oceanic rifted margins, the Resolution and Southwest Campbell Rifted Margins, which are visible in satellite-derived gravity images [*Sandwell and Smith*, 1997; *Sutherland*, 1995]. Magnetic anomalies adjacent to the southeast side of the Resolution Rifted Margin indicate that this younger stage of seafloor spreading propagated northeast toward New Zealand. Magnetic anomalies as old as chron 29 (64.5 Ma) have been identified in the Balleny Corridor adjacent to the Nella Dan Rift, the southwest extension of the Resolution Rifted Margin [*Cande et al.*, 2000]. Chron 18 (42 Ma) is the oldest anomaly identified adjacent to the Resolution Rifted Margin, indicating that spreading along the Macquarie Spreading Center initiated at roughly 42 Ma [*Weissel et al.*, 1977; *Wood et al.*, 1996]. This age coincides with geological evidence in New Zealand, which suggests an early Eocene age for the onset of this stage of rifting [*Carter and Norris*, 1976; *Kamp*, 1986].

Orthogonal Australia-Pacific seafloor spreading continued along the Macquarie Spreading Center until approximately chron 10 (29 Ma), forming a wedge-shaped region of new ocean crust. Subsequent gradual migration of the instantaneous pole of rotation to the southeast caused the spreading direction along this boundary to become progressively more oblique to the plate boundary in a right-lateral sense [*Walcott*, 1984; *Lamarche et al.*, 1997]. As the pole continued to migrate, the ridge segments shortened and the transform faults lengthened in response to the change in spreading direction [*Massell et al.*, 2000]. The orientation of Chron 7, the youngest magnetic anomaly identified adjacent to the Macquarie Ridge Complex, indicates that motion along this plate boundary was predominantly strike slip by 25 Ma. This transition to right-lateral strike slip motion along the Macquarie Ridge caused crust on the Australia side of the boundary to be translated to the northeast (Pacific Plate fixed) and then partially subducted under the South Island of New Zealand at the

Puysegur Trench [*Collot et al.*, 1995; *Lamarche and Lebrun*, 2000; *Sutherland et al.*, 2000].

We present a new shipboard data set collected during several geophysical cruises including the EW9513 cruise aboard the R/V Ewing and the NBP9702, NBP0007B, and NBP0209 cruises aboard the R/VIB Nathaniel B. Palmer. In addition, several profiles were collected by the Japan National Oil Corporation on cruises TH91B and TH92B aboard the R/V Hakurei Maru [*Tanahashi et al.*, 1997]. This new data set is combined with all currently available magnetic and multibeam data from previous cruises in the Southeast Tasman Sea in order to determine revised interpretations of magnetic anomaly and fracture zone locations within the Macquarie Basin. In Chapter 2, I present the revised data and use it to generate a series of finite rotations that reconstruct the configuration of the Macquarie Basin at various times spanning chrons 18-11 (42-30 Ma). In addition, magnetic, gravity, multibeam bathymetry, and seismic data collected aboard these cruises allow me to determine the geophysical structure and precise location of the Resolution and Southwest Campbell Rifted Margins. I present these results in Chapter 3 and calculate a best-fit finite rotation that reconstructs the Resolution and South Campbell Rifted Margins to their locations prior to the formation of the Macquarie Basin.

While new seafloor was being generated along the Macquarie Spreading Center, new oceanic crust was also being created in the Adare Basin, north of the Ross Sea, Antarctica. For many years, Cenozoic plate tectonic reconstructions in the Southwest Pacific which have treated Antarctica as a single rigid plate have been plagued by large misfits. Early plate reconstructions predicted a large gap along the Australia-Pacific boundary between the North and South Islands of New Zealand, and it was proposed that including roughly 500 km of motion between East and West Antarctica could account for this misfit [*Molnar et al.*, 1975]. Continued improvements in our knowledge of the plate circuit have reduced the amount of misfit in plate reconstructions in the Southwest Pacific from its original estimates [*Stock and Molnar*, 1987]. However, the most recent reconstructions still suggest that significant extension between East and West Antarctica was accommodated during this time period [*Cande*

et al., 2000]. Cenozoic extension in the Ross Sea is accommodated along the Adare Trough, a prominent NW trending graben aligned with the major sedimentary basins of the Ross Sea Embayment. Because of the Adare Trough's resemblance to known oceanic rifts, the magnitude and nature of its extension has remained an issue of debate. In Chapter 4, I present further evidence from bathymetry, seismic, and well data that suggests the Adare Basin was formed by seafloor spreading along the now extinct Adare Trough.

Chapter 2

Cenozoic Australia-Pacific plate tectonic reconstructions in the southeast Tasman Sea

Abstract

The Macquarie Ridge Complex, the boundary between the Australia and Pacific plates southwest of New Zealand, is a complicated system that acted as a spreading ridge from roughly 40-30 Ma and then evolved over the last 30 million years from a divergent plate boundary to one that is dominated by right-lateral strike-slip and compression. We refer to this plate boundary as the Macquarie Spreading Center during the period of Eocene seafloor spreading that resulted in the formation of the Emerald Basin and South Tasman Ocean Crust, collectively referred to here as the Macquarie Basin. The large amount of strike-slip motion coupled with the paucity of data within this region has placed major limitations on previous attempts to reconstruct the seafloor spreading history along this boundary. We utilize a new shipboard geophysical data set collected during several recent cruises in the southeast Tasman Sea to create a revised set of magnetic anomaly and fracture zone interpretations for this region. By combining these revised magnetic anomaly interpretations with seafloor spreading fabric directions interpreted from currently available multibeam data, we are able to successfully match fracture zones on either side of the Macquarie Ridge Complex for the first time. This knowledge allows us to calculate relative motions between the Australia and Pacific plates and their associated uncertainties for the time period between 40 and 30 Ma (chrons 18-11).

2.1 Introduction

Seafloor spreading along the Macquarie Spreading Center in Eocene and Oligocene time resulted in the formation of new oceanic crust in the Emerald Basin and South Tasman Ocean Crust (STOC), collectively referred to here as the Macquarie Basin (Figure 2.1). During the initial stages of rifting, extension propagated northward and stepped progressively eastward along zones of weakness parallel to fracture zones associated with an earlier stage of seafloor spreading along the Tasman Ridge [*Sutherland et al.*, 2000]. This pattern of rifting produced two distinctively shaped conjugate intra-oceanic rifted margins, the Resolution and Southwest Campbell Rifted Margins, which are visible in satellite-derived gravity images [*Sandwell and Smith*, 1997; *Sutherland*, 1995]. The formation of these rifted margins denotes the initial stages of rifting along the Macquarie Spreading Center and marks a dramatic 90 degree change in spreading direction relative to previous seafloor spreading along the Tasman Ridge from chron 34 to chron 24 (83-52 Ma) [*Weissel and Hayes*, 1972; *Hayes and Ringis*, 1973; *Weissel et al.*, 1977; *Gaina et al.*, 1998]. Magnetic anomalies adjacent to the southeast side of the Resolution Rifted Margin indicate that this younger stage of seafloor spreading propagated northeast toward New Zealand. Magnetic anomalies as old as chron 29 (64.5 Ma) have been identified in the Balleny Corridor adjacent to the Nella Dan Rift, the southwest extension of the Resolution Rifted Margin [*Cande et al.*, 2000]. Chron 18 (42 Ma) is the oldest anomaly identified adjacent to the Resolution Rifted Margin, indicating that spreading along the Macquarie Spreading Center initiated at roughly 42 Ma [*Weissel et al.*, 1977; *Wood et al.*, 1996]. This age coincides with geological evidence in New Zealand which suggests an early Eocene age for the onset of this stage of rifting [*Carter and Norris*, 1976; *Kamp*, 1986].

Figure 2.1: (caption on following page)

Figure 2.1: Major tectonic features and classification of regions of ocean crust in the Southeast Tasman Sea by the spreading ridge at which they were formed. The yellow region indicates crust that was formed along the Tasman Ridge between chrons 34 and 24. The pink region was formed by Australia-Pacific spreading along the Macquarie Spreading Center between chrons 20 and 7, and the dark green region east of the Balleny Fracture Zone was generated by Australia-West Antarctic spreading prior to chron 8. The light green and blue regions were formed by Australia-East Antarctic and Pacific-West Antarctic spreading respectively. Dark green lines show the tracks of recent geophysical cruises, and solid black lines indicate tectonic features. Intra-oceanic rifted margins are shown with thick black lines and dots. White circles numbered 1-3 indicate conjugate segments of these rifted margins. Satellite derived gravity [*Sandwell and Smith*, 1997] is shown in shaded relief. MRC=Macquarie Ridge Complex, STOC=South Tasman Ocean Crust, EMB=Emerald Basin, SEIR=Southeast Indian Ridge. Figure after *Cande et al.* [2000].

Orthogonal Australia-Pacific seafloor spreading continued along the Macquarie Spreading Center until approximately chron 10 (29 Ma), forming a wedge-shaped region of new ocean crust. Subsequent gradual migration of the instantaneous pole of rotation to the southeast caused the spreading direction along this boundary to become progressively more oblique to the plate boundary in a right-lateral sense [*Walcott*, 1984; *Lamarche et al.*, 1997]. As the pole continued to migrate, the ridge segments decreased in length and the transforms increased in length in response to the change in spreading direction [*Massell et al.*, 2000]. Chron 7 is the youngest magnetic anomaly identified adjacent to the Macqarie Ridge Complex indicating that motion along this plate boundary was predominantly strike slip by 25 Ma. This transition to right-lateral strike slip motion along the Macquarie Ridge caused crust on the Australia side of the boundary to be translated to the northeast (Pacific Plate fixed) and then partially subducted under the South Island of New Zealand at the Puysegur Trench [*Collot et al.*, 1995; *Lamarche and Lebrun*, 2000; *Sutherland et al.*, 2000].

We present a new shipboard data set collected during several geophysical cruises including the EW9513 cruise aboard the R/V Ewing, cruise NBP0007B aboard the R/VIB Nathaniel B. Palmer, and Japan National Oil Corporation cruises TH91B and TH92B aboard the R/V Hakurei Maru [*Tanahashi et al.*, 1997]. This new data set is combined with all currently available magnetic and multibeam data from previous

cruises in the Southeast Tasman Sea in order to determine revised interpretations of magnetic anomaly and fracture zone locations for this region.

2.2   Multibeam bathymetry

Shipboard multibeam bathymetry data from geophysical cruises in the Macquarie Basin (Figures 2.2 and 2.3) are used to identify major tectonic features including fracture zones and abyssal hill fabric related to seafloor spreading. Because of the paucity of data and complex fracture zone patterns in the Macquarie Basin, identification of abyssal hill fabric orientation is a vital constraint when mapping magnetic isochron trends throughout the region. *Massell et al.* [2000] identified fracture zones related to seafloor spreading along the Macquarie Spreading Center within their survey region and then extrapolated the location of these fracture zones away from the plate boundary by following anomaly trends in the satellite derived gravity field. We have identified additional fracture zones based on observations of offsets in magnetic anomaly trends, so we re-numbered all known fracture zones from FZ1-FZ9. Multibeam swath width varies from roughly 2-3 times the water depth and is dependent on the beam width of each system that was used during data collection. The data from cruise EW9513 were collected with an Atlas DS Hydrosweep multibeam system, the data from cruises NBP9702 and NBP0007b were collected with a Seabeam 2100 multibeam system, and the data from cruise NBP0209 were collected using a Simrad EM120 multibeam system. Data along the northeast part of the Macquarie Ridge and South Tasman Ocean Crust were collected aboard the Geodynz-sud leg 2 cruise aboard the R/V L'Atalante using a Simrad EM12 multibeam system [*Collot et al.*, 1995; *Delteil et al.*, 1996; *Lamarche et al.*, 1997]. Ship tracks from this cruise are labeled GEODYNZ2 in Figures 2.2 and 2.3. Data along the central and southern Macquarie Ridge were collected on cruise RS124 aboard the R/V Rig Seismic using the Hawaii-HMR1 multibeam system which was towed behind the ship [*Massell et al.*, 2000]. MB-System software [*Caress and Chayes*, 1996] was used to process all of the multibeam data.
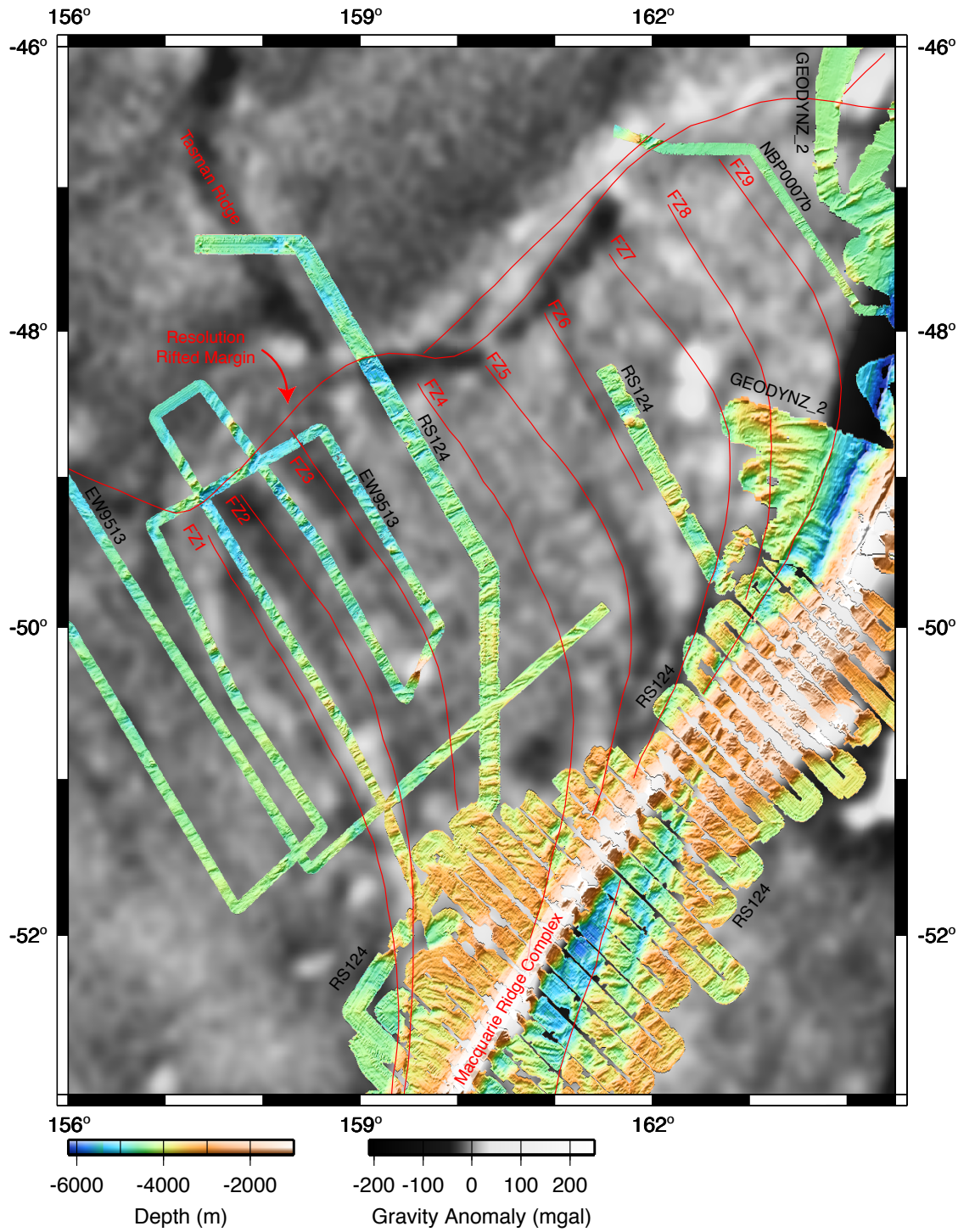
Figure 2.2: (caption on following page)

Figure 2.2: Multibeam map of the northern Macquarie Ridge Complex and South Tasman Ocean Crust. Multibeam data are plotted in color on top of a satellite-derived gravity basemap, which is shown in grayscale [*Sandwell and Smith*, 1997]. The multibeam data are from several sources including R/V Ewing cruise EW9513, R/VIB Nathaniel Palmer cruise NBP0007b, R/V L'Atalante cruise Geodynz-sud leg 2, and R/V Rig Seismic cruise RS124. Tectonic features and associated labels are shown in red, and ship tracks are labeled with geophysical cruise codes. Artificial illumination from the north-northwest is applied to the multibeam data to accentuate abyssal hill fabric orientation. Multibeam and satellite gravity data are used to constrain the location of fracture zones which are NW trending and then rotate in a clockwise fashion to become sub-parallel to the Macquarie Ridge Complex close to the active plate boundary.

Interaction between the Deep Western Boundary Current and the Antarctic Circumpolar Current has caused widespread abyssal erosion in areas throughout the Macquarie Basin [*Carter and McCave*, 1997; *Carter and Wilkin*, 1999]. However, thick lenses of sediment are deposited in localized areas in the western part of the Emerald Basin as eastward flowing bottom currents flow through topographic breaks in the Macquarie Ridge Complex. Two EW9513 lines at roughly 57° S, 159°-162° E (Figure 2.3) cross a mounded contourite deposit called the Emerald Basin Drift [*Schuur et al.*, 1998], thus obscuring the identification of abyssal hill trends along these two lines. However, sediment cover within most of the Macquarie Basin is thin and confined to valleys between elongate abyssal hill basement ridges that typically form as a result of extensional faulting and changes in magma flux near the ridge crest during seafloor spreading [*Pezard et al.*, 1992; *Macdonald et al.*, 1996]. The general lack of thick sediment cover in the Southern Emerald Basin allows abyssal hill spreading fabric to be imaged in this region with multibeam systems. Abyssal hill fabric is most apparent in areas where sediment fills the valleys between basement ridges because the flat level surface of the sediment contrasts with the more irregular topography associated with the exposed basement rocks.

The Resolution Rifted Margin denotes the NW boundary of STOC and is marked by a negative gravity anomaly that is visible in satellite gravity images (Figure 2.2) [*Sutherland*, 1995]. Multibeam data NW of the rifted margin reveal NW-trending
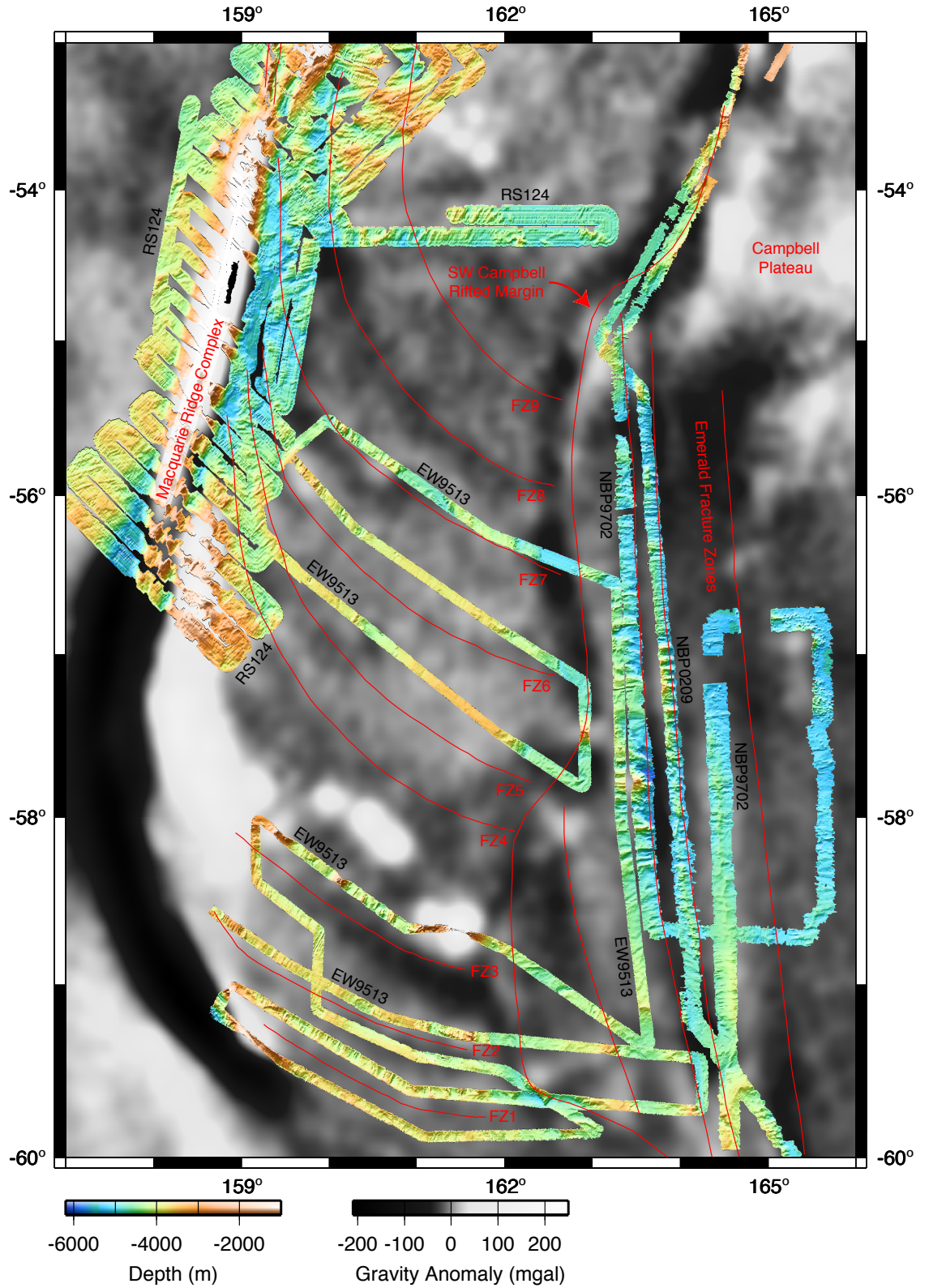
Figure 2.3: Multibeam map of the Emerald Basin. The format of the figure follows that of Figure 2.2. Data sources include R/V Ewing cruise EW9513, R/VIB Nathaniel Palmer cruises NBP9702 and NBP0209, and R/V Rig Seismic cruise RS124.

abyssal hill fabric, while multibeam data adjacent to this boundary in STOC reveal NE-trending abyssal hill fabric. Abyssal hill orientation is perpendicular to STOC fracture zones and is uniformly NE trending for approximately 200 km southwest of the rifted margin along the trend of fracture zones FZ1-FZ9. As these fracture zones curve southward and become asymptotic to the present plate boundary along the Macquarie Ridge Complex, abyssal hill fabric orientation rotates clockwise to become more E-W oriented. Adjacent to the Macquarie Ridge Complex, abyssal hill fabric trends E-SE and is best seen in the spreading corridors northeast of FZ8 and in the corridor between FZ2 and FZ3. This pattern of change in abyssal hill fabric direction is mirrored in the conjugate ocean crust of the Emerald Basin (Figure 2.3).

2.3 Magnetic anomaly and spreading corridor identification

Magnetic anomaly locations within the Macquarie Basin were identified and compiled (Figures 2.4 and 2.5, Appendix A). Because abyssal hill fabric is oriented parallel to magnetic isochrons, we use multibeam data to supplement this magnetic anomaly dataset whenever possible. Along tracks with multibeam coverage, magnetic anomaly picks are extrapolated to the edges of the multibeam data swath along the abyssal hill fabric direction (see small circles, Figures 2.4 and 2.5). This provides us better control on isochron orientations, and it also enables us to include fracture zone corridors with sparse data. (Our software requires at least three picks per fracture zone corridor with a minimum of one pick from each plate.)

Chron 21o is identified adjacent to the Resolution Rifted Margin southwest of FZ1 (Figure 2.4). Farther to the northeast, chron 19 is the oldest identifiable anomaly between FZ1 and FZ3. Between FZ3 and FZ9, chron 18o is the oldest anomaly identified adjacent to the rifted margin, and chron 17o is the oldest anomaly identified northeast of FZ9. This age progression places strong constraints on the pattern of early rifting as it propagated to the northeast along the Resolution Rifted Margin and new seafloor
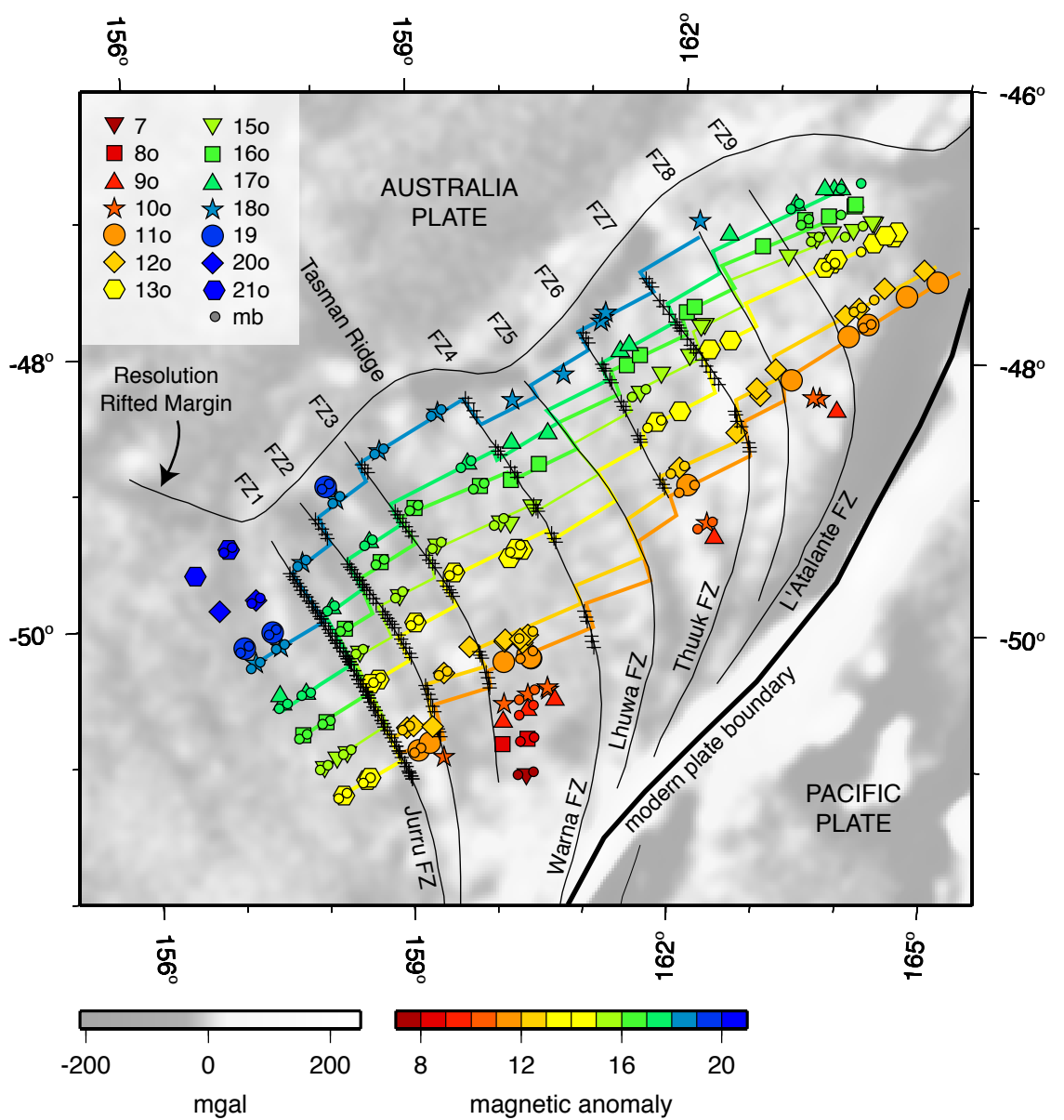
Figure 2.4: Stereographic projection showing magnetic anomaly identifications in the South Tasman Ocean Crust. Colored symbols indicate the location of magnetic anomaly picks from shipboard magnetic data. For simplicity, only the location of the old edge is shown for anomalies that are conventionally indicated by a young and old edge [*Cande and Kent*, 1995]. For areas with multibeam coverage, magnetic anomaly picks are extrapolated to the edges of the multibeam data swath along the abyssal hill fabric direction (shown by small circles and indicated by mb in the legend). Hot colors indicate younger anomalies and cool colors indicate older anomalies. Magnetic isochrons are shown with solid colored lines and are located by taking into account data from both sides of the plate boundary. Fracture zones are labeled with numerical codes (FZ1-FZ9) as well as with the Aboriginal names assigned by *Massell et al.* [2000], and fracture zone picks used in our reconstructions are shown with small crosses. Satellite-derived gravity is shown in grayscale for reference.
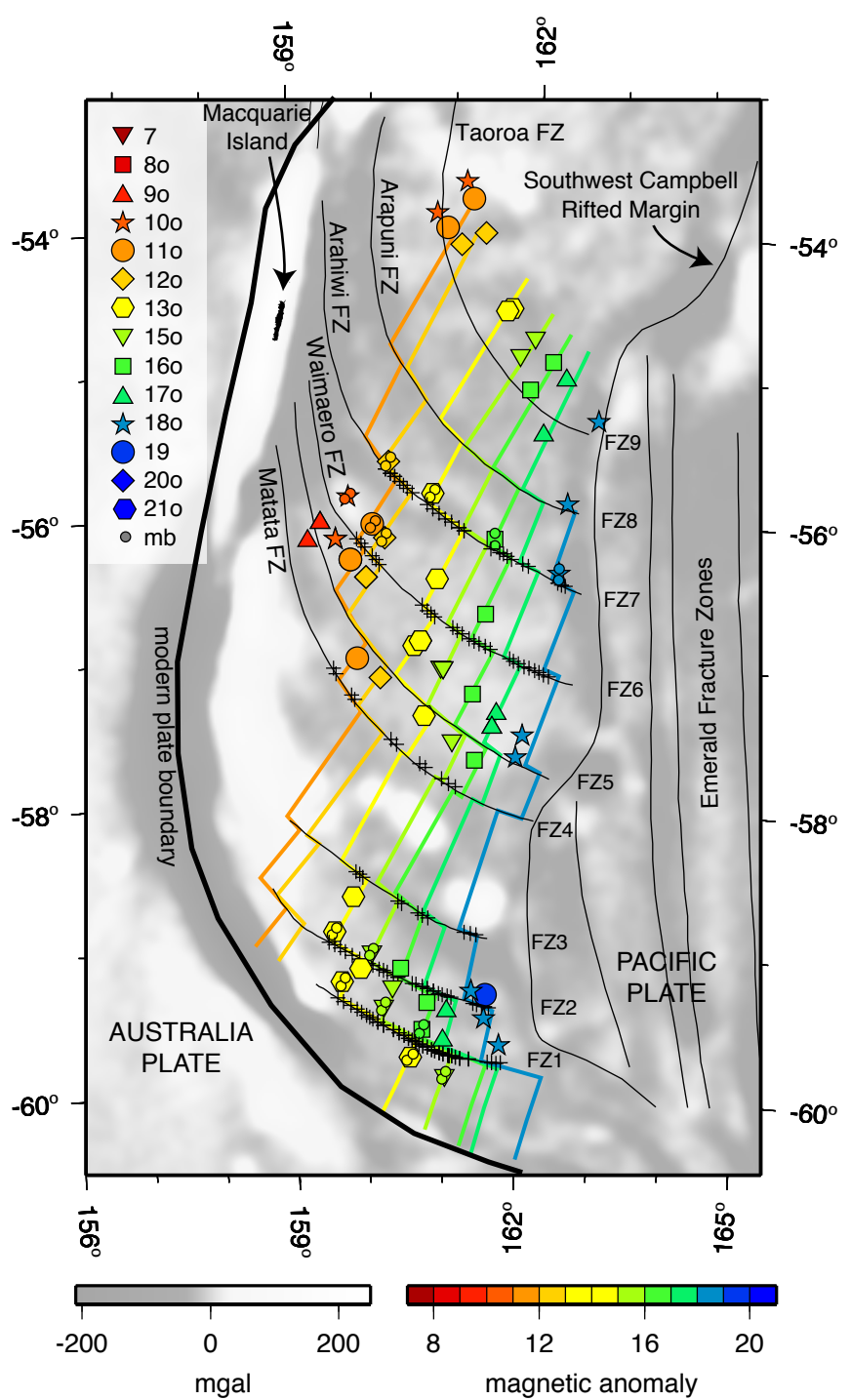
Figure 2.5: Stereographic projection showing magnetic anomaly identifications in the Emerald Basin. The format of the figure follows that of Figure 2.4. Fracture zones are labeled with numerical codes as well as the Maori names assigned by *Massell et al.* [2000].

was generated along the Macquarie Spreading Center. A similar, although less well constrained, age progression is found along the Southwest Campbell Rifted Margin along the eastern boundary of the Emerald Basin (Figure 2.5). Magnetic anomalies in the northeast part of STOC are closer together than anomalies farther to the southwest, indicating that the instantaneous pole of rotation was located relatively close to the northern end of the Macquarie Basin during this period of orthogonal spreading along the Macquarie Spreading Center.

In order to determine a set of finite rotations that reconstructs magnetic anomalies on the Australia plate back to their locations on the Pacific Plate, it is absolutely vital to match correctly the spreading corridors and fracture zones across the plate boundary. Along most mid-ocean ridges, this task is relatively straightforward because fracture zones can in many cases be traced continuously back to the ridge crest and are perpendicular to the ridge close to the active plate boundary. Matching spreading corridors across the Australia-Pacific boundary in the Macquarie Basin has proven to be a very difficult problem because of the large amount of right lateral strike-slip motion that has occurred along this boundary in the last 30 Ma.

The best way to match spreading corridors across the Macquarie Ridge Complex is to use patterns in the spacing of fracture zones as well as the amount and sense of offset across them as indicated by magnetic anomaly identifications. Patterns of offset that are unique to a particular fracture zone are difficult to identify because magnetic data are sparse and numerous closely spaced fracture zones exist in the Macquarie Basin, almost all of which are left-stepping (i.e. they offset magnetic anomalies in a left-lateral sense). Multibeam bathymetry is a crucial component in solving this problem because it provides a valuable constraint on the location of fracture zones close to the Macquarie Ridge Complex, and it reveals the orientation of abyssal hill fabric in spreading corridors between fracture zones. Abyssal hill fabric forms parallel to spreading ridges, so its orientation places a strong constraint on the strike of magnetic isochrons.
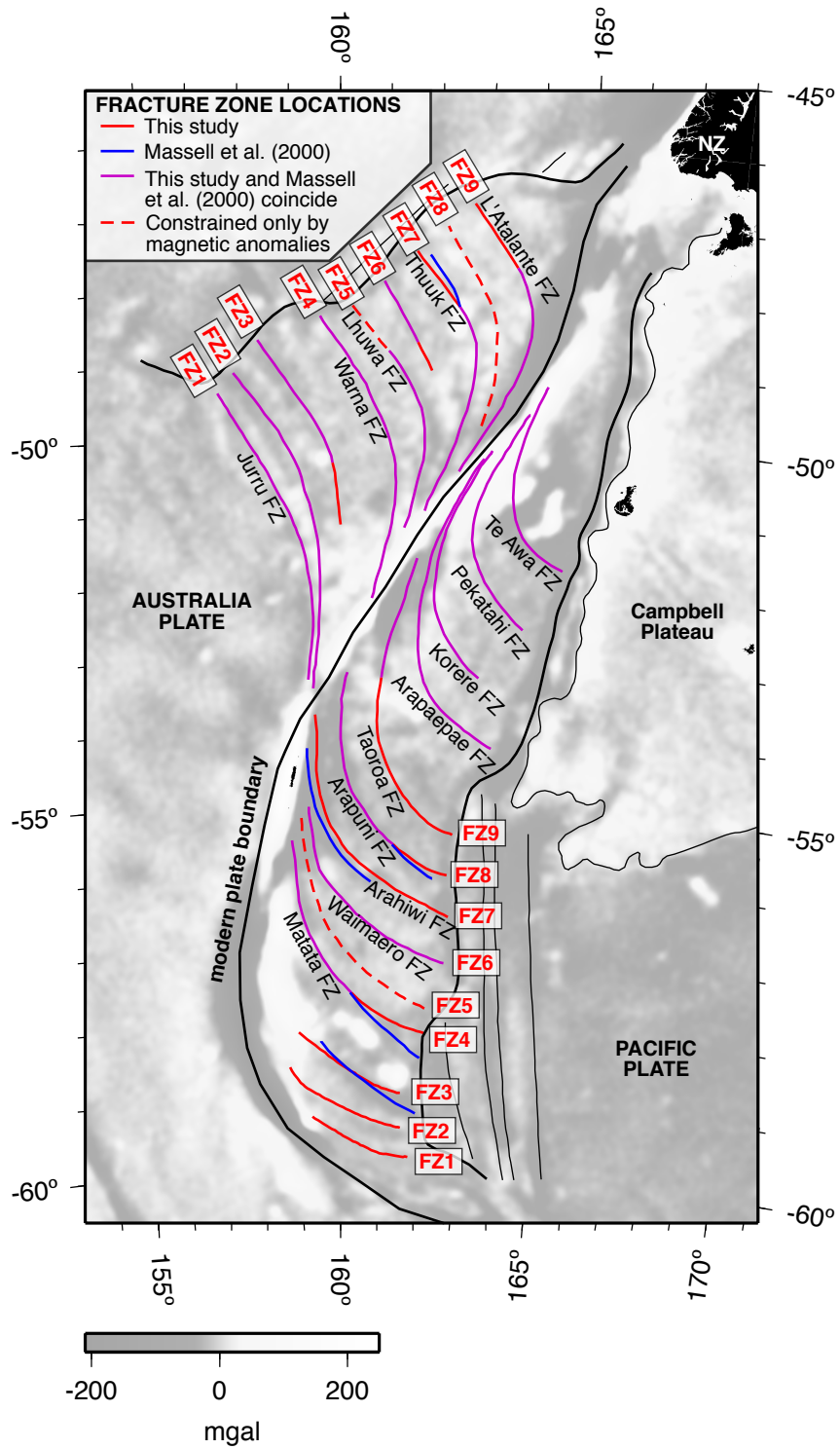
Figure 2.6: (caption on following page)

Figure 2.6: Stereographic projection showing fracture zone locations in the Macquarie Basin. Fracture zones are separated into four groups depending upon how they were identified: 1) purple - this study agrees with the fracture zone identification of *Massell et al.* [2000], 2) blue - *Massell et al.* [2000] interpretation deviates from this study, 3) red - new fracture zone identified or existing location revised for this study, 4) red dashed - new fracture zone identification based only on magnetic anomaly data from this study. Aside from the fracture zones shown by red dashed lines, all locations are constrained by multibeam and/or satellite-derived gravity. Conjugate fracture zone pairs are numbered FZ1-FZ9 (see Table 2.1) and are labeled with their Aboriginal (Australia Plate) and Maori (Pacific Plate) names [*Massell et al.*, 2000].

We see evidence for magnetic isochron offset across the fracture zones identified by *Massell et al.* [2000], and we identify additional fracture zones based on obvious magnetic anomaly offsets and gravity anomaly trends in the satellite-derived gravity field (Figure 2.6). By combining magnetic anomaly interpretations with abyssal hill spreading fabric directions obtained from multibeam data, we are able to identify several unique patterns of offset across these fracture zones. FZ1 is characterized by a large left stepping offset in magnetic isochrons 18o-13o and is coincident with a large offset in the Resolution Rifted Margin (Figure 2.4). This offset is mirrored in the Southwest Campbell Rifted Margin along the eastern boundary of the Emerald Basin where the large left-stepping offset of FZ1 is also easily identifiable. The spreading corridor between FZ3 and FZ4 is wider than the other spreading corridors, allowing it to be matched with confidence to its conjugate on the other side of the plate boundary. In the South Tasman Ocean Crust, there is an obvious right-stepping offset in chron 18 across FZ4, the Warna Fracture Zone (Figure 2.4). This offset coincides with the southern end of a prominent right stepping offset in the Resolution and Southwest Campbell Rifted Margins but becomes less prominent for chrons 17-13. The fracture zone then changes polarity and is left-stepping for chrons 12-11. This pattern of offset is not easily recognized when looking at data from each plate individually; however, the pattern becomes apparent when one does a series of best-fit reconstructions using data from other spreading corridors along the plate boundary. A similar scenario may exist for FZ9, the L'Atalante Fracture Zone. However, offset across this fracture zone is small, and the spreading corridors flanking this fracture zone are treated as a

Table 2.1: List of STOC fracture zones and their Emerald Basin conjugates. Fracture zone names are from *Massell et al.* [2000].

FZ number	Australia Plate FZ	Pacific Plate FZ
FZ9	L'Atalante FZ	Taoroa FZ
FZ8		Arapuni FZ
FZ7	Thuuk FZ	Arahiwi FZ
FZ6		Waimaero FZ
FZ5	Lhuwa FZ	
FZ4	Warna FZ	Matata FZ
FZ3		
FZ2		
FZ1	Jurru FZ	

single corridor in our plate reconstruction calculations.

These unique patterns of spacing and sense of offset across fracture zones in the South Tasman Ocean Crust and Emerald Basin allow us to confidently match fracture zones and spreading corridors on either side of the plate boundary (Table 2.1). *Massell et al.* [2000] identify the Arapaepae, Korere, Pekatahi, and Te Awa Fracture Zones in the Emerald Basin north of the Taoroa Fracture Zone (Figure 2.6). However, the conjugate fracture zones on the Australia Plate have been translated to the northeast as a result of right-lateral strike-slip motion along the Macquarie Ridge Complex and have been subsequently subducted under the Puysegur Trench.

2.4   Australia-Pacific finite rotations

Using magnetic and multibeam data from recent cruises in the Macquarie Basin, we have greatly increased the accuracy of magnetic isochron and fracture zone locations and have confidently matched conjugate spreading corridors across the Macquarie Ridge Complex for the first time. We have divided magnetic anomaly and fracture zone picks on either side of this plate boundary into as many as 12 segments and used the fitting algorithm of *Hellinger* [1981] to determine finite rotations for chrons 11o, 12o, 13o, 15o, 16o, 17o, and 18o (approximately 30-40 Ma). All times assigned to magnetic isochrons are from *Cande and Kent* [1995]. The best-fit finite rotations are

determined by minimizing the sum of the weighted misfits of these conjugate sets of points along great circle segments. We used the statistical methods of *Chang* [1987] and *Royer and Chang* [1991] to determine rotation parameters and their associated 95% confidence limits.

Uncertainties were assigned to each point based on a combination of 1) the navigational uncertainty of the ship, and 2) the uncertainty associated with picking the magnetic anomaly itself. An interactive program in which magnetic anomaly profiles are directly associated with navigation was used to pick anomalies on screen and assign associated uncertainties. These uncertainties were then combined with a navigational uncertainty that is based on the accuracy of navigational systems that have changed and evolved over the last 35 years. Navigational uncertainties ranged from 10 km for cruises from the late 1960s prior to satellite navigation to 0.1 km for more recent cruises with P-code GPS navigation. Whenever multibeam data were available along a particular ship track, we extrapolated magnetic anomaly identifications to the edge of the swath along the trend of the abyssal hill fabric. These points were digitized from multibeam maps and were assigned uncertainties of 3 km. Fracture zone locations were extrapolated away from areas of multibeam coverage by following negative anomalies in the satellite-derived gravity field. Points associated with these fracture zones were assigned uncertainties of 7 km. A maximum of 4-5 points were used on each fracture zone segment to avoid placing too much weight on the fracture zone segments relative to the magnetic anomaly segments used in our calculations.

Each resultant best-fit finite rotation is described by a pole location and angle (Table 2.2). The uncertainty associated with each rotation (Table 2.3) is given by a covariance matrix that describes an ellipsoidal confidence region about the pole location. The three eigenvectors and eigenvalues of the covariance matrix represent the directions and lengths of the principal axes of the ellipsoid respectively. More specifically, the square roots of the eigenvalues represent three small rotations about the axes defined by their corresponding eigenvectors. These three rotations can be thought of as the statistical equivalents of the Partial Uncertainty Rotations described by *Stock and Molnar* [1983]. (See *Chang et al.* [1990] for a comprehensive discussion

of uncertainties associated with plate reconstructions.)

The quality factor, $\hat{\kappa} = (\hat{\sigma}/\sigma)^2$, is a statistical parameter that relates the uncertainties assigned to the data ($\hat{\sigma}$) to their estimated true uncertainties (σ) based on the data distribution and total misfit of the reconstruction (Table 2.3). As such, $\hat{\kappa}$ is a measure of whether the uncertainties assigned to the points used in the reconstruction are statistically correct ($\hat{\kappa} = 1$), overestimated ($\hat{\kappa} >> 1$), or underestimated ($\hat{\kappa} << 1$). The quality factor was estimated from the data as follows [*Royer and Chang*, 1991]:

$$\hat{\kappa} = (N - 2s - 3)/r$$

where N is the number of points, s is the number of great circle segments, and (N - 2s -3) is the number of degrees of freedom. The total misfit (r) is the sum of the squares of the weighted distances of data points to their best-fit great circle segments.

The values we obtained for $\hat{\kappa}$ are all greater than 1 and range from approximately 1 for chron 15o to approximately 4 for chron 18o. This indicates that the errors assigned to our points are in general slightly overestimated. This overestimation is the result of the comparatively large uncertainties assigned to fracture zone points picked from the satellite-derived gravity field. Because lowering the value of these uncertainties caused little change in the location of the rotation poles or the size of their associated 95% confidence regions, we chose to retain the original uncertainty estimates.

Table 2.2: Finite rotations of Australia relative to Pacific.

Chron	Age (Ma)	Latitude (°N)	Longitude (°E)	Angle (deg)
11o	30.10	-53.19	-178.74	33.73
12o	30.94	-52.83	-178.81	34.58
13o	33.55	-51.70	-178.45	35.99
15o	34.94	-51.19	-178.62	37.49
16o	36.34	-50.82	-179.30	39.61
17o	37.47	-50.36	-178.97	39.62
18o	40.13	-49.81	-179.55	41.77

Table 2.3: Covariance matrices for finite rotations in Table 2.2

Chron	$\hat{\kappa}$	a	b	c	d	e	f	g
11o	2.22	5.01	-1.36	5.78	0.377	-1.57	6.69	4
12o	3.04	5.56	-1.62	6.45	0.475	-1.87	7.48	4
13o	2.07	7.79	-2.93	9.56	1.13	-3.55	11.9	6
15o	1.14	2.05	-0.780	2.65	0.305	-1.00	3.45	5
16o	1.58	1.17	-0.433	1.48	0.169	-0.542	1.89	5
17o	1.98	3.02	-1.12	3.83	0.432	-1.42	4.88	5
18o	4.06	24.0	-8.36	28.6	2.96	-9.99	34.1	5

The covariance matrix is given by the formula:

$$\frac{1}{\hat{\kappa}} * \begin{pmatrix} a & b & c \\ b & d & e \\ c & e & f \end{pmatrix} \times 10^{-g}$$

where a-f are given in radians squared

Finite pole locations and their associated 95% confidence regions are shown in Figure 2.7. Between chrons 18o and 11o, a very consistent southward migration of finite rotation poles is seen from 49.8° S to 53.2° S. The size of the confidence regions is controlled primarily by limitations due to inconsistencies in data distribution. Chrons 11o and 12o are not identified south of 57.5° S in the southern Emerald Basin (Figure 2.5), so only ridge and fracture zone segments north of this latitude were used to calculate these finite rotations. Because the data for these chrons are confined to a relatively small area along the length of the plate boundary, the error ellipses are correspondingly larger than the error ellipses for other chrons. Figure 2.8 shows the magnetic anomaly and fracture zone fits that were used to constrain the finite rotation poles. Points on the Australia Plate (white symbols) have been rotated using the finite rotations described in Table 2.2 and generally match the location and trend of their Pacific Plate conjugates (black symbols) very closely. Magnetic and fracture zone fits are also shown individually for chrons 11o, 13o, 16o, and 18o (Figure 2.10 parts A-D). Significant non-systematic scatter in the chron 18 fit exists and is likely due to inconsistencies in the shape of magnetic anomalies that were formed close to the rifted margin during the early stages of seafloor spreading along the Macquarie Spreading Center.
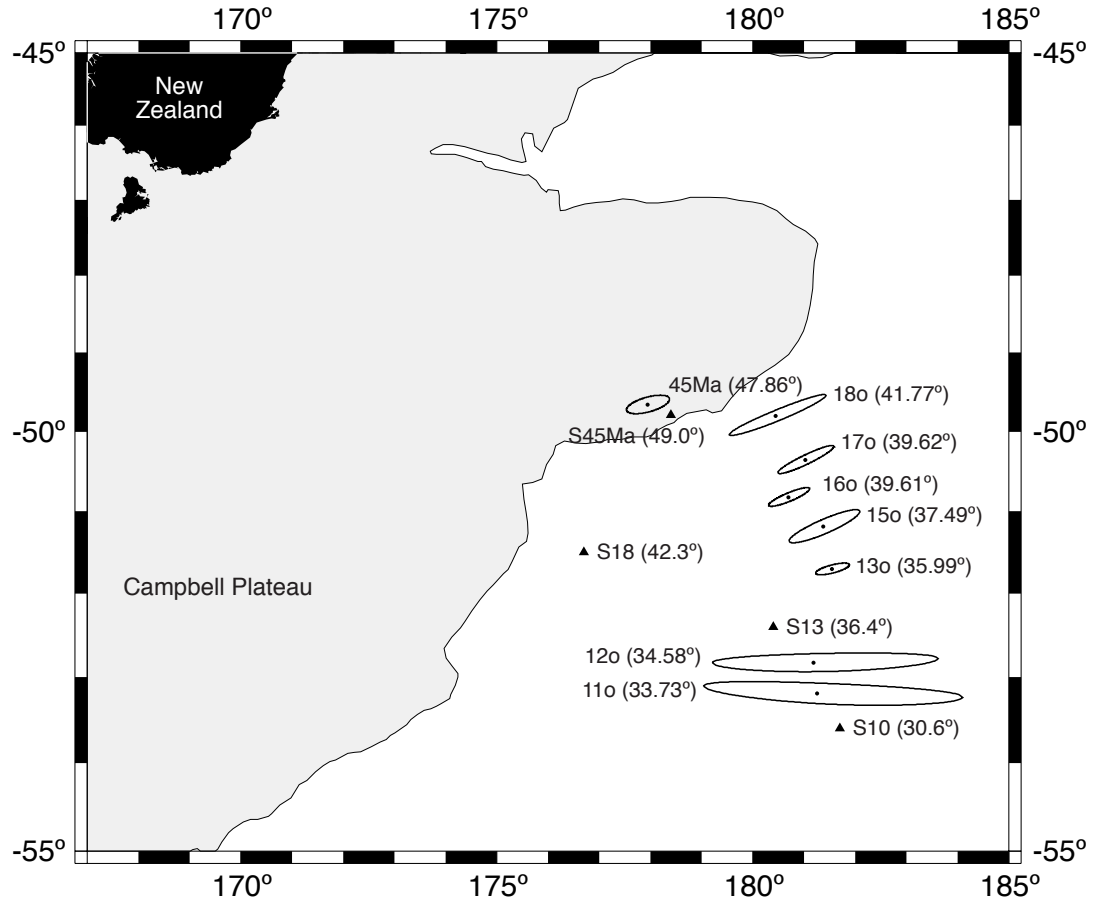
Figure 2.7: Location of AUS-PAC finite rotation poles and associated 95% confidence regions. Each pole is labeled with its associated magnetic isochron, and the rotation angle is shown in parentheses. Pole locations are shown with small black dots, and confidence regions are outlined with solid black lines. The 45 Ma pole and angle, Chapter 3, reconstructs the Australia Plate back to its location prior to rifting along the Macquarie Spreading Center. *Sutherland* [1995] poles are shown with black triangles and labeled with annotations of the form "Sxx", where "xx" is the isochron that denotes the age of the rotation. The 2000 m contour is shaded with gray and represents the approximate location of the New Zealand continental shelf. The South Island of New Zealand is seen in the far NW side of the figure and is shaded black.

24
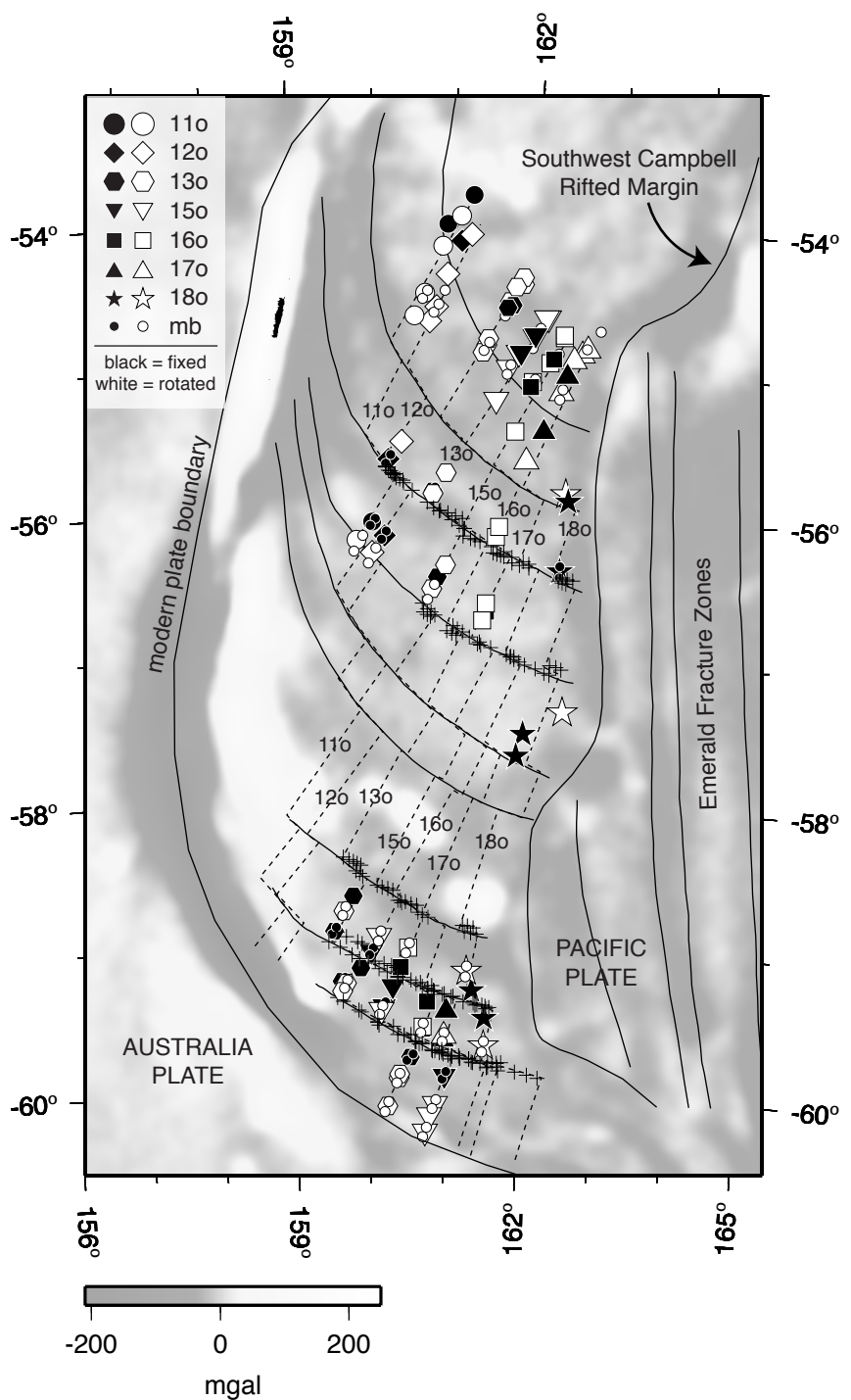
Figure 2.8: Magnetic anomaly and fracture zone points used to constrain AUS-PAC finite rotations. Fixed points on the Pacific Plate are shown by black symbols. White symbols are Australia Plate points that have been rotated using the finite rotations described in Table 2.2. Fracture zone points are indicated by small crosses, and magnetic isochrons are shown with dotted lines. The lack of 11o and 12o points south of 56.5° S is the cause of the larger uncertainties associated with these two finite rotations. Magnetic and fracture zone fits are shown individually for chrons 11o, 13o, 16o, and 18o in Figure 2.10 parts A-D.

2.5 Plate tectonic reconstructions of the Macquarie Basin

Previous attempts to find a set of finite rotations that reconstructs the spreading history along the Macquarie Spreading Center [*Sutherland*, 1995] have been primarily based on reconstructing tectonic features interpreted from the satellite-derived gravity field [*Sandwell and Smith*, 1997]. *Sutherland* [1995] constructed estimated magnetic isochrons from sparse shipboard identifications of magnetic anomalies to help constrain the rotations; however, this study marks the first attempt at calculating finite rotations and associated uncertainties using shipboard observations of magnetic anomalies and fracture zones in the Macquarie Basin. As an example of the misfit inherent in prior finite rotations, we have generated a reconstruction in the Pacific Plate reference frame using the chron 13 finite rotation described by *Sutherland* [1995] (Figure 2.9). This reconstruction indicates that the *Sutherland* [1995] finite rotation is a significant underestimate, leaving a more than 100 km wide gap between the chron 13o isochrons identified in this study. Figure 2.10 part C shows that our 13o finite rotation correctly accounts for the misfit inherent in the *Sutherland* [1995] finite rotation.

The finite rotations described in Table 2.2 are used to produce a series of reconstructions of the Macquarie Basin (Figure 2.10 parts A-D). During the early stages of seafloor spreading along the Macquarie Spreading Center at chron 18o (40 Ma), rifting was propagating northward toward the Campbell Plateau/New Zealand continental block (Figure 2.10A). Active seafloor spreading was just becoming established during this time along the Macquarie Spreading Center between roughly 49.5° S and 56° S; however, seafloor spreading had been established south of approximately 59.5° S since chron 21o (48 Ma). As seafloor spreading continued to propagate to the northeast, a wedge shaped region of new ocean crust was formed in the Macquarie Basin (Figure 2.10 parts B-D). NW-trending gravity lows related to fracture zones in the southern part of the Macquarie Basin match very closely across the active plate boundary for reconstructions younger than chron 16o (Figure 2.10B-D). At chron

11o, the oceanic transform and ridge segments of the Macquarie Spreading Center are rotated slightly in a clockwise fashion in response to the southward migration of the finite rotation pole. This marks the initial stages of transition from oceanic spreading to right-lateral strike-slip faulting along this plate boundary.
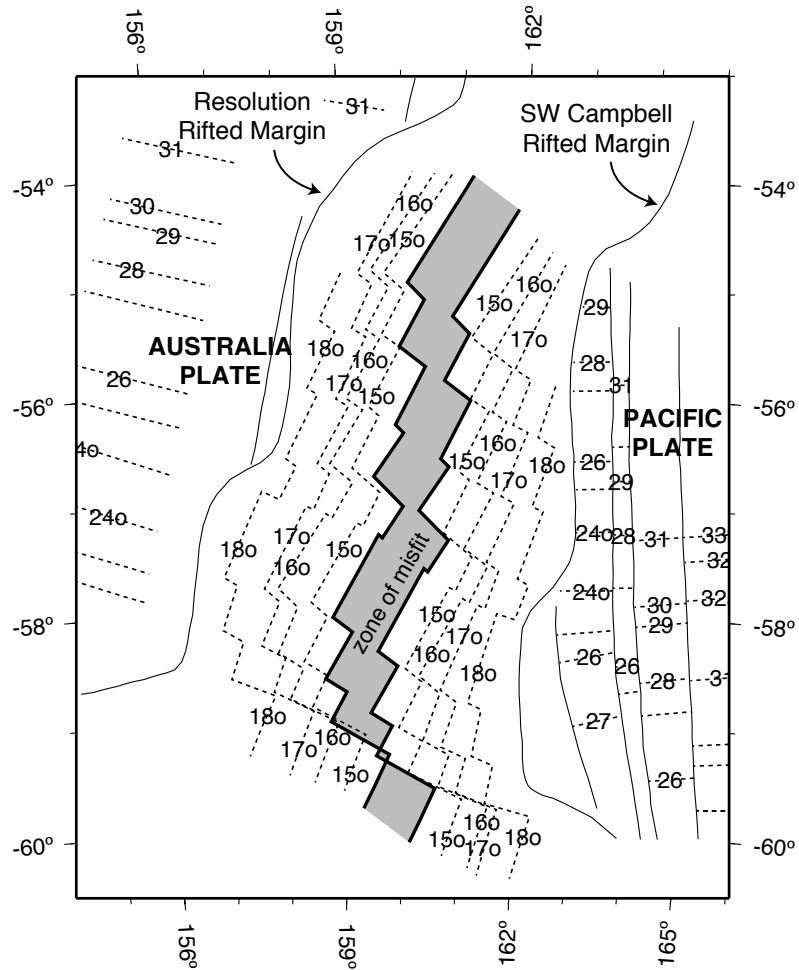
Figure 2.9: *Sutherland* [1995] chron 13 reconstruction of the Macquarie Basin. The Pacific Plate is held fixed, and tectonic features on the Australia Plate have been rotated using the chron 13 finite rotation described by *Sutherland* [1995]. The 13o isochrons from this study are shown by thick black lines, and the shaded gray area represents over 100 km of misfit between them.

28
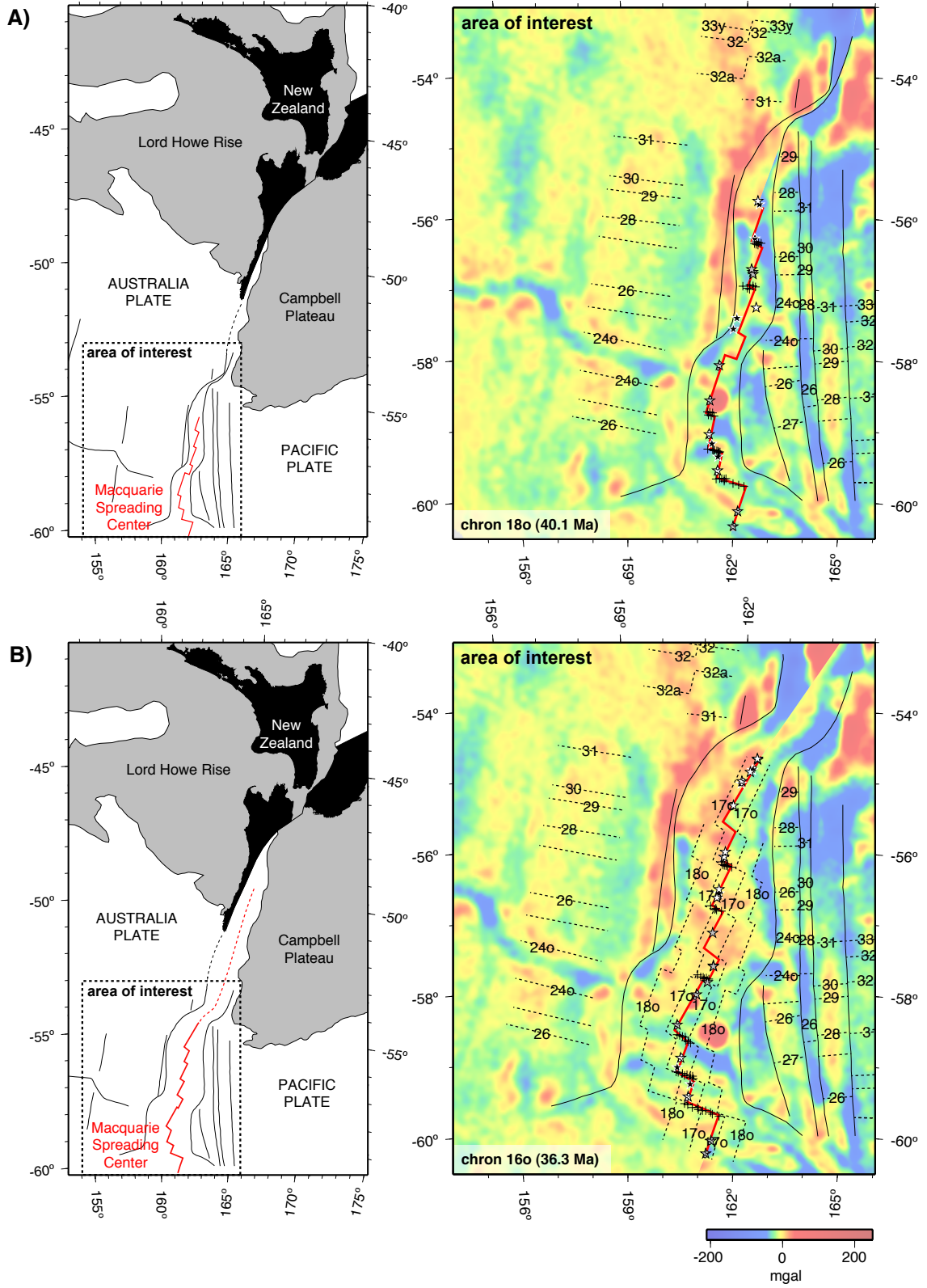
Figure 2.10: (continued on following page...)
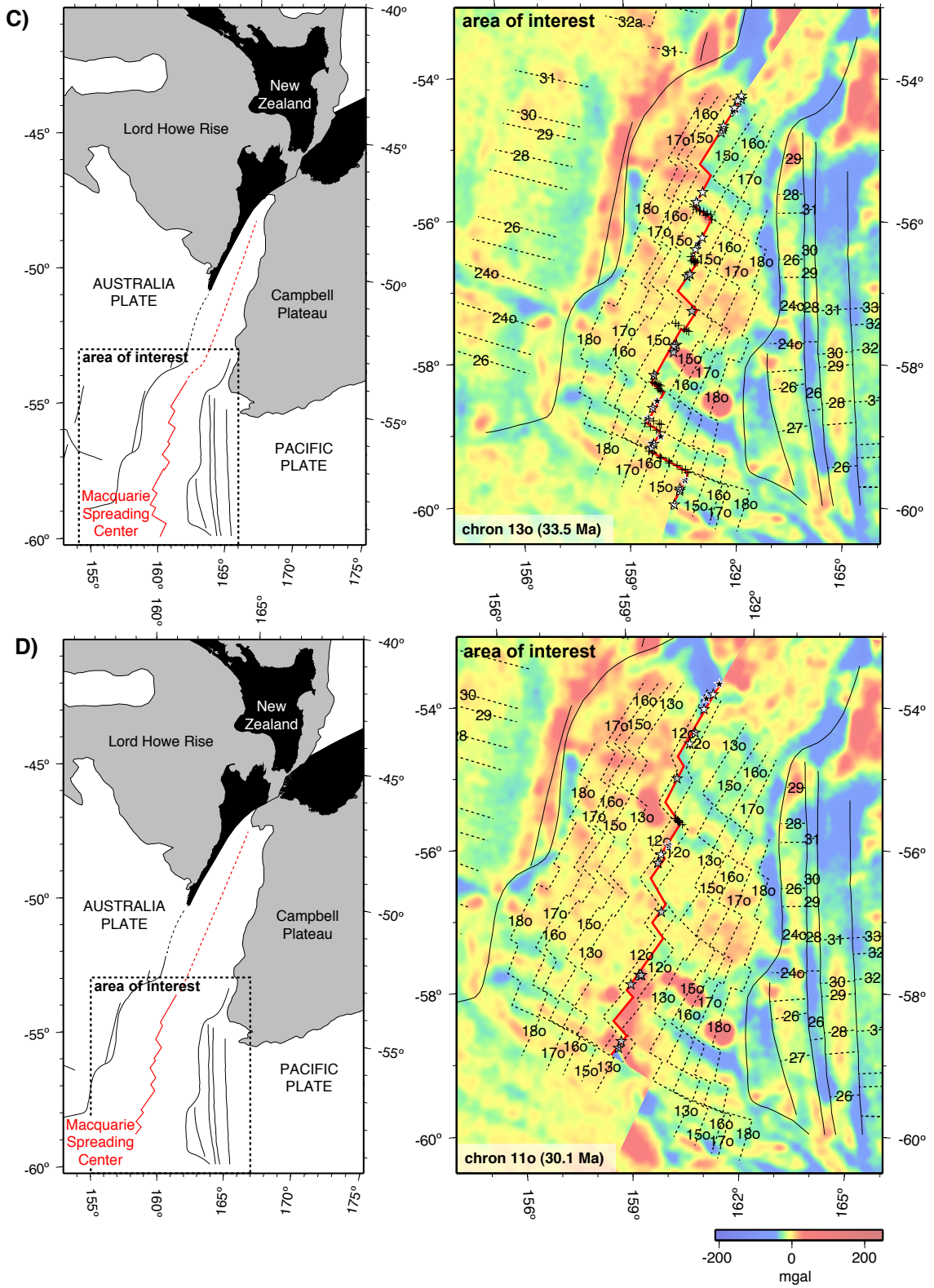
Figure 2.10: (caption on following page)

Figure 2.10: Plate tectonic reconstructions of the Macquarie Basin. The Pacific Plate is held fixed, and the satellite gravity field and tectonic features on the Australia Plate have been rotated using the finite rotations described in Table 2.2. The gravity field of the Australia Plate has been clipped along the active plate boundary, which is shown with the solid red line in each figure. Magnetic anomaly points (stars and small circles) and fracture zone points (crosses) used to constrain the rotations are shown in their reconstructed positions along the active plate boundary. Black symbols indicate fixed points on the Pacific Plate, white symbols indicate rotated Australia Plate points, and gray symbols indicate points that were not used in the calculation because they did not have conjugates on the opposing plate. Fracture zone points are indicated by small crosses.

2.6   Implications for New Zealand tectonics

Stage rotations spanning chrons 18o-15o and chrons 15o-11o were calculated in order to better understand the position of the instantaneous AUS-PAC rotation pole through time and its relationship to the tectonics of New Zealand (Tables 2.4 and 2.5, Figure 2.11). A stage rotation was also calculated for the entire interval spanning chrons 18o-11o, the time period during which spreading along the Macquarie Spreading Center was predominantly orthogonal. At younger times, right-lateral strike slip motion became progressively more dominant. The 95% confidence regions for these stage poles are larger than those for the finite rotations largely because the stage poles represent a much smaller total angle of rotation. The 30-35 Ma (roughly chrons 11o-15o) and 35-40 Ma (roughly chrons 15o-18o) stage poles described by *Sutherland* [1995] fall to the south and just outside the error ellipses of the corresponding stage poles described in this study (Figure 2.11).

Table 2.4: Australia-Pacific Stage Rotations (Pacific Plate reference frame).

Chron	Age (Ma)	Latitude (°N)	Longitude (°E)	Angle (deg)
18o-15o	40.13-34.94	-40.03	168.99	-4.40
15o-11o	34.94-30.10	-34.66	175.53	-3.96
18o-11o	40.13-30.10	-37.44	172.08	-8.34

Table 2.5: Covariance matrices for finite rotations in Table 2.4

Chron	$\hat{\kappa}$	a	b	c	d	e	f	g
18o-15o	1.56	0.174	-6.18	0.286	2.24	-0.102	0.472	5
15o-11o	1.26	3.81	-1.27	5.65	43.3	-1.89	8.41	4
18o-11o	3.30	5.30	-1.87	8.03	68.1	-2.85	0.122	4

The covariance matrix is given by the formula:

$$\frac{1}{\hat{\kappa}} * \begin{pmatrix} a & b & c \\ b & d & e \\ c & e & f \end{pmatrix} \times 10^{-g}$$

where a-f are given in radians squared

The chron 18o-15o stage pole described in this study is located on the north edge of the reconstructed New Zealand continental shelf and then migrates to the northeast through time as shown by the location of the chron 15o-11o stage pole. This stage pole configuration predicts minor extension within the South Island of New Zealand from chrons 18o-15o followed by a more pronounced period of extension as the stage pole migrates farther away from the continent during the time spanning chrons 15o-11o. This relationship is evident when viewing reconstructions of New Zealand and its associated continental shelf for chrons 11o, 15o, and 18o (Figures 2.11 and 2.12). Assuming perfectly rigid plates split along the present day location of the Alpine Fault, the Lord Howe Rise continental block significantly overlaps the South Island of New Zealand and Campbell Plateau continental block when reconstructed back to its chron 18o location (Pacific Plate reference frame). Farther south, however, the Lord Howe Rise and the northern part of the Resolution Rifted Margin fit very closely along the western edge of the Campbell Plateau. By chron 15o, a narrow wedge of new ocean crust exists between the Resolution Rifted Margin and the western edge of the Campbell Plateau as a result of seafloor spreading along the Macquarie Spreading Center. To the north, the overlap between the Lord Howe Rise continental block and the South Island of New Zealand has only been slightly reduced due to the proximity of the stage pole. By chron 11o, this overlap has been almost entirely removed and the eastern margin of the Lord Howe Rise continental block very closely follows what is now the west coast of the South Island of New Zealand (Figure 2.12). The overlap

described above may be accounted for by distributed crustal extension during the time period spanning chrons 18o-11o with most of the extension occurring at younger times. This idea is supported by observations of large extensional basins related to rifting in the southern South Island during this time period.

To quantify the amount of crustal extension expected during the time period spanning chrons 18o-11o, the positions of a series of arbitrary points on the South Island of New Zealand were predicted forward in time relative to a fixed Pacific Plate (Figure 2.12). The positions of the points at chron 11o were calculated using the 18o-11o stage rotation described in Table 2.4, and their present day positions were calculated using the inverse of the 18o finite rotation described in Table 2.2. From their original chron 18o positions, the points move W-NW to their positions at chron 11o indicating a period of continental extension that is most pronounced in the south during this time. The magnitude of extension decreases from 140±80 km at the southernmost point to 90±105 km at the northernmost point, a value that is well within the error of the measurement. From their positions at chron 11o, the points move NE to their current positions. The paths the points take from chron 11o to present are schematic and are thus shown as dashed lines in Figure 2.12. However, it is clear by visual inspection that motion across the plate boundary during this time was dominantly right-lateral strike slip. From observations of magnetic anomalies and fracture zone orientations in the Macquarie Basin, the transition from extension to right lateral strike slip initiated shortly after chron 11 (30 Ma). Chron 7 is the youngest magnetic anomaly identified in the Macquarie Basin (Figure 2.4), indicating that right-lateral motion across the plate boundary was well established by 25 Ma. Although an exact measurement is not possible given the lack of sufficient data younger than chron 11o, the distances between the present day and chron 11o locations of the points in Figure 2.12 are consistent with roughly 800 km of post 30 Ma dextral displacement across the plate boundary. This motion is likely accommodated by a combination of distributed crustal shear and strike-slip motion along the Alpine Fault [*Sutherland*, 1999].
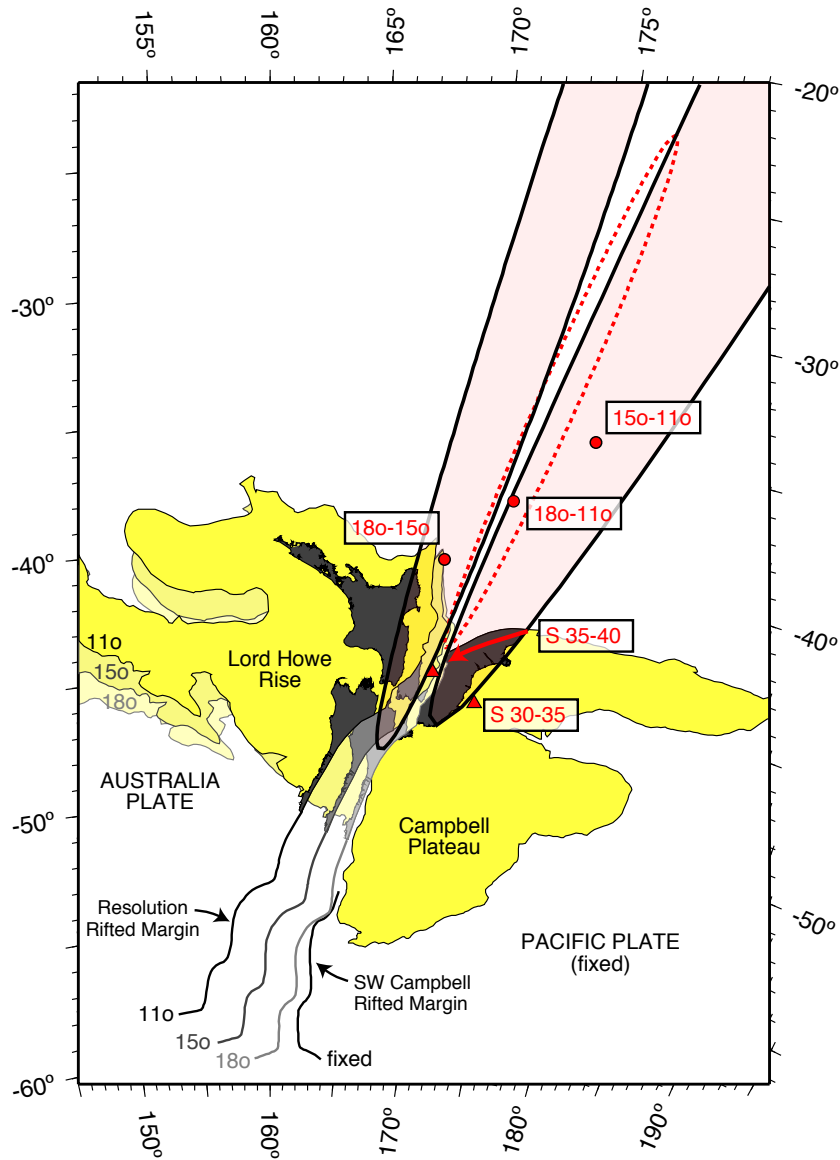
Figure 2.11: Location of 18o-15o and 15o-11o AUS-PAC stage poles (red circles) are shown with their associated 95% confidence regions (ellipses outlined in black). Seafloor spreading along the Macquarie Spreading Center was predominantly orthogonal from chrons 18o-11o, and the 95% confidence region for the stage pole spanning this time period is shown by the red dashed ellipse. The locations of the *Sutherland* [1995] 35-40 Ma (roughly chrons 15o-18o) and 30-35 Ma (roughly chrons 11o-15o) stage poles are shown with red triangles. New Zealand and its continental shelf are shown in dark gray and yellow respectively. The Resolution Rifted Margin, the Lord Howe Rise, and the Australia Plate side of New Zealand are reconstructed back to their locations at chrons 18o, 15o, and 11o and labeled accordingly. For clarity, these features at older times are shown in progressively lighter colors.
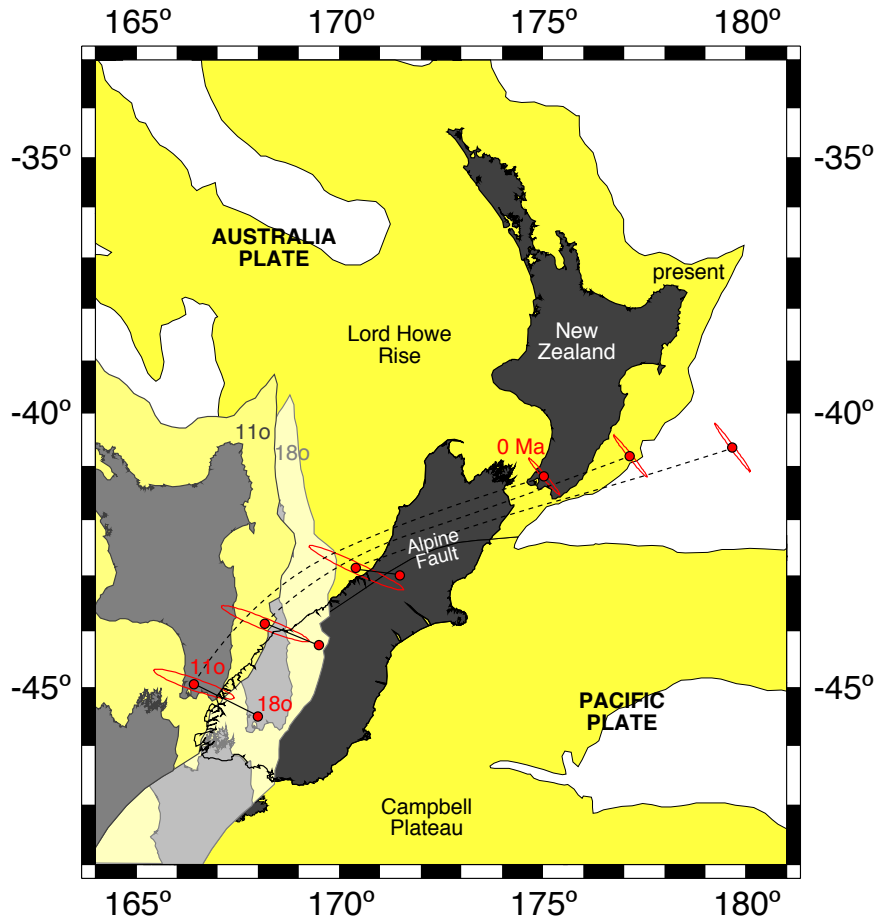
Figure 2.12: Arbitrary points that originally lay west of the South Island of New Zealand and their positions predicted forward in time relative to a fixed Pacific Plate, chron 18o to present. The points were rotated to their 11o locations using the 11o-18o stage rotation from this study and were rotated to their present locations using our chron 18o finite rotation. 95% confidence regions are shown by red ellipses. Our model predicts approximately 140±80 km of extension in the southern South Island of New Zealand from chron 18o-11o, a value that decreases toward the stage pole location to the north. The paths the points take from chron 11o to present are schematic and are thus shown as dashed lines. The colors of present day and reconstructed continental blocks follow Figure 2.11.

2.7 Discussion

Analysis of new shipboard data, including magnetic and multibeam bathymetry data from recent geophysical cruises, has greatly improved the accuracy of fracture zone locations and magnetic anomaly trends in the Macquarie Basin. Because the scouring activity of bottom water currents has eroded much of the sediment cover over large areas of the ocean floor in this region, the Macquarie Basin is an ideal environment in which to image tectonic features with multibeam bathymetry data. Multibeam bathymetry clearly images abyssal hill fabric that formed parallel to ridge segments during seafloor spreading along the Macquarie Spreading Center. In the South Tasman Ocean Crust, abyssal hill fabric on seafloor that was created between chron 21 and chron 11 (48-30 Ma) trends NE. As previous authors have noted, abyssal hill fabric at younger times is progressively rotated in a clockwise sense and generally trends SE adjacent to the Macquarie Ridge Complex. *Massell et al.* [2000] identified fracture zones using multibeam bathymetry close to the Macquarie Ridge Complex and extrapolated their locations outside of their data coverage area by following anomaly trends in the satellite-derived gravity field. Magnetic anomaly offsets confirm the location of these fracture zones, and we identify several additional fracture zones based on observed magnetic anomaly offsets and anomaly trends in the satellite-derived gravity field.

Magnetic anomalies identified adjacent to the Resolution and Southwest Campbell Rifted Margins reveal the pattern of early seafloor spreading along the Macquarie Spreading Center. This pattern of rifting is best observed in the South Tasman Ocean Crust along the Resolution Rifted Margin because of sparse data coverage in the Emerald Basin. Magnetic anomalies adjacent to the Resolution Rifted Margin are younger to the northeast - chron 21 is observed southwest of FZ1 (Jurru FZ), chron 19 is observed between FZ1 and FZ3, chron 18 is observed between FZ3 and FZ9, and chron 17 is observed northwest of FZ9 (L'Atalante FZ). This pattern indicates that early seafloor spreading between the Australia and Pacific plates propagated to the northeast toward New Zealand. Chron 7 is identified in one spreading corridor in the

South Tasman Ocean Crust and is the youngest magnetic anomaly identified close to the Macquarie Ridge Complex. This indicates that new crust was being created along this plate boundary until at least 25 Ma. However, chron 7 is over 100 km away from the modern plate boundary along the trend of fracture zones close to the Macquarie Ridge Complex, indicating that a significant amount of ocean crust was formed after chron 7.

Fracture zones identified in the Macquarie Basin are closely spaced and almost exclusively left-stepping. This geometry coupled with the paucity of shipboard geophysical data in the region and the large amount of strike-slip motion that occurred subsequent to seafloor spreading has hampered previous attempts to match fracture zones across the modern plate boundary. By combining our magnetic anomaly dataset with abyssal hill spreading fabric directions identified in available multibeam data, we are able to confidently match fracture zones and spreading corridors on either side of the Macquarie Ridge Complex for the first time. We match 9 fracture zones and 10 spreading corridors across the modern plate boundary. Fracture zones north of FZ9 (Taoroa FZ) are the Pacific Plate conjugates to fracture zones on the Australia Plate that have been subducted under the Puysegur Trench. We use conjugate magnetic anomaly and fracture zone points to calculate finite rotations for chrons 18-11 (40-30 Ma); however, we have insufficient data to calculate rotation parameters for younger times.

When the New Zealand continental shelf is reconstructed back to its chron 18o (40 Ma) configuration, the Lord Howe Rise continental block significantly overlaps the South Island of New Zealand. This overlap is removed by chron 11o (30 Ma), when the eastern edge of the Lord Howe Rise continental block fits nicely against the present day west coast of the South Island of New Zealand. The overlap seen during the time spanning 40-30 Ma can be accounted for by approximately 140±80 km of W-NW crustal extension that decreases in magnitude towards the 18o-11o stage pole to the north. Roughly 800 km of dextral motion has been accommodated across the Australia-Pacific Plate boundary through New Zealand since chron 11o (30 Ma). Fracture zone orientations and magnetic anomaly identifications within the

Macquarie Basin suggest that the Alpine Fault was well established by 25 Ma (chron 7).

Chapter 3

A Middle Eocene Australia-Pacific pre-rift reconstruction of the southeast Tasman Sea

Abstract

Seafloor spreading along the Macquarie Ridge Complex in Eocene and Oligocene time formed new oceanic crust in the Emerald Basin and South Tasman Ocean Crust (STOC). During the initial stages of rifting, extension migrated northward along zones of weakness parallel to fracture zones associated with the Tasman Ridge and along the western edge of the Campbell Plateau. The margins separating younger crust created along the Macquarie Ridge Complex from older crust created along the Tasman and Pacific-Antarctic Ridges are identified as the Resolution Rifted Margin (on the Australia Plate), and the Southwest Campbell Rifted Margin (on the Pacific Plate). We use geophysical data from recent surveys along with satellite derived gravity to map precisely the location of these rifted margins and older fracture zones that predate seafloor spreading along the Macquarie Ridge Complex. These tectonic features are then used to calculate a new best-fit Australia-Pacific pre-rift finite rotation including associated uncertainties. This is the first time that uncertainties have been calculated for this rotation. The age associated with the best-fit pre-rift rotation (45 ± 5 Ma) is not precisely constrained because it is not directly associated with a magnetic isochron. However, the rotation is known to postdate the cessation of spreading along the Tasman Ridge (chron 24, 52 Ma) and to predate the initiation of spreading along the Macquarie Ridge Complex (chron 18, 40 Ma).

3.1   Introduction

Seafloor spreading along the Tasman Ridge initiated at roughly 83 Ma (chron 34), opening the Tasman Sea ocean basin between Australia and the Lord Howe Rise-New Zealand continental block [*Weissel and Hayes*, 1972]. Continental extension between East Antarctica and Australia and subsequent slow spreading along the Southeast Indian Ridge (SEIR) were also occurring during this time period. As spreading along the SEIR became more established, the ridge lengthened eastward toward the Tasman and Pacific-Antarctic ridge systems. Spreading along the Tasman Ridge continued until roughly 52 Ma (chon 24) when spreading ceased and the Lord Howe Rise became part of the Australia Plate (e.g., *Hayes and Ringis* [1973]; *Weissel et al.* [1977]; *Gaina et al.* [1998]). Seafloor spreading between the Australia and Pacific plates was initiated along the Macquarie Spreading Center just prior to 40 Ma (chron 18), marking a 90 degree change in spreading direction relative to the previous Tasman Ridge spreading direction *Weissel et al.* [1977]. The Macquarie Ridge Complex has a complicated history in which it evolved from a spreading center to a predominantly strike-slip boundary. We use "Macquarie Spreading Center" when referring to the time period during which this feature acted as an orthogonal spreading center between the Australia and Pacific Plates.
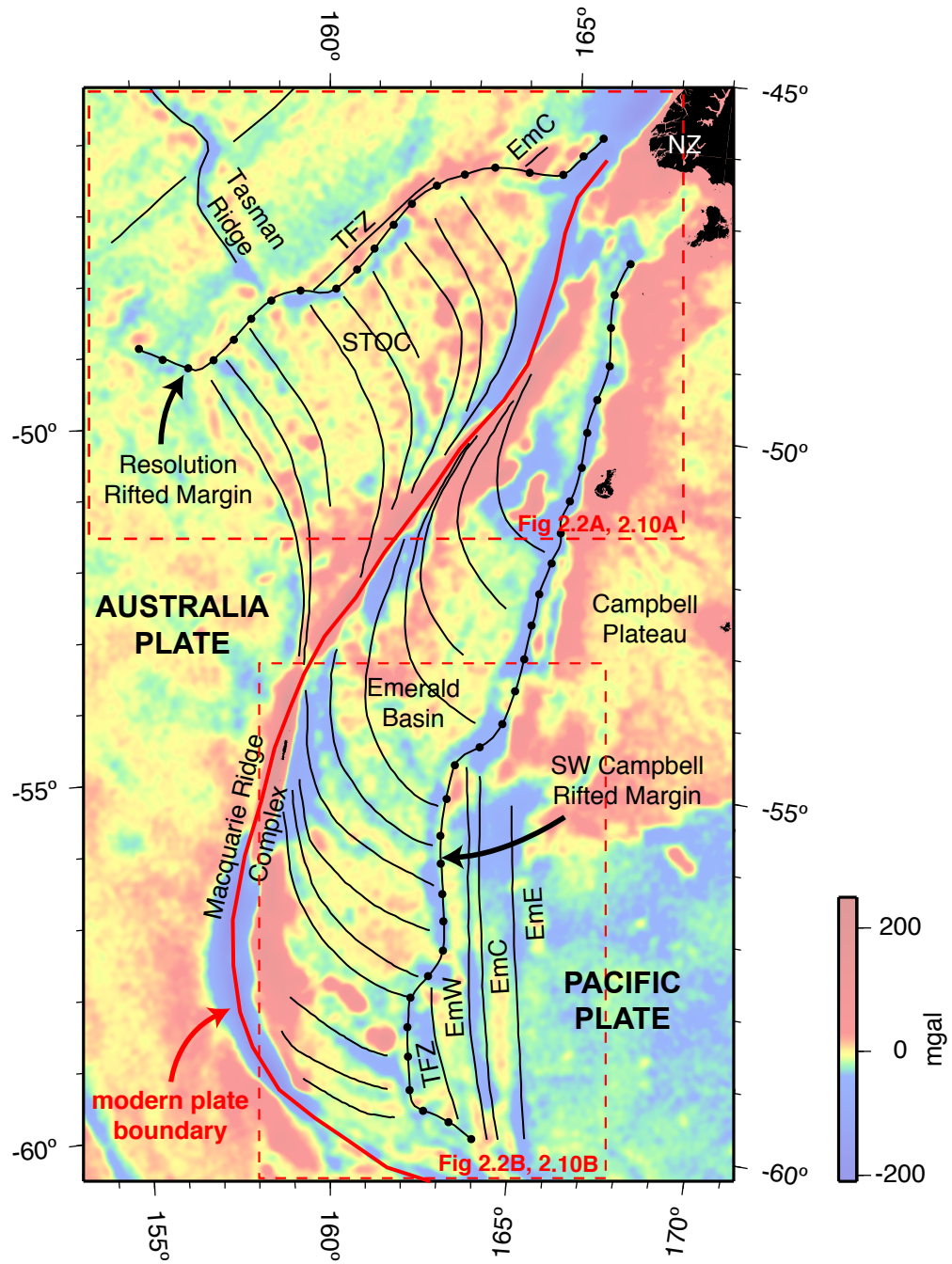
Figure 3.1: (caption on following page)

The boundary between older Tasman Ridge crust and younger Macquarie Ridge crust is marked by the Resolution Rifted Margin on the Australia Plate and the Southwest Campbell Rifted Margin on the Pacific Plate. These two rifted margins are clearly visible in satellite-derived gravity anomaly maps [*Sutherland*, 1995], and the present day locations of these and other important tectonic features in the Southeast Tasman Sea are shown in Figure 3.1. We present a new shipboard data set collected during several geophysical cruises including the EW9513 cruise aboard the R/V Ewing and the NBP9702, NBP0007B, and NBP0209 cruises aboard the R/VIB Nathaniel B. Palmer. In addition, several profiles were collected by the Japan National Oil Corporation on cruises TH91B and TH92B aboard the R/V Hakurei Maru [*Tanahashi et al.*, 1997]. Magnetic, gravity, multibeam bathymetry, and seismic data collected aboard these cruises allow us to determine the geophysical structure and precise location of the Resolution and Southwest Campbell Rifted Margins.

3.2 Shipboard bathymetry, gravity, and magnetics across the Resolution and Southwest Campbell Rifted Margins

Single beam bathymetry, magnetic, and gravity data collected along selected profiles across the Resolution and Southwest Campbell Rifted Margins (Figure 3.2) reveal that older crust created along the Tasman Ridge is separated from the younger crust

Figure 3.1: Major tectonic features in the Southeast Tasman Sea. The South Tasman Ocean Crust (STOC) and Emerald Basin were formed by seafloor spreading along the Macquarie Ridge Complex and are collectively referred to here as the Macquarie Basin. Fracture zones are shown with thin black lines, the rifted margins denoting the edge of the Macquarie Basin are shown with black dotted lines, and the modern plate boundary is shown in red. Red dashed lines delineate regions shown in Figures 3.2a and 3.2b. Satellite derived gravity is the basemap [*Sandwell and Smith*, 1997]. NZ=New Zealand, TFZ=Tasman Fracture Zone, EmW=West Emerald Fracture Zone, EmC=Central Emerald Fracture Zone, and EmE=East Emerald Fracture Zone.

of the Emerald Basin and South Tasman Ocean Crust by a roughly 20-30 km wide zone of extended oceanic crust. The structure of this zone varies along strike, but is typically characterized by a prominent gravity low that coincides with a bathymetric depression between the old side (RM2) and the young side (RM1) of the rifted margin (eg. Figure 3.3 lines S7-S11, Figure 3.4 lines E8-E11). The location of tectonic features is interpolated between shipboard control points in map view by following anomaly trends in the satellite derived gravity field [*Sandwell and Smith*, 1997].

The geometry of the Southwest Campbell Rifted Margin is very distinct and can be divided into three N-S segments that are offset by two shorter E-W oriented segments at roughly 54° S and 57.5° S. These E-W segments are right stepping (i.e. they offset the rifted margin in a right-lateral sense). The Resolution Rifted Margin is the conjugate to the Southwest Campbell Rifted Margin and mimics its geometry on the Australia Plate with right stepping offsets at roughly 46.5° S, 164° E and 48.25° S, 159.5° E. The exception is a large left stepping offset near the southern end of the Southwest Campbell Rifted Margin at roughly 59.5° S, 163° E, which is mirrored on the Australia Plate by a right stepping offset in the Resolution Rifted Margin at 49° S, 157° E. Magnetic anomalies adjacent to the rifted margin south and southwest of these offsets are progressively older than along the rest of the boundary to the north and represent an earlier stage of extension as rifting propagated north toward the New Zealand continental block (Figure 3.3 lines S1 and S2, Figure 3.4 lines E0a and E0b). In the Balleny Corridor, anomalies as old as chron 29 have been identified adjacent to the Nella Dan Rift, the continuation of the Resolution Rifted Margin southwest of the right stepping offset at 59.5° S, 163° E [*Cande et al.*, 2000]. The magnetic isochrons adjacent to the Nella Dan Rift are related to seafloor spreading between Australia and West Antarctica, and the conjugate isochrons on the Antarctic Plate are located adjacent to the Scott Rift north of the Ross Sea, Antarctica.
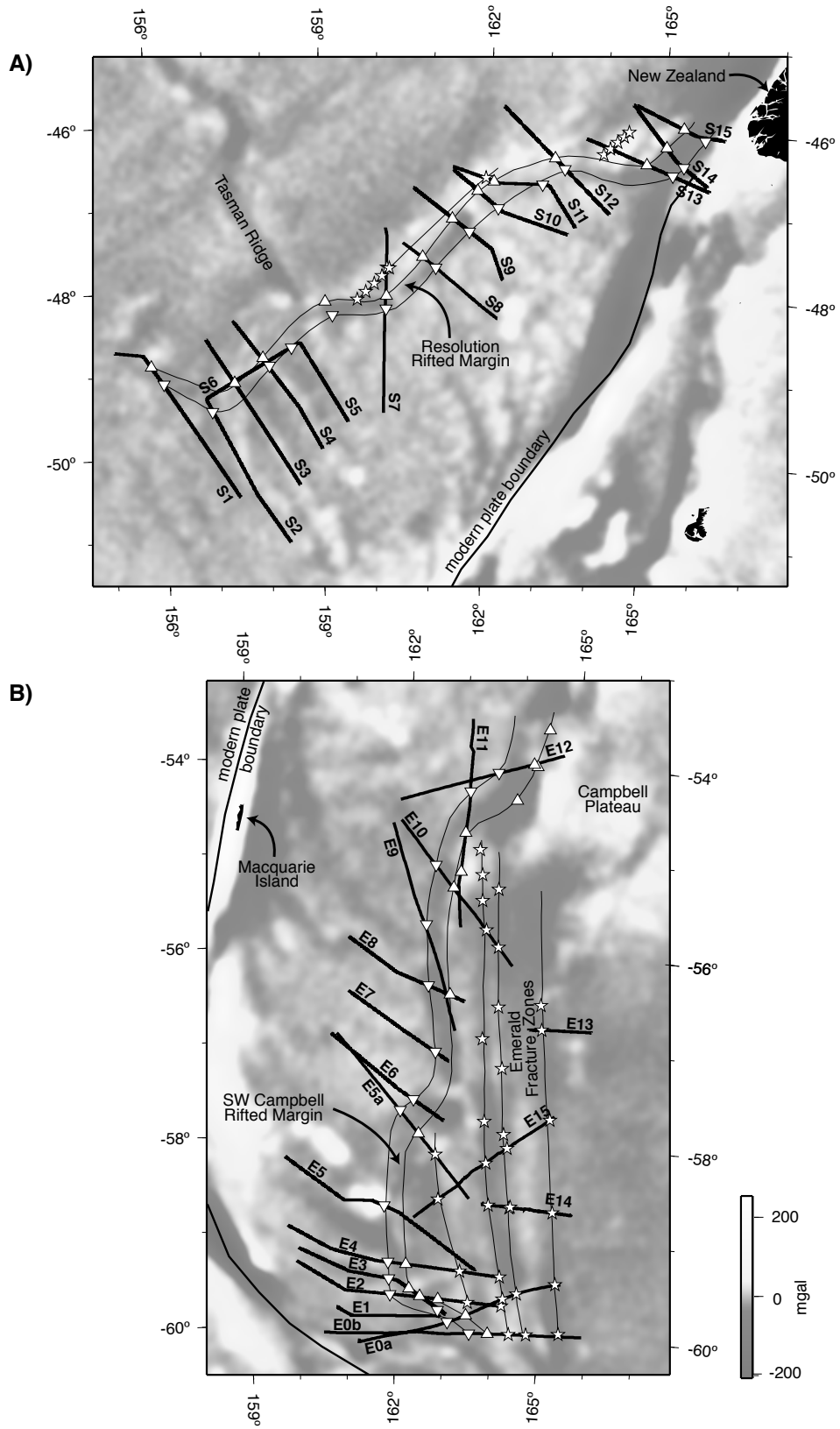
Figure 3.2: (caption on following page)

Profiles crossing the Resolution Rifted Margin (Figure 3.3) and the Southwest Campbell Rifted Margin (Figure 3.4) constrain the location of the zone of rifted oceanic crust that defines these margins. We use single beam bathymetry (black silhouettes), free air gravity anomaly profiles (solid lines), and magnetic anomaly profiles (dashed lines) to define the zone between the old and young edges of the rifted margin (RM2 and RM1 respectively). This zone is marked by a prominent gravity low and bathymetric depression on most profiles. The width of the rifted margin zone varies along strike from roughly 20-30 km and is typically bounded on both sides by normal faults (e.g. Figure 3.3 lines S6-S9 and Figure 3.4 lines E8-E11). Along line E10, the old side of the rifted margin (RM2) has a very distinct bathymetric signature (Figure 3.4). There is a large offset in the seafloor at RM2 and the dip on the older Tasman Sea crust gradually decreases to the east. The conjugate to this segment on the Australia side has a similar signature (Figure **??**, line S11). We interpret this bathymetric signature to be caused by flexural uplift of the oceanic plate on the old side of the rifted margin due to isostatic rebound after mechanical unloading of the lithosphere during the initial phase of rifting. This lithospheric flexure is typical of what is found in other known oceanic rift systems [*Weissel and Karner*, 1989] and is most pronounced on the segment of the Southwest Campbell Rifted Margin between 54.5° S and 57° S (Figure 3.4 lines E8-E11) and the conjugate section of the Resolution Rifted Margin on the Australia Plate (Figure 3.3 lines S8-S11).

Figure 3.2: Tectonic features and shiptrack line locations for profiles crossing A) the Resolution Rifted Margin, and B) the Southwest Campbell Rifted Margin (see dashed red boxes in Figure 3.1 for location of subregions A and B). Thin solid lines show the location of tectonic features, and locations of profiles (Figures 3.3 and 3.4) are shown with thick solid lines. White filled symbols indicate rifted margin and fracture zone locations picked from shipboard bathymetry, gravity, magnetics, multibeam and seismic data. Inverted triangles indicate the young edge of the rifted margin (RM1), triangles indicate the old edge of the rifted margin (RM2), and stars indicate the location of older fracture zones related to spreading along the Tasman Ridge. Location of tectonic features are interpolated between these points by following anomaly trends in the satellite derived gravity basemap [*Sandwell and Smith*, 1997].
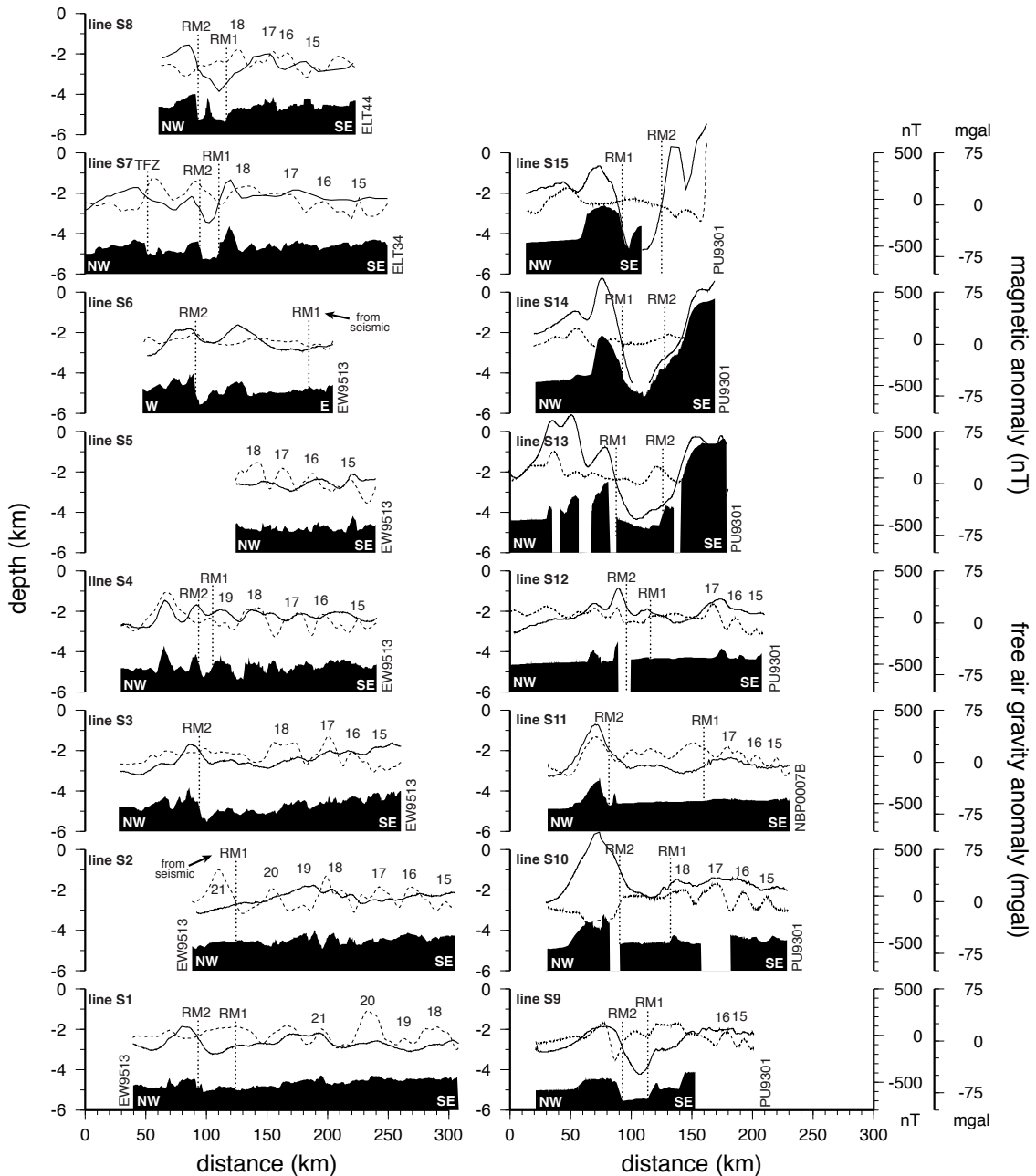
Figure 3.3: Magnetic, gravity, and depth profiles for lines crossing the Resolution Rifted Margin. Black silhouettes show single beam bathymetry, gravity data are shown with solid lines, and magnetic data are shown with dashed lines. Magnetic anomalies are labeled above each profile, and tectonic features are marked by vertical dotted lines (RM1=young edge of rifted margin, RM2=old edge of rifted margin, TFZ=Tasman Fracture Zone, EmW/EmC/EmE=West/Central/East Emerald Fracture Zones). Geophysical cruise identification codes are shown at the end of each profile. Tectonic feature and magnetic anomaly picks from cruise PU9301 follow *Wood et al.* [1996].
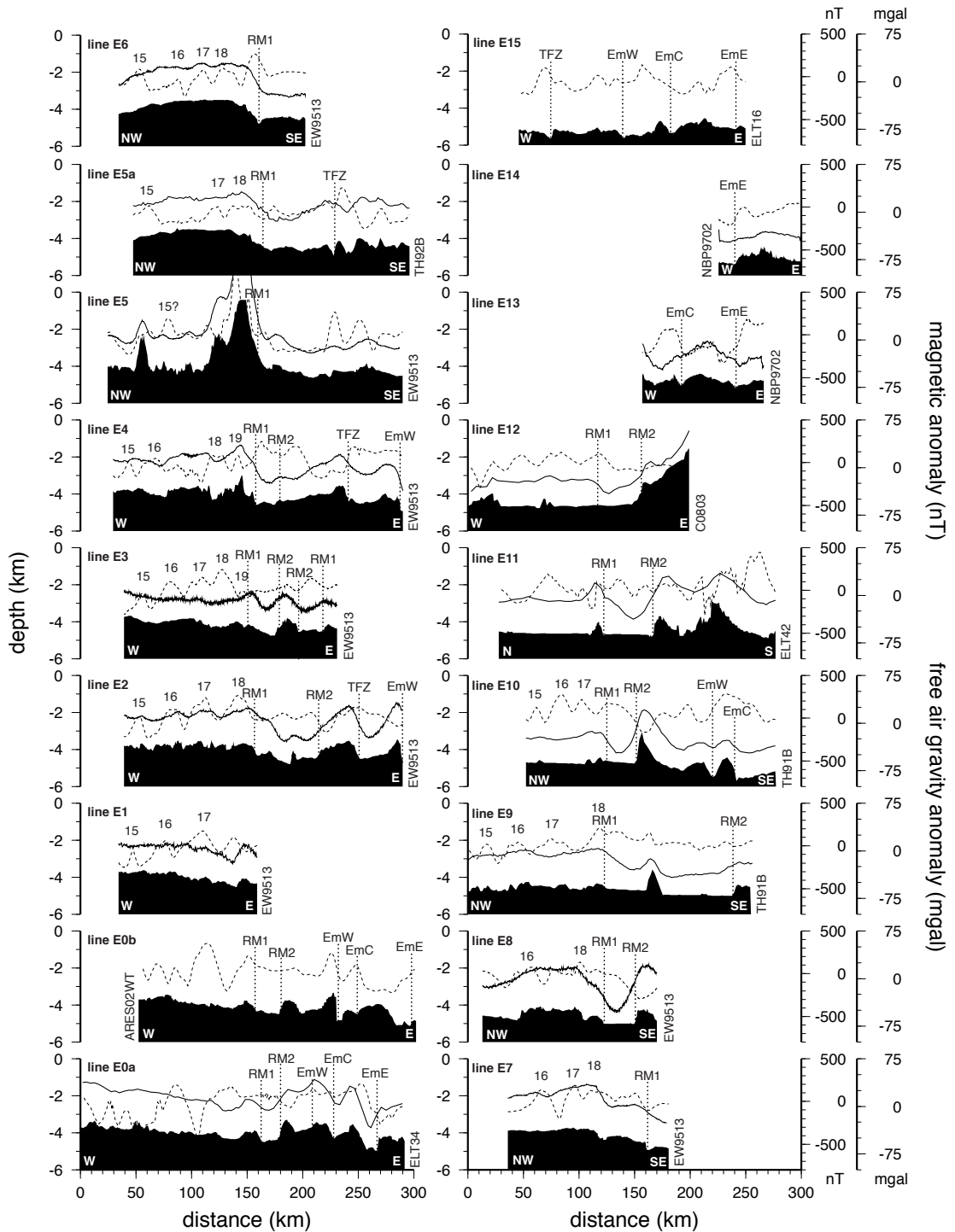
Figure 3.4: Magnetic, free-air gravity anomaly, and depth profiles for lines that cross the Southwest Campbell Rifted Margin. Plot format and annotations follow the conventions described in Figure 3.3.

The Tasman Fracture Zone (TFZ) is related to spreading along the Tasman Ridge and is typically denoted by a bathymetric step in cross section with the high side to the west, and it is also marked by an associated step in the shipboard gravity anomaly (i.e. Figure 3.3 lines S7 and Figure 3.4 lines E2, and E4). The West and Central Emerald Fracture Zones (EmW and EmC respectively) are characterized by a relatively narrow central valley and associated gravity low similar to medium-offset fracture zones in the slow spreading regimes of the Atlantic and western Indian Oceans [*Van Andel*, 1971; *Fox and Gallo*, 1986]. The East Emerald Fracture Zone (EmE) has a similar morphology, but its central valley is typically wider.

3.3 Seismic data

Single channel seismic data were collected on several crossings of the Resolution and Southwest Campbell Rifted Margins on the R/V Ewing EW9513 cruise. A four channel analog streamer was utilized in the data collection process, and the seismic source consisted of two 80 cubic inch SSI air guns. Channels 3 and 4 were stacked and then filtered using a high pass linear ramp filter from 20-30 Hz and a notch filter at 60 Hz to obtain the constant offset sections shown in Figures 3.5 and 3.6. Locations of the profiles are shown in Figure 3.2. Because of their proximity to the ship, channels 1 and 2 were extremely noisy and were not used when the traces were stacked. With these parameters, penetration of 1.0-1.5 seconds was consistently achieved, and a strong acoustic basement reflector is clearly distinguishable in most locations.

Sediment thickness is highly variable in the Emerald Basin (Figure 3.6) as a result of the interaction of the eastward flowing Antarctic Circumpolar and Deep Wester Boundary Currents with the elevated topography of the Macquarie Ridge Complex [*Carter and McCave*, 1997; *Carter and Wilkin*, 1999]. Lines E1 and E2 (Figure 3.6) cross ocean floor that has been scoured by the Western Boundary Current and is relatively free of sediment cover. Lines E6 and E7 (Figure 3.6) cross the Emerald Basin Drift [*Schuur et al.*, 1998] where there is an extremely thick layer of sediment overlaying acoustic basement. Sediment thickness on these seismic lines is typically greater

than 1.0 second thick and reaches up to 1.5 seconds two way travel time (TWTT) in some places. The Emerald Basin Drift exhibits an elongate mounded shape which is a characteristic of mounded contourite drifts [*Faugères et al.*, 1993, 1999] This shape is particularly apparent on line E6. Continuous, wavy reflections on seismic sections along these profiles form elongate depositional highs and lows that do not directly mirror the basement topography and are truncated at the seafloor in several locations. The top of the high amplitude package of reflectors seen at roughly 0-0.3 seconds sub-bottom (black dots on Figure 3.6 lines E6 and E7) marks an angular unconformity that is thought to be Pliocene in age based on stratigraphic ties to DSDP hole 278 [*Kennett et al.*, 1973; *Schuur et al.*, 1998]. This unconformity may be related to a change in depositional environment caused by evolving bottom water circulation patterns related to the opening of the 53.5° S passage in the Macquarie Ridge Complex.
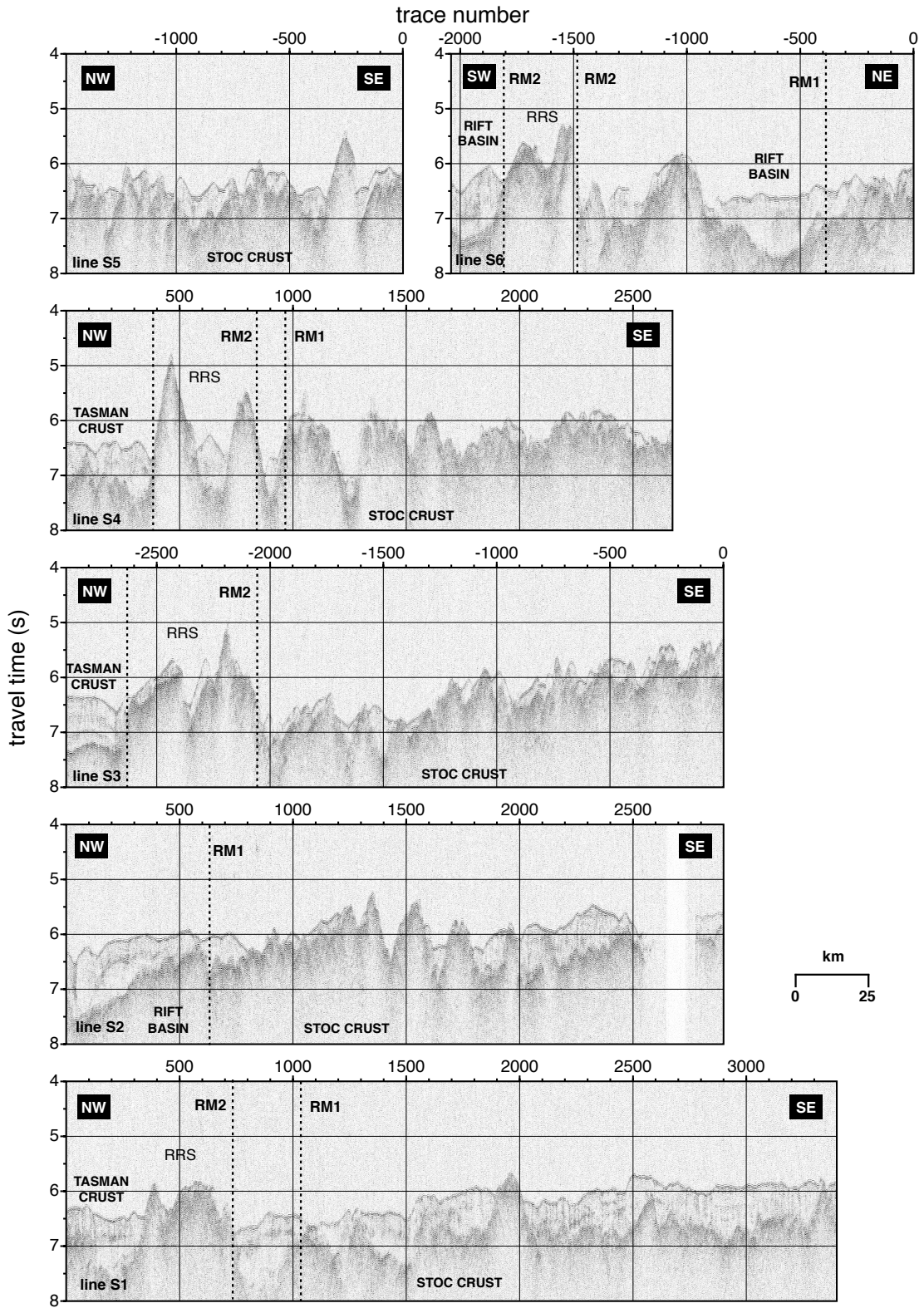
Figure 3.5: (caption on following page)

Figure 3.5: Single channel constant offset seismic sections across the southwestern Resolution Rifted Margin. All seismic data were collected aboard the R/V Ewing, cruise EW9513. STOC crust is young (less than 45 Ma) oceanic crust that was formed at the Macquarie Ridge, and Tasman crust is older (greater than 50 Ma) crust that was formed along the Tasman Ridge (RM1=young edge of rifted margin, RM2=old edge of rifted margin, RRS=Resolution Ridge System). Small dots on lines E6 and E7 denote an unconformity of probable Pliocene age within the Emerald Basin Drift.
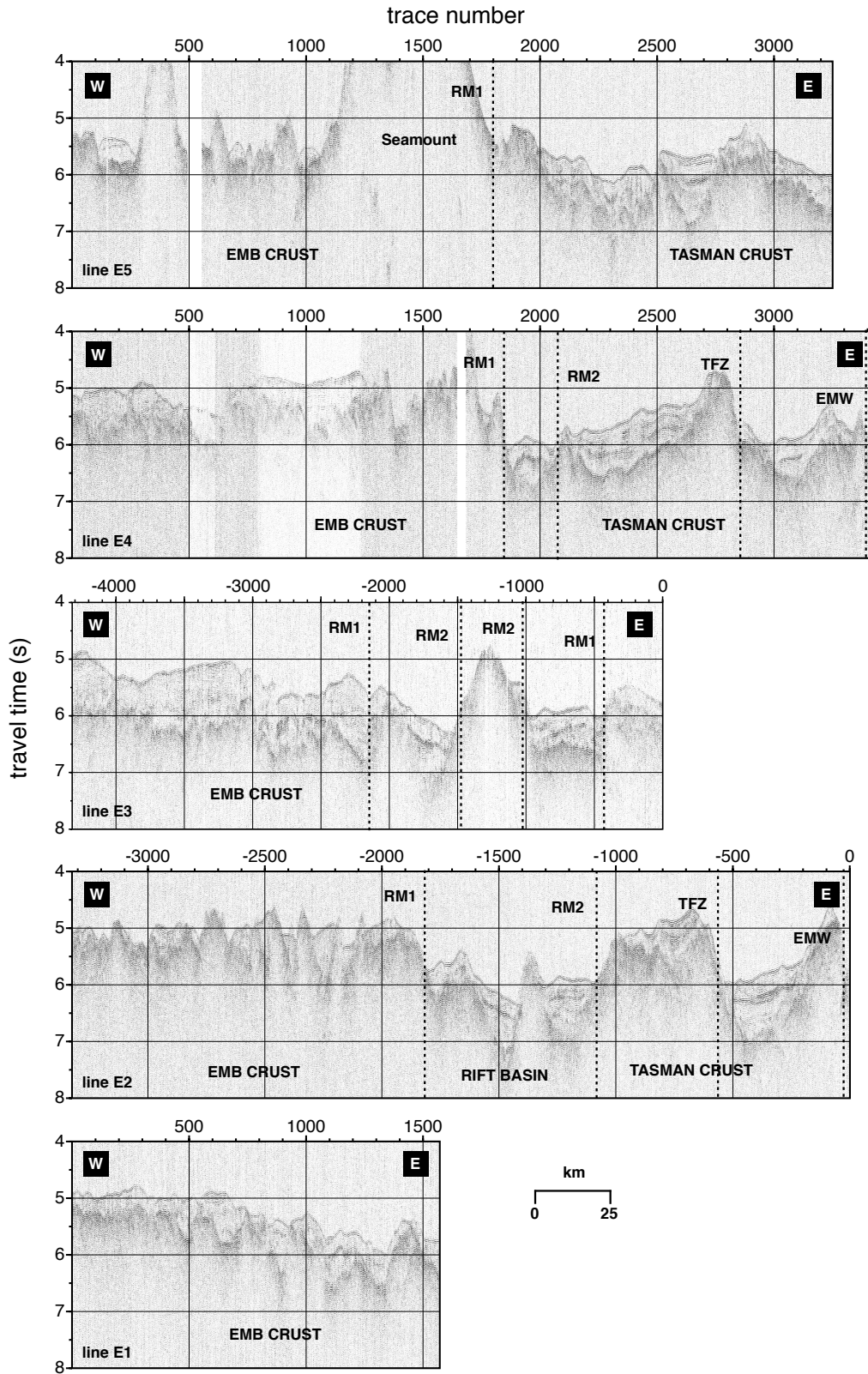
Figure 3.6: (continued on following page...)
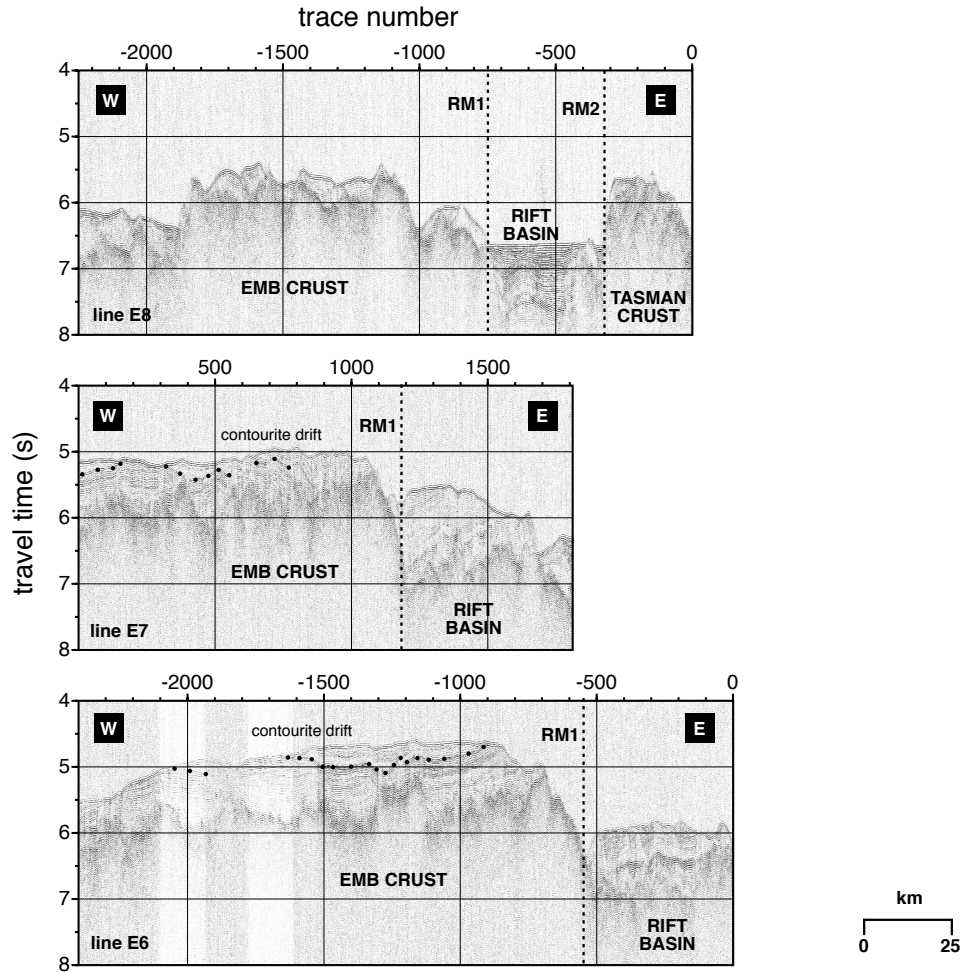
Figure 3.6: (continued from previous page...) Single channel constant offset seismic sections across the Southwest Campbell Rifted Margin. All seismic data were collected aboard the R/V Ewing, cruise EW9513. EMB crust is young (less than 45 Ma) oceanic crust that was formed at the Macquarie Ridge, and Tasman crust is older (greater than 50 Ma) crust that was formed along the Tasman Ridge. All other annotations follow Figure 3.3.

On a few seismic profiles, the rifted margin zone is characterized by a tilted half graben bounded by a large normal fault on the old side of the margin (e.g. Figure 3.5 line S2 and Figure 3.6 line E3). However, most of the rifted margin consists of a roughly symmetric graben bounded on both sides by normal faults (e.g. Figure 3.5 line S1 and Figure 3.6 lines E2, E4 and E8).

The Resolution Ridge System is a topographic high that runs along the northwest

edge of the Resolution Rifted Margin and has previously been described east of 160°
E longitude [*Wood et al.*, 1996]. The Resolution Ridge is identified on EW9513
seismic lines S1, S3, S4, and S6 (Figure 3.5) where it is associated with acoustic
basement relief of approximately 2 seconds TWTT, a value similar to that observed
farther to the northeast [*Wood et al.*, 1996]. The Resolution Ridge is also associated
with a positive gravity anomaly of roughly 40 mgal along these profiles (Figure 3.3).
Sediment thickness northwest of the Resolution Ridge on crust created at the Tasman
Ridge is up to 1.0 seconds TWTT while sediment thickness southeast of the Resolution
Ridge on younger STOC crust is typically less than 0.5 seconds TWTT (Figure 3.5
lines S3 and S4). The difference in sediment thickness on line S1 is not as pronounced
because the crustal age difference across the Resolution Rifted Margin is much less
in this location.

The younger crust of the STOC and Emerald Basins is in general elevated relative
to the older crust created along the Tasman and Pacific-Antarctic Ridges. The base-
ment reflector in the STOC and Emerald Basins generally deepens with increasing
crustal age away from the ridge crest. This reflector is also offset by numerous small
abyssal hill faults related to seafloor spreading along the Macquarie Ridge Complex.
However, the acoustic basement reflector on older Tasman and Pacific-Antarctic crust
is apparently more coherent because the azimuth of our seismic profiles is roughly par-
allel to the abyssal hill spreading fabric direction. This difference in seismic character
of the acoustic basement reflector between these two stages of rifting is an important
indicator of the location of the Resolution and Southwest Campbell Rifted Margins,
especially in areas where there is not a well defined rift basin between the young and
old edges of the rifted margins.

3.4 Multibeam bathymetry data

Multibeam bathymetry data illustrate the major tectonic features in the southern
Emerald Basin (Figure 3.7). Swath width varies from roughly 2-3 times the water
depth and is dependent on the beam width of the multibeam system that was used

during data collection. The data were collected using several different hull-mounted multibeam systems: Atlas DS Hydrosweep (EW9513), Seabeam 2100 (NBP9702), and Simrad EM120 (NBP0209). All of these multibeam systems were hull mounted. Cruise RS124 aboard the R/V Rig Seismic used the Hawaii-HMR1 multibeam system which was towed behind the ship [*Massell et al.*, 2000]. MB-System software [*Caress and Chayes*, 1996] was used to process all of the multibeam data.
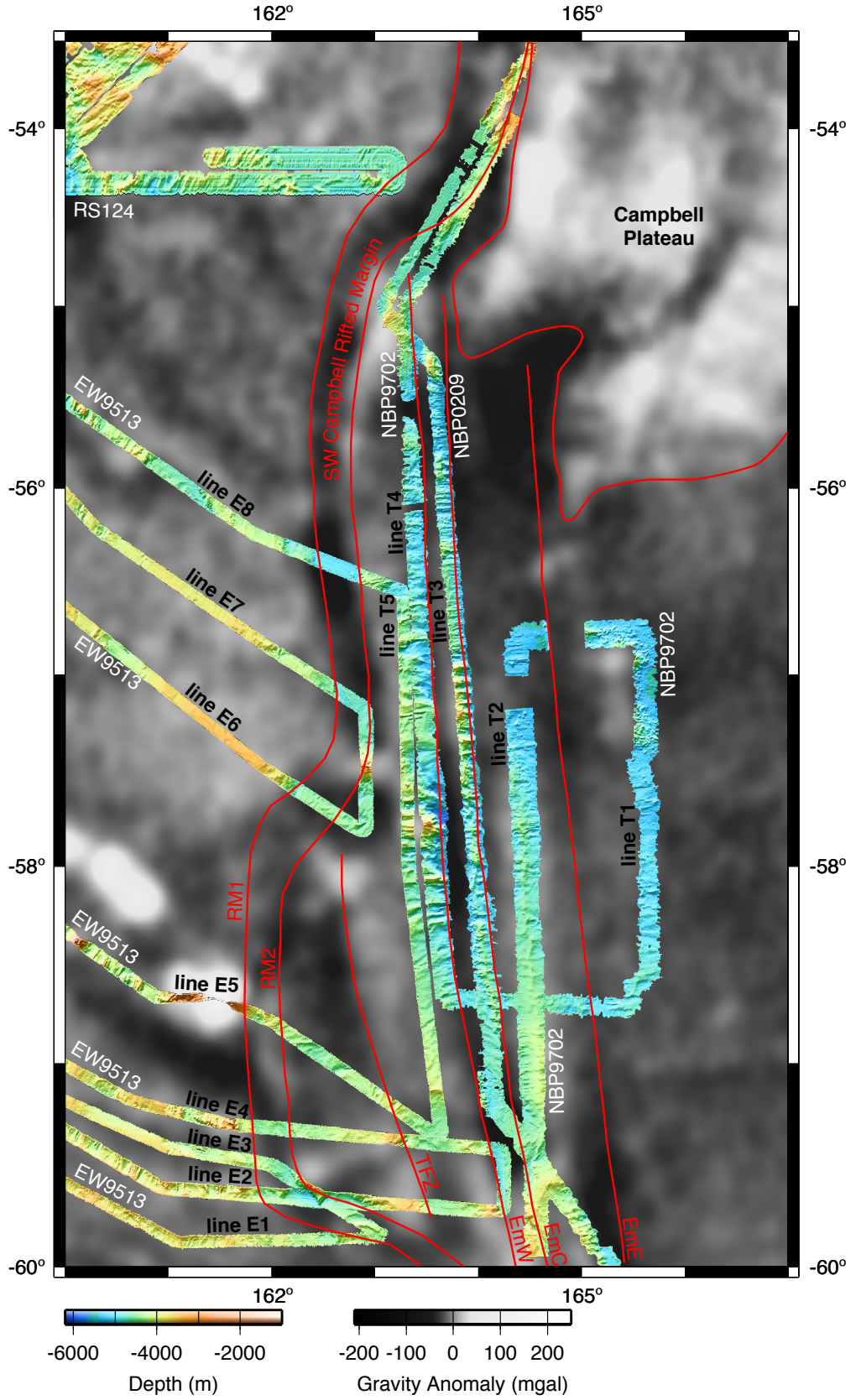
Figure 3.7: (caption on following page)

As the Antarctic Circumpolar Current flows east around the southern end and through topographic breaks in the Macquarie Ridge Complex, it is reinforced by the Deep Western Boundary Current and turns northeast to follow the southeast side of the Campbell Plateau. This interaction results in the generation of deep reaching eddies that are responsible for widespread abyssal erosion throughout the region [*Carter and McCave*, 1997; *Carter and Wilkin*, 1999]. The ocean floor along lines T1-T5 (Figure 3.7) is characterized by thin sediment cover that is confined mainly to low-lying areas between basement ridges even though magnetic anomalies show that the ocean crust along those profiles is more than 52 million years old. Abyssal hill topography is characterized by a series of bathymetric highs and lows that form parallel to mid-ocean ridges as a result of extensional faulting and changes in magma flux near the ridge crest during seafloor spreading [*Pezard et al.*, 1992; *Macdonald et al.*, 1996], and a general lack of thick sediment cover in the Southern Emerald Basin allows abyssal hill spreading fabric to be well-imaged in this region with multibeam systems.

Multibeam data in Figure 3.7 show a change in abyssal hill fabric orientation across the Southwest Campbell Rifted Margin. Abyssal hills east of the rifted margin trend E-W while abyssal hills immediately west of the rifted margin trend N-NW. This change in spreading fabric marks the boundary between older crust formed at the Tasman and Pacific-Antarctic Ridges to the east and younger crust formed along the Macquarie Ridge Complex to the west. Abyssal hill fabric along lines E6 and E7 is obscured by the thick sediment cover of the Emerald Basin Drift (Figure 3.6)

Figure 3.7: Multibeam map of the eastern Emerald Basin and the Southwest Campbell Rifted Margin. Multibeam data are plotted in color on top of a satellite derived gravity basemap which is shown in grayscale. The multibeam data are from several sources including R/V Ewing cruise EW9513 and R/VIB Nathaniel Palmer cruises NBP9702 and NBP0209. Multibeam data west of 163.5° and north of -54.5° were collected aboard the R/V Rig Seismic cruise RS124 [*Massell et al.*, 2000]. Tectonic features are indicated by solid red lines and are annotated with red labels following the conventions of Figure 3.3. Ship tracks are labeled with white geophysical cruise codes.

[*Schuur et al.*, 1998]. The rift basin between the young and old edge of the Southwest Campbell Rifted margin is visible in several locations and is characterized by the smooth, level surface of the thickened package of sediments within the rift basin (e.g. Figure 3.7 line E8). The rift basin along line E5 is not well defined, likely in part due to the large seamount just west of the rifted margin. However, the location of the old edge of the rifted margin (RM2) is well constrained along this line by E-W trending abyssal hill fabric clearly visible at roughly 162° E longitude.

Figure 3.7 reveals several N-S trending gravity lows that coincide with fracture zones revealed in the multibeam data. These fracture zones are related to spreading along the Tasman and Pacific-Antarctic Ridges prior to Middle Eocene rifting and the formation of the Southwest Campbell Rifted Margin. Lines T3 and T4 closely follow the western edge of the Central Emerald and West Emerald Fracture Zones respectively. By running tracklines parallel to the fracture zones, we are able to measure a continuous set of magnetic anomalies along these profiles while at the same time imaging at least one edge of the fracture zone. At the northern end of line T3 between 55° S and 55.5° S, the NBP0209 track crosses the West Emerald Fracture Zone and reveals a relatively narrow central valley associated with a symmetric gravity low visible in the satellite gravity. The western edge of the West Emerald Fracture Zone is clearly visible on the N-S trending EW9513 track between lines E2 and E4 at roughly 164.3° E longitude. The Tasman and East Emerald Fracture Zones are not as readily identifiable from the multibeam data; however, the signature of these fracture zones is seen in both satellite and shipboard gravity measurements.

The southwest end of the Resolution Rifted Margin is also easily visible in the multibeam data in Figure 3.8. It is most immediately evident on the RS124 track on the NE side of the figure where it is marked by a very distinct rift basin depression. Along lines S3 and S4, a series of tilted and faulted blocks comprising the Resolution Ridge System are visible northwest of and parallel to the rifted margin. Abyssal hill fabric northwest of the Resolution Ridge System along these lines is masked by thick sediment cover; however, abyssal hill fabric south of the rifted margin trends NE and is clearly visible on all tracklines. NW-trending abyssal hill fabric related to spreading

along the Tasman Ridge is seen along the RS124 track NW of the rifted margin.

Multibeam data reveal fracture zones related to Tasman Sea spreading in two areas close to the Resolution Rifted Margin: the Central Emerald Fracture Zone (Figure 3.9A) and the Tasman Fracture Zone (Figure 3.9B). These multibeam data were collected aboard the R/V L'Atalante using a hull mounted Simrad EM12 multibeam system. The Resolution Ridge, the wide prominent ridge whose western edge is marked by a dashed line in Figure 3.9A, is inferred to be composed of continental crust that was rifted apart from the southern end of the Campbell Plateau during the early stages of Eocene rifting along the Macquarie Ridge Complex [*Wood et al.*, 1996]. There are two elongate NE trending ridges that emerge from the thick sediment to the west of the Resolution Ridge (Figure 3.9A). The western ridge has a very sharp step or valley running along its crest, and several low amplitude NW trending undulations in the seafloor are visible near the crest of both ridges. The projected northward continuation of this sharp step is crossed by Ewing line P3 on the southern Caswell High [*Wood et al.*, 2000] where a distinct fault that does not appear to have been active during post Eocene time is imaged in seismic section. We interpret the sharp step at the crest of the western ridge to be a fracture zone and the undulations to be abyssal hill fabric related to spreading along the Tasman Ridge prior to Eocene rifting. This interpretation is consistent with nearby magnetic anomaly trends identified by *Wood et al.* [2000] (Figure 3.12 lines T6-T8). We identify this fracture zone as the Central Emerald Fracture Zone based on its distance from the Tasman Fracture Zone and its consistency with the spacing between conjugate fracture zones east of the Southwest Campbell Rifted Margin (Figure 3.7).
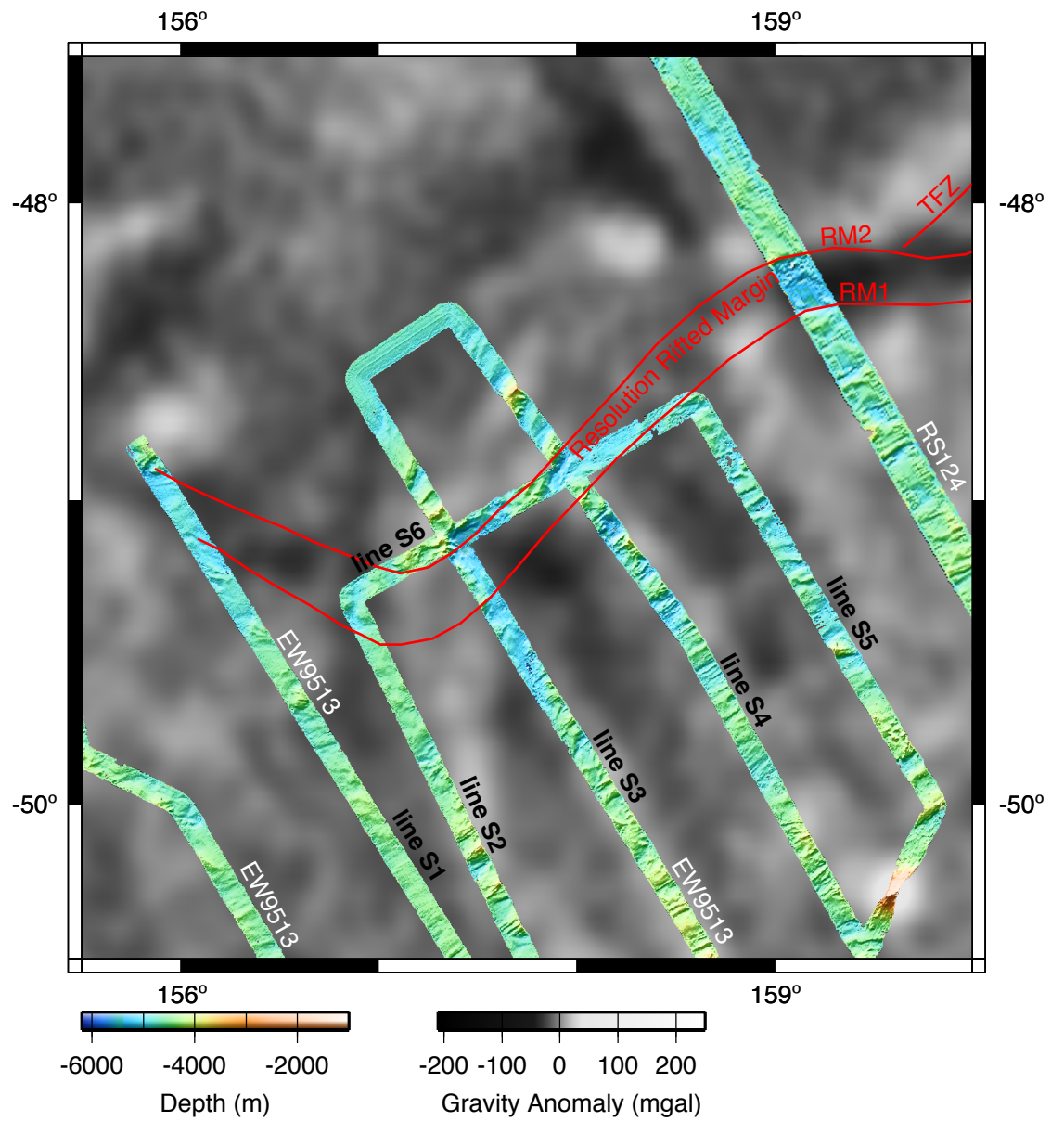
Figure 3.8: Multibeam map of the southwest region of the South Tasman Ocean Crust and the Resolution Rifted Margin. The format of the figure follows the conventions of Figure 3.7. All multibeam data shown here were collected aboard the R/V Ewing cruise EW9513 except for the easternmost line which was collected aboard the R/V Rig Seismic cruise RS124 [*Massell et al.*, 2000].

A) satellite bathymetry

multibeam data coverage

Resolution Ridge

B) satellite bathymetry

multibeam data coverage

?
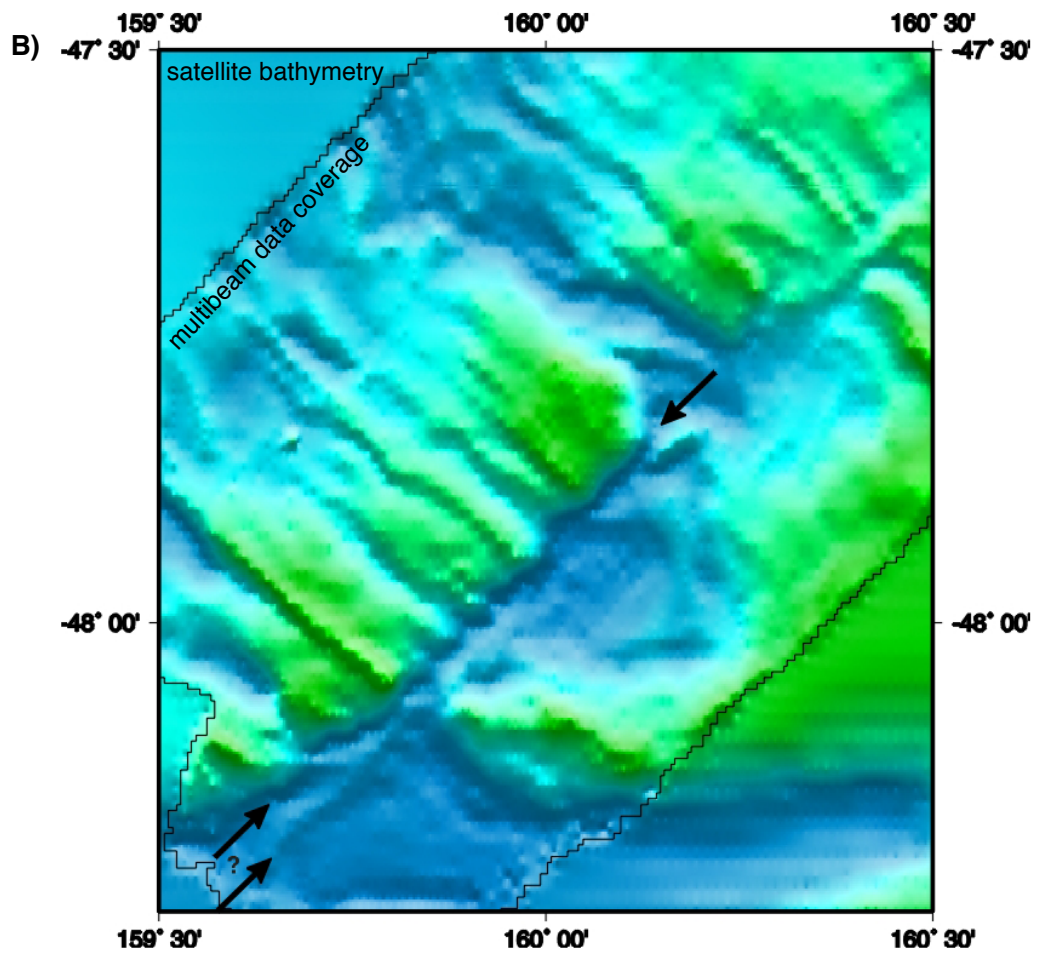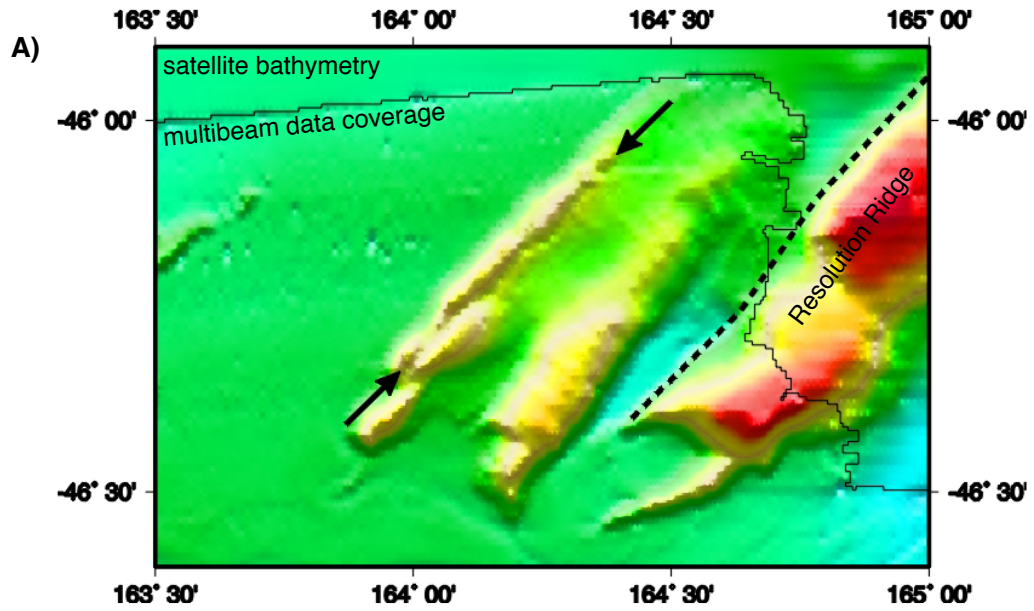
Figure 3.9: (caption on following page)

NW-trending abyssal hill fabric is also visible near the Resolution Rifted Margin at roughly 48° S, 160° E (Figure 3.9B). Again, this abyssal hill fabric is related to spreading along the Tasman Ridge prior to Eocene rifting along the Macquarie Ridge Complex. A prominent NE-trending step in the bathymetry (arrows in Figure 3.9B) is very clearly the offset conjugate of the Tasman Fracture Zone described in Figure 3.7. The step is high on the northwest side and low on the southeast side, consistent with other crossings of this fracture zone (Figure 3.4). At its intersection with the Resolution Rifted Margin, the southern termination of the Tasman Fracture Zone bifurcates and may have been affected by Eocene rifting. However, this and other fracture zones on both sides of the rift do not appear to have been significantly affected by crustal deformation during rifting.

3.5 Magnetic anomalies on pre-Eocene Tasman Sea crust

Ship tracks in the region show the location of magnetic anomalies associated with spreading along the Tasman Ridge from chron 34 to chron 24 (83-52 Ma) (Figure 3.10). Magnetic isochron trends are constrained by multiple magnetic anomaly picks where possible; however, abyssal hill fabric orientation identified on the multibeam data is used to extrapolate isochron orientations away from the ship track when necessary. As a result, magnetic isochron orientations are more reliable in fracture zone corridors with multiple ship tracks (i.e. Figure 3.10B Line T1) as compared to corridors with only one ship track (i.e. Figure 3.10A Line T9). Chron 24o is the youngest magnetic

Figure 3.9: Multibeam maps show the location of A) the Central Emerald Fracture Zone, and B) the Tasman Fracture Zone close to the Resolution Rifted Margin. Fracture zones are marked by arrows. The edge of multibeam coverage is indicated by thin black lines, and bathymetry outside of that is derived from satellite altimetry and ship depth soundings [*Smith and Sandwell*, 1997]. The western edge of the continental crust of the Resolution Ridge [*Wood et al.*, 1996] is marked by a dashed line.

anomaly identified along Line T9, marking the cessation of spreading along the Tasman Ridge [*Gaina et al.*, 1998]. We identify a similar magnetic anomaly sequence located east of the SW Campbell Rifted Margin between the Tasman Fracture zone and the West Emerald Fracture Zone (Figure 3.10B Lines T4 and T5). The magnetic anomaly sequence within this spreading corridor is also centered about chron 24o, which suggests that crust to the west of the West Emerald Fracture Zone was formed by spreading at the southern end of the Tasman Ridge. Subsequent rifting along the Resolution and SW Campbell Rifted Margins transferred this conjugate sliver of Tasman Sea crust to the Pacific Plate during Eocene rifting.

Magnetic isochron patterns northwest of the Resolution Rifted Margin (Figure 3.11) reveal the approximate location of the northeast extension of the Tasman Fracture Zone as well as another left stepping fracture zone to the northwest. Our observations indicate the Tasman Fracture zone is a left-stepping fracture zone in contrast to the large right-stepping Emerald Fracture Zones east of the Southwest Campbell Rifted Margin. Between the Tasman and West Emerald Fracture Zones, chrons 24o-29 are identified on the Pacific Plate (Figure 3.10B Lines T4 and T5), and chron 31-33y are identified on the Australia Plate (Figure 3.10A Lines T6-T8 and Figure 3.11). When the Resolution and SW Campbell Rifted Margins are reconstructed to their pre-rift configurations, the restoration of this continuous magnetic anomaly sequence from 24o-33y provides an important independent constraint on the accuracy of the reconstruction.
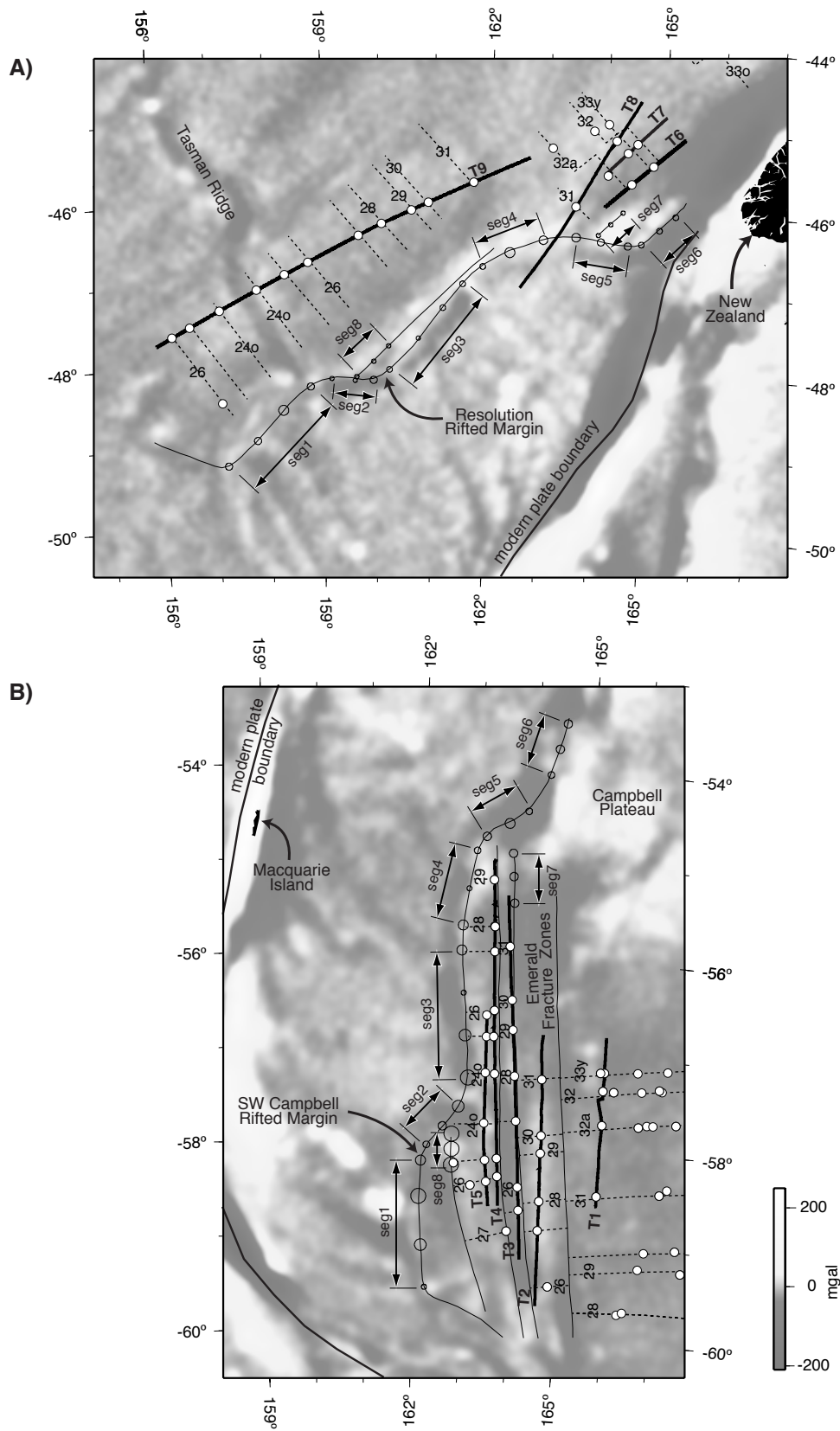
Figure 3.10: (caption on following page)

Despite the complicated tectonic setting and numerous closely spaced fracture zones throughout the area, interpretation of magnetic anomalies along Lines T1-T9 (Figure 3.12) was fairly straightforward. This is true because efforts were taken to follow fracture zone trends and stay within a single spreading corridor when most recent magnetic lines were acquired. Magnetic interpretations along profiles T6-T8 follow *Wood et al.* [2000]. A synthetic magnetic anomaly profile is shown in the middle graph of Figure 3.12, and all other profiles are projected onto an azimuth parallel to fracture zone orientations and then shifted horizontally to line up with this profile. The magnetic model used to calculate the synthetic magnetic anomaly assumes a flat 500 meter thick magnetized layer at a depth of 5000 meters. Other model parameters include: magnetization = 5 A/m, present inclination = -78°, present declination = 30°, and profile azimuth = 0°. In addition, the model assumes that the phase shift due to the remnant inclination and declination of the magnetic field is negligible. The magnetic time scale of *Cande and Kent* [1995] is used for all calculations and is shown by the block model directly below the calculated synthetic magnetic profile in Figure 3.12. The half-spreading rates used in the calculation decrease with time from 30 mm/yr to 18 mm/yr. These rates are slightly greater than those modeled by *Gaina et al.* [1998], a discrepancy most likely caused because the profiles used for our model were farther from the rotation pole at the time of formation. Additional uncertainty in our result arises from the fact that we are modeling numerous segmented profiles

Figure 3.10: Magnetic anomaly picks, magnetic isochron locations, and shiptrack line locations for profiles located on crust formed along the Tasman Ridge prior to rifting along the Macquarie Spreading Center (see dashed red boxes in Figure 3.1 for location of subregions A and B). Filled white circles indicate magnetic anomaly picks, magnetic isochrons are shown with dashed lines, and locations of profiles (Figure 3.12) are shown with thick solid lines. The old edge of the Resolution and Southwest Campbell Rifted Margins (RM2) and older fracture zones are shown with thin solid lines. For the best fit pre-rift Australia-Pacific reconstruction, RM2 was approximated by 6 great circle segments, indicated by arrows and associated annotations. Close to RM2, the Central Emerald Fracture Zone and Tasman Fracture Zone are approximated by segments 7 and 8 respectively. Open circles represent the 95% confidence regions of picks used in the best-fit reconstruction.
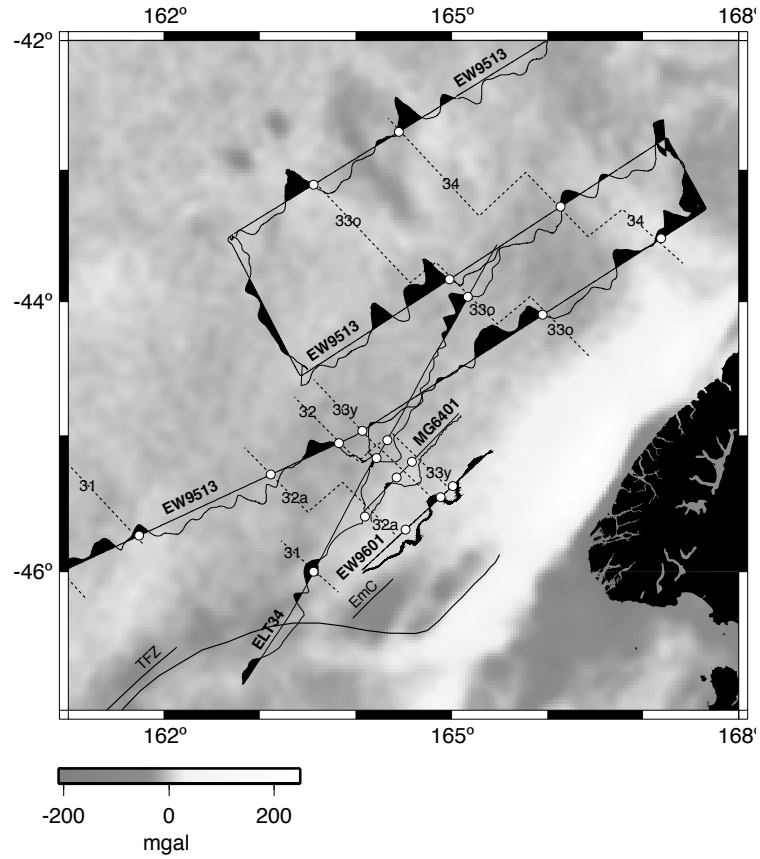
Figure 3.11: Magnetic anomaly plotted perpendicular to shiptracks for lines located on crust created at the Tasman Ridge. Positive excursions in the magnetic anomaly are filled with black. Magnetic isochron lines are dashed, and white circles indicate magnetic anomaly picks.

that have been transported and potentially disrupted during subsequent periods of tectonic activity.
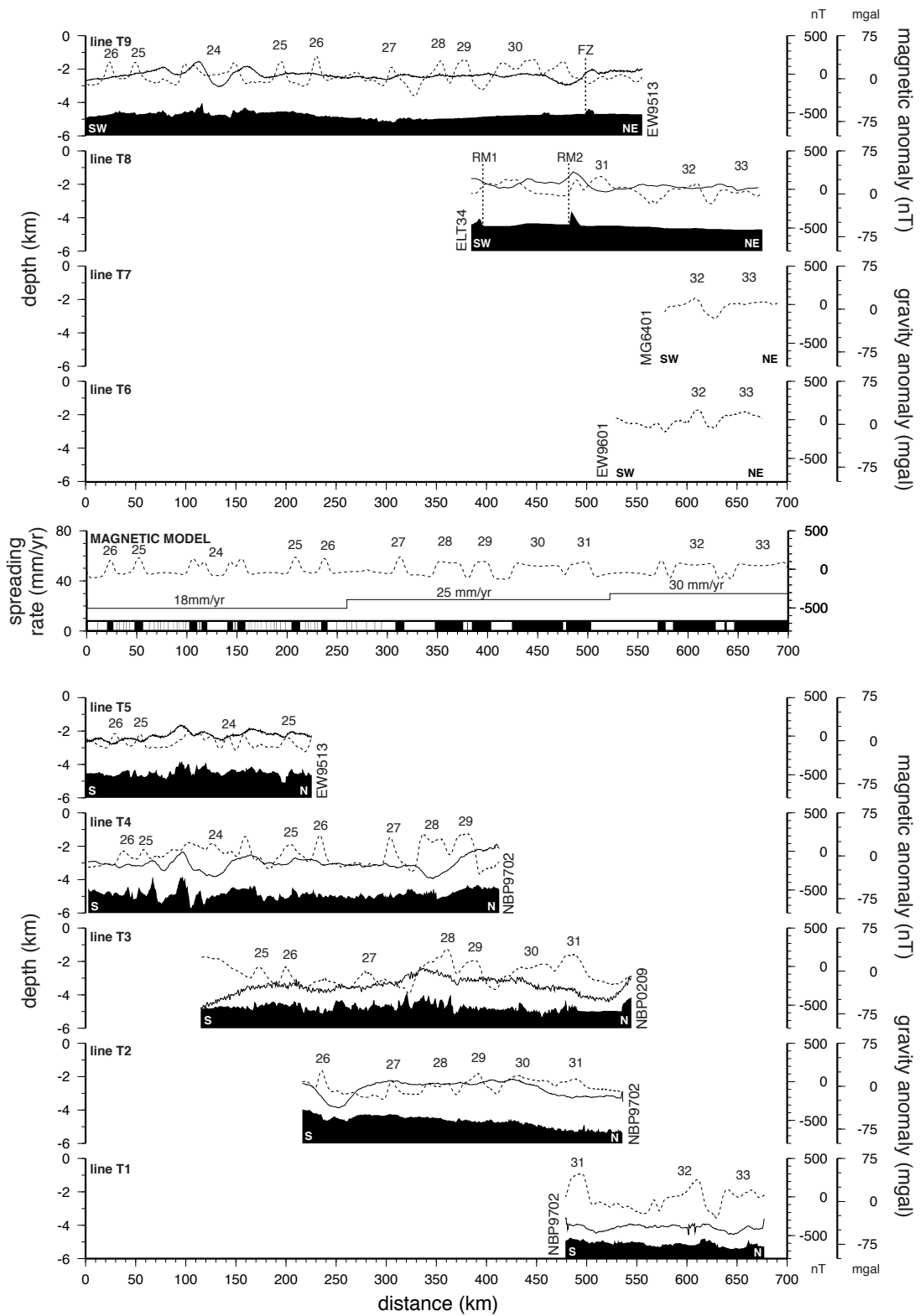
Figure 3.12: (caption on following page)

3.6 Middle Eocene pre-rift finite rotation

New shipboard datasets in the southeast Tasman Sea have allowed us to constrain the location of the Resolution and Southwest Campbell Rifted Margins more accurately than was previously possible, and we have also been able to better constrain the location of fracture zones related to spreading along the Tasman and Pacific-Antarctic Ridges on older crust adjacent to these rifted margins. The locations of these tectonic features have been used to calculate a new Australia-Pacific finite rotation that reconstructs features on the Australia Plate back to their locations prior to their translation by Eocene rifting and subsequent right-lateral strike-slip motion along the Macquarie Ridge Complex. This finite rotation has been calculated using an inversion based on the fitting algorithm of *Hellinger* [1981] and the statistical methods of *Chang* [1987] and *Royer and Chang* [1991].

The best-fit finite rotation is determined by minimizing the sum of the misfits of conjugate sets of points along great circle segments. In order to perform the inversion, we have divided the smooth, curvilinear Resolution and Southwest Campbell Rifted margins into six great circle segments (see arrows and associated annotations in Figure 3.10). We have treated the Central Emerald and Tasman Fracture Zones as great circle segments 7 and 8 respectively, and we only used segments of these fracture zones closest to the rifted margin in order to minimize the effect of changes in fracture zone orientation far away from the boundary. We picked roughly equally spaced points along each of the great circle segments used in the inversion and assigned them 95% confidence regions (Figure 3.10). The uncertainties assigned to these points range from 3-5 km depending on the type of data used to constrain their location. Points

Figure 3.12: Magnetic, gravity, and depth profiles for crust created at the Tasman Ridge. Plot format and annotations follow the conventions described in Figure 3.3. The *Cande and Kent* [1995] magnetic reversal time scale was used for the magnetic model shown in the middle figure. Spreading rates are shown above the reversal pattern. Profiles are projected onto azimuths parallel to fracture zone orientations and then horizontally shifted to line up with the calculated magnetic anomaly profile from this model. Magnetic anomaly picks on profiles T6-T8 follow *Wood et al.* [2000].

that are tightly constrained by nearby shipboard observations with accurate navigation are assigned uncertainties of 3 km, and points that are constrained almost entirely by satellite derived gravity data are assigned uncertainties of 9 km. Points along the old edge of the Resolution and Southwest Campbell Rifted Margins (RM2) were used in the inversion in order to best approximate the plate configuration prior to the onset of Eocene rifting. By choosing RM2 for the reconstruction, we are making the assumption that there was no pre-existing crust between the old edges of the rifted margins before the onset of rifting. However, there must have been some undetermined amount of extension of pre-existing crust in order to explain the observed structure of the rifted margins (i.e. normal faulting and formation of a central graben between RM1 and RM2; flexural signature due to mechanical unloading of the lithosphere). If a significant amount of pre-existing extended Tasman Sea crust exists beneath the rift basin between the old and young edges of the rifted margin, then the resultant angle of the finite rotation may be slightly overestimated. However, we note that the amount of pre-existing crust must be relatively small because the pre-rift Tasman and Central Emerald Fracture Zones line up nicely across the rifted margin when only the rifted margin segments (Figure 3.10 segments 1-6) are included in the reconstruction calculation.

The inversion yielded a best-fit pole and rotation (Table 3.1) and a covariance matrix that constrains its associated 95% confidence limit. The value of the quality factor, $\hat{\kappa}$, is a measure of whether the uncertainties assigned to the points used in the reconstruction are statistically correct ($\hat{\kappa} = 1$), overestimated ($\hat{\kappa} > 1$), or underestimated ($\hat{\kappa} < 1$). The value of $\hat{\kappa}$ for this finite rotation is 2.01, which suggests that these uncertainties are slightly overestimated.

The best-fit pre-rift Australia-Pacific rotation pole is located on the east side of the Campbell Plateau (Figure 3.13). It has an elongate 95% confidence ellipse because the reconstruction is more strongly constrained in an E-W sense than in a N-S sense in a Pacific Plate reference frame. This is due to the fact that the best N-S constraint on the rotation comes from the two short E-W offsets in the rifted margin (Figure 3.10 segments 2 and 5), while the fracture zone segments along with

Table 3.1: Finite rotation and covariance matrix for the best fit pre-rift AUS-PAC reconstruction. The Pacific Plate is held fixed.

Finite rotation pole and angle		
Lat	Lon	Angle
+°N	+°E	deg
-49.666	177.946	47.857

Covariance matrix							
$\hat{\kappa}$	a	b	c	d	e	f	g
2.01	0.219	-7.15	0.254	2.51	-8.09	0.301	6

The covariance matrix is given by the formula:

$$\frac{1}{\hat{\kappa}} * \begin{pmatrix} a & b & c \\ b & d & e \\ c & e & f \end{pmatrix} \times 10^{-g}$$

where a-f are given in radians squared

the long N-S segments of the rifted margin place a stronger constraint on the E-W component of the rotation. New Zealand is reconstructed back to its configuration prior to rifting and subsequent right-lateral strike slip motion along the Macquarie Ridge Complex in Figure 3.13. No attempt has been made to account for distributed continental deformation within New Zealand and its associated continental shelf.

The best-fit pre-rift reconstruction described in Table 3.1 closes the STOC and Emerald Basins, thereby matching the old edge of the Resolution and Southwest Campbell Rifted Margins with a high level of accuracy (Figure 3.14). To illustrate the uncertainty associated with this rotation, we rotated several points along the Resolution Rifted Margin to their pre-rift locations and plotted their confidence ellipses (Figure 3.14). Excluding a small part of the northernmost segment (segment 6) of the rifted margin, the rifted margins fit within the confidence limits placed on defining their present day locations (Figure 3.10). The Tasman and Central Emerald Fracture Zones also line up nicely on either side of the rifted margin, and the magnetic isochrons west of the rifted margin are rotated to a parallel orientation with those east of the rifted margin. The N-S trending gravity low that rotates into a position north of the rifted margin near 54.3° S, 162.2° E in the Pacific reference frame (Figure 3.14) likely marks the Australia Plate equivalent of the West Emerald Fracture
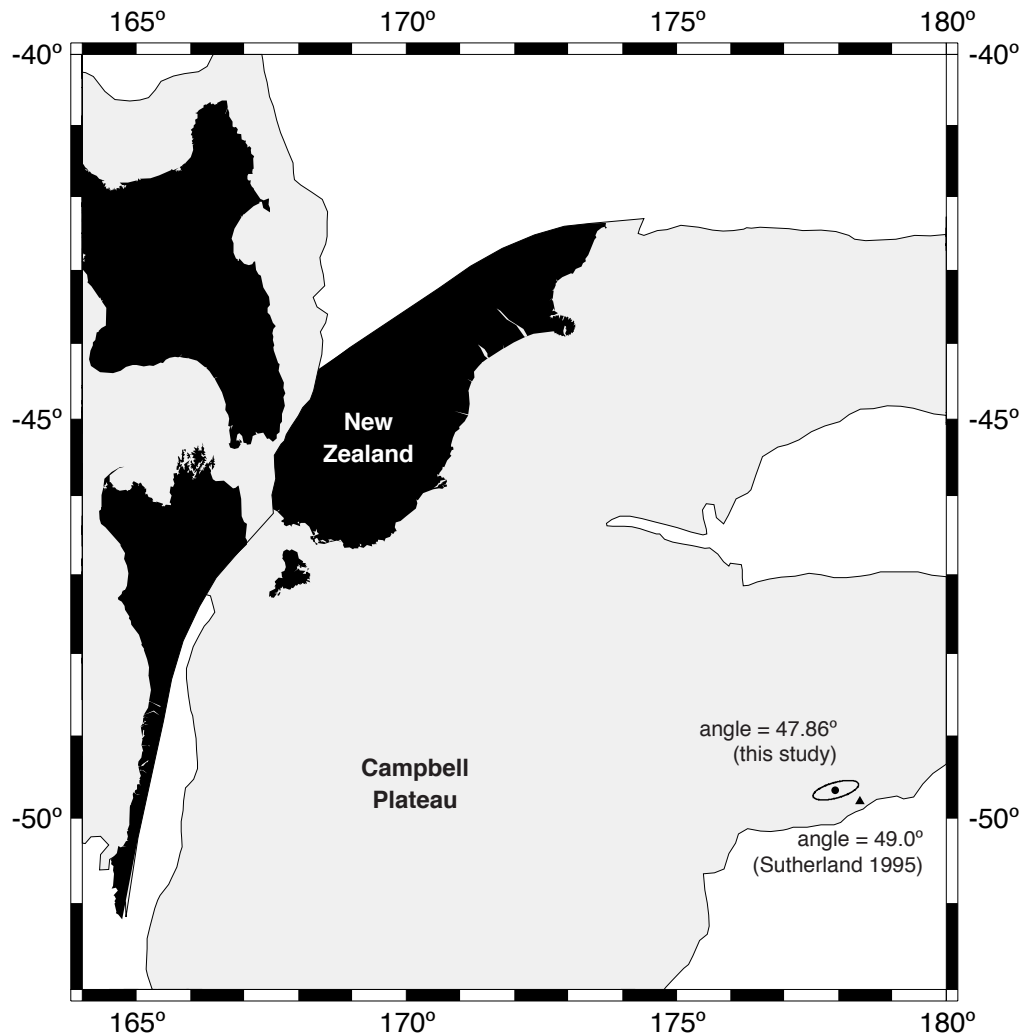
Figure 3.13: The best-fit pre-rift finite rotation pole is indicated by the small black circle with the 95% confidence ellipse. The best fit pole of *Sutherland* [1995] is shown with the small black triangle. New Zealand is shown in black, and its associated continental shelf is represented by the 2000 m contour and shown in gray. New Zealand is divided along the present day location of the Alpine Fault. The Australia plate portion of the continental shelf, west of the Alpine Fault, has been rotated back to its pre-rift configuration using the best-fit finite rotation from this study. No attempt has been made to account for distributed continental deformation.

Zone. However, the West Emerald Fracture zone was not included when calculating the pre-rift reconstruction because of a lack of shipboard controls on its location on the Australia side of the plate boundary.

To check the accuracy of the best-fit reconstruction in the N-S direction, we calculated the distance between chron 29 and chron 31 across the rifted margin in the spreading corridor between the Tasman and West Emerald Fracture Zones (97.5±6 km). The uncertainty in this number is largely controlled by 1) the uncertainty due to the best-fit finite rotation, and 2) the uncertainty associated with locating the chron 31 pick used in the calculation. Chron 31 was picked on the ELT34 ship track, a legacy Eltanin cruise that lacks accurate satellite navigation. We compared our calculated distance across the rifted margin to the distance between chron 29 and chron 31 in spreading corridors that do not cross the rifted margin (98.6 km in the corridor between EmW and EmC, 87.5 km in the corridor between EmC and EmE, and 88.1 km in the corridor east of EmE). From these numbers, the distance between chrons 29 and 31 seen in spreading corridors that do not cross the rifted margin is approximately 93±5 km. The agreement between this distance and the distance calculated across the rifted margin (97.5±6 km) indicates that, within the limits of uncertainty, the reconstruction has accurately rotated these magnetic isochrons back to their correct pre-rift locations in a N-S sense.

3.7 Implications for reconstruction of New Zealand basement terranes

We use the best-fit pre-rift finite rotation to reconstruct the pre-rift geometry of the Maitai Terrane (dotted white lines, Figure 3.14), a Permian age basement terrane in New Zealand that consists of the Dun Mountain ophiolite assemblage [*Coombs et al.*, 1976]. The Maitai Terrane is associated with the Junction Magnetic Anomaly [*Hunt*, 1978] which can be mapped accurately throughout New Zealand, and its geometry provides a useful marker when estimating the timing and magnitude of Cenozoic
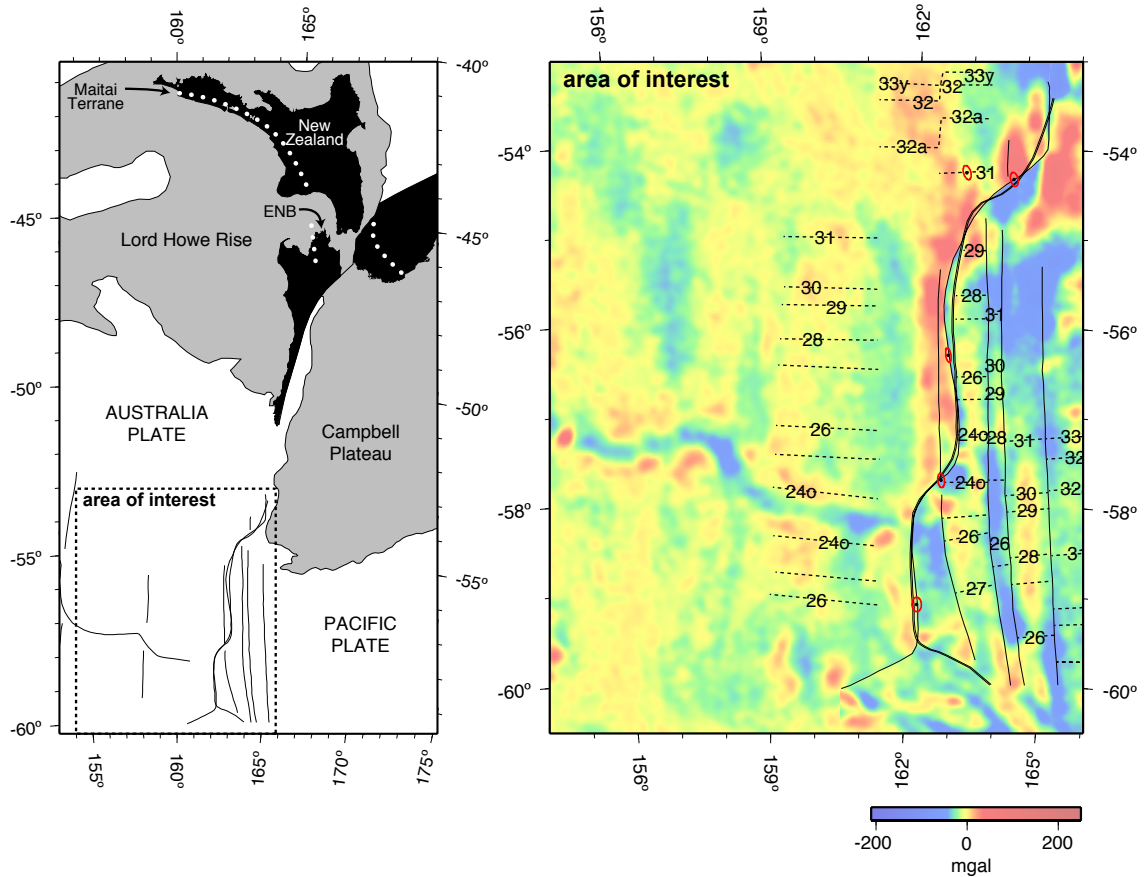
Figure 3.14: Best-fit pre-rift Australia-Pacific reconstruction for the Emerald Basin and South Tasman Ocean Crust. The Pacific Plate is held fixed, and the gravity field and tectonic features of the Australia Plate have been rotated using the best-fit pre-rift finite rotation (Table 3.1). This figure represents the plate configuration at roughly 45 Ma, prior to the initiation of seafloor spreading along the Macquarie Ridge Complex. Selected points along the Resolution Rifted Margin have been rotated to their pre-rift locations using our best-fit finite rotation, and their associated 95% confidence regions are shown in red. The Permian Dun Mountain - Maitai Terrane is shown by the white dotted line through New Zealand. ENB=East Nelson Block.

movement along the Alpine Fault. We reconstruct New Zealand and the Maitai Terrane by dividing the continental shelf along the present location of the Alpine Fault and then treating the two plates as perfectly rigid since the initiation of Eocene rifting. Taking this rigid plate assumption at face value, the Maitai Terrane is left with an apparent pre-existing sinistral offset of over 300 km when reconstructed back to its pre-rift orientation. However, excluding the zone of curvature within 100-200 km of the Alpine Fault, the Maitai Terrane matches across the boundary in a broad continuous arc oriented roughly NW-SE. Much of the apparent misfit within 100-200 km of the plate boundary can be explained by distributed dextral shear adjacent to the Alpine Fault during the last 30 Ma [*Sutherland*, 1999]. *King* [2000] uses paleomagnetic and geologic evidence to suggest that the East Nelson Block (northern end of the South Island, Figure 3.14) has acted as a mini-plate that moved independently from the rest of the Australia Plate. In either case, it is likely that post Eocene plate boundary deformation has been distributed over a wide zone rather than being confined entirely to the Alpine Fault. Taking this into account, our reconstruction favors the interpretation that the Maitai Terrane formed a continuous arc across New Zealand prior to Eocene rifting.

3.8   Summary and conclusions

A new shipboard dataset from various cruises in the Southeast Tasman Sea allows the location and structure of the Resolution and Southwest Campbell Rifted Margins to be determined with greater accuracy than was previously possible. The Southwest Campbell Rifted Margin is shown to comprise three relatively long N-S trending segments that are separated by two right stepping offsets, one at roughly 54° S and the other at approximately 57.5° S. The conjugate segments of the Resolution Rifted Margin mimic this geometry on the Australia Plate. These conjugate rifted margins were formed at 45±5 Ma during the initial stages of rifting between the Australia and Pacific Plates along a boundary that later evolved into the Macquarie Ridge Complex. This age is constrained by magnetic anomaly identifications adjacent to

the rifted margin as well as anomalies close to the crest of the extinct Tasman Ridge spreading center. Rifting propagated N-NW towards the New Zealand continental block, likely exploiting pre-existing zones of weakness parallel to fracture zones related to spreading along the Tasman Ridge.

Along with other shipboard geophysical measurements, seismic data reveal a 20-30 km wide zone of extended oceanic crust between the young and old edges of the Resolution and Southwest Campbell Rifted Margins. This zone comprises a rifted basin which is typically bounded by normal faults on both sides but is shown to be a tilted fault block bounded by a single normal fault in some locations. Sediment thickness in this region is highly variable due to the interaction of the eastward flowing Antarctic Circumpolar Current and Great Western Boundary Current with elevated topography along the Macquarie Ridge Complex. This interaction has resulted in the deposition of thick mounded contourite sequences in localized areas and has resulted in vigorous scouring and abyssal erosion throughout large regions of the Emerald Basin and South Tasman Ocean Crust.

Multibeam data in the Southeast Tasman Sea reveal abyssal hill fabric that is left exposed as a result of the scouring activity of currents throughout the region. Abyssal hill fabric is aligned parallel to the axis of spreading centers and is created through a complex combination of extensional faulting and changes in magma flux that occur during seafloor spreading. Abyssal hill fabric in the Emerald Basin and South Tasman Ocean Crust is oriented roughly parallel to the Eocene rifted margins while abyssal hill fabric on older Tasman Sea crust is oriented roughly perpendicular to the rifted margins. This dramatic 90° change in abyssal hill fabric direction marks the boundary between seafloor created along the Tasman Ridge prior to chron 24 (52 Ma) and newer seafloor created along the Macquarie Ridge Complex after chron 18 (40 Ma). Fracture zones related to the earlier period of seafloor spreading along the Tasman Ridge are also located very accurately in several locations with multibeam images.

We used the location of these fracture zones along with the location of the old edge of the Resolution and Southwest Campbell Rifted Margins in order to determine

an Australia-Pacific pre-rift finite rotation. We divided the rifted margins into 6 segments approximated by great circles in order to perform the calculation. The resultant finite rotation reconstructs the Resolution Rifted Margin back to its pre-rift location directly adjacent to the Southwest Campbell Rifted Margin. The fit obtained from this reconstruction is quite good and is accurate within the limits of the uncertainty associated with determining the location of the rifted margin. When the Australia Plate side of the New Zealand continental shelf is reconstructed back to its pre-rift configuration and distributed dextral shear across the Alpine Fault is taken into account, the Permian Maitai Terrane matches across the plate boundary in a broad continuous arc. This suggests that the present day curvature of the New Zealand basement terranes can be accounted for by dextral motion and distributed crustal shear close to the Alpine Fault during the time period following Eocene rifting along the Macquarie Ridge Complex.

Chapter 4

Geophysical structure of the Adare Trough: a Cenozoic boundary between East and West Antarctica

Abstract

The Adare Trough is a prominent N-NW trending extensional feature that is aligned with sedimentary basins in the western Ross Sea and is located roughly 100 km NE of Cape Adare, Antarctica. A distinct series of magnetic lineations has been identified parallel to and flanking the Adare Trough. This, along with magnetic anomalies on the Australia Plate, indicates that this structure was actively spreading during Eocene and Oligocene time until approximately 28 Ma, forming a new wedge of ocean crust called the Adare Basin [*Cande et al.*, 2000]. We analyze multi-channel seismic and multibeam bathymetry data collected aboard the R/VIB Nathaniel B. Palmer in 1997 in order to better understand the formation, history, and tectonic role the Adare Trough has played in the Cenozoic history of the Antarctic Region. Multi-beam bathymetry data on the flanks of the Adare Trough reveals seafloor spreading fabric aligned parallel to the trough's axis. Spreading fabric in the deeper parts of the Adare Basin is obscured by thick sedimentary cover. We also present stacked and migrated seismic sections along two 48-channel seismic lines across the Adare Trough. Minor faults within the trough as well as drag folds related to movement along the bounding faults of the Adare Trough are clearly visible. The uppermost sedimentary units are horizontal and undisturbed by faulting which indicates that the Adare Trough is no longer active. Seismic stratigraphic units identified on our

seismic lines are correlated to DSDP hole 274 via the Eltanin 52 seismic line. Ties to DSDP 274 suggest that the oldest sediments in the Adare Trough are Early Oligocene in age, in general agreement with the magnetic models of *Cande et al.* [2000].

4.1 Introduction

For many years, Cenozoic plate tectonic reconstructions in the Southwest Pacific which have treated Antarctica as a single rigid plate have been plagued by large misfits. Early plate reconstructions predicted a large gap along the Australia-Pacific boundary between the North and South Islands of New Zealand, and it was proposed that including roughly 500 km of motion between East and West Antarctica could account for this misfit [*Molnar et al.*, 1975]. Further studies indicated that early Tertiary spreading along the easternmost part of the Southeast Indian Ridge (SEIR) had occurred as an apparently faster rate than along the rest of the SEIR [*Stock and Molnar*, 1982; *Royer and Sandwell*, 1989]. Because magnetic lineations along most of the length of the SEIR lie adjacent to stable East Antarctica whereas magnetic lineations associated with the easternmost part of the SEIR lie to the east of the axes of Cenozoic extensional basins in the western Ross Sea, the observed discrepancy in spreading rates was attributed to motion between East and West Antarctica. Continued improvements in our knowledge of the plate circuit have reduced the amount of misfit in plate reconstructions in the Southwest Pacific from its original estimates [*Stock and Molnar*, 1987]. However, the most recent reconstructions involving a single rigid Antarctic Plate still predict a gap of over 150 km along the Pacific-Australia plate boundary south of New Zealand in the early Tertiary, again suggesting that significant extension between East and West Antarctica was accommodated during this time period [*Cande et al.*, 2000].

Geological and geophysical evidence for significant amounts of extension between East and West Antarctica goes beyond predictions from plate reconstructions. West Antarctica is an amalgamation of smaller continental blocks [*Dalziel and Elliot*, 1982] that is separated from the stable craton of East Antarctica by the West Antarctic

Rift System (WARS), an extensional province that is comparable in size to the Basin and Range Province in North America [*LeMasurier*, 1990]. The WARS consists of the Ross Sea Embayment which is flanked by the Transantarctic Mountains to the west and the Marie Byrd Land Block to the east (Figure 4.1) and is considered active because of extensive young volcanism in the region [*Behrendt et al.*, 1991; *Behrendt and Cooper*, 1991]. The exact timing and amount of extension that has occurred across the Ross Sea Embayment has remained controversial. Numerous authors have proposed that the formation of the major basins in the western Ross Sea initiated with an extensional episode in the Ross Sea Embayment during middle and Late Cretacous time (e.g. *Davey* [1981], *Cooper and Davey* [1985] ,*Brancolini et al.* [1995] ,*Davey and Brancolini* [1995]). Evidence for a major Cenozoic rifting event comes from recent drilling in the western part of the Victoria Land Basin near Cape Roberts which has revealed a thick section of Oligocene sedimentary rock that can be correlated to the stratigraphy in the deeper parts of the basin. This suggests that much of the sediment in the Victoria Land Basin is latest Eocene and younger, an age much younger than previously thought [*Hamilton et al.*, 2001]. The existence of a major Cenozoic rifting episode is also supported by apatite fission track analysis which suggests that uplift and exhumation of the Transantarctic Mountains initiated at roughly 50-55 Ma [*Fitzgerald et al.*, 1986; *Fitzgerald*, 1992, 1994].

Cenozoic extension in the Ross Sea may be related to the Adare Trough, which is a prominent NW trending graben aligned with the major sedimentary basins of the Ross Sea Embayment. The Adare Trough was first described by *Ewing et al.* [1969] and in further detail by *Houtz and Davey* [1973]. More recently, *Cande et al.* [2000] identified magnetic anomalies parallel to and flanking the trough, which suggests that it was an active spreading center during Eocene and Oligocene time until approximately 28 Ma. We look in detail at bathymetry and seismic data from the Adare Trough region and present further evidence that the Adare Trough is an extinct spreading center.
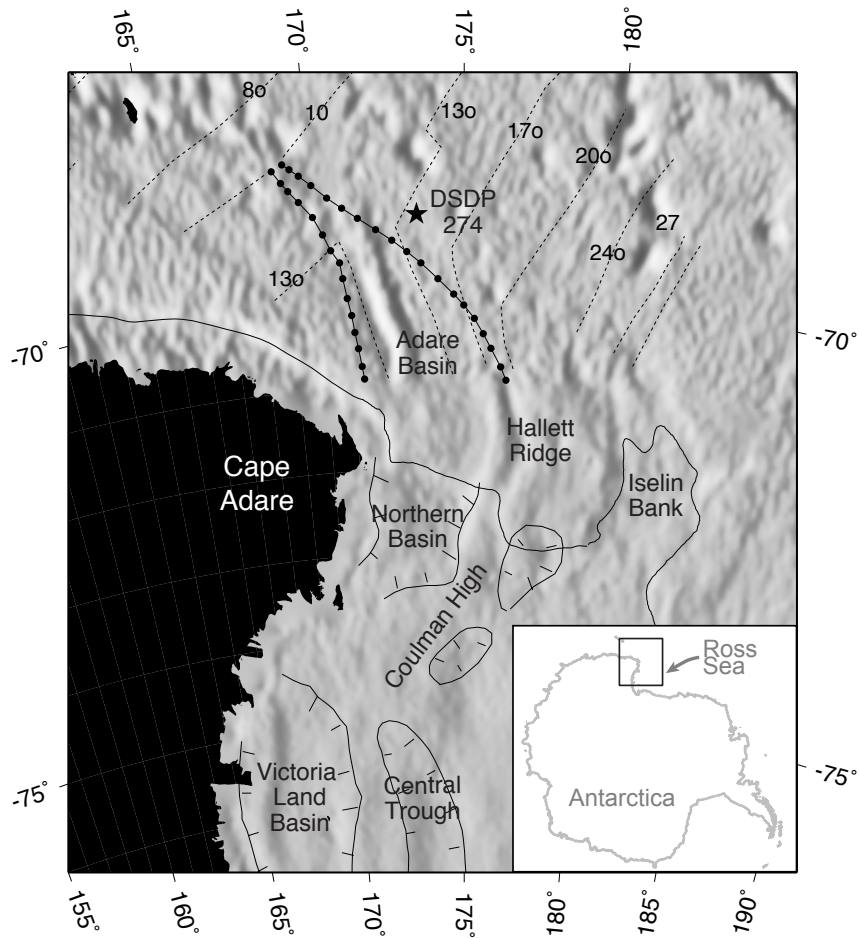
Figure 4.1: Location figure showing the major tectonic features of the region surrounding the Adare Basin and Ross Sea Embayment. A shaded relief image of the satellite derived free air gravity anomaly is shown for reference *Sandwell and Smith* [1997]; *McAdoo and Laxon* [1997]. Magnetic anomalies showing the East Antarctica - Australia - West Antarctica triple junction are from *Cande et al.* [2000], and the location of the major sedimentary basins of the Ross Sea Embayment are from *Davey and Brancolini* [1995]
.

4.2 Bathymetry

Single beam bathymetry data collected with the Bathy2000 3.5 kHz bottom profiler along lines AA to E[1] (Figure 4.2) reveal that the Adare Trough is a NW trending feature with a prominent 40 km wide central graben that is bounded by large normal faults (Figure 4.3). There is approximately 1.5 km of relief on the western bounding fault and 1 km of relief on the eastern bounding fault of the central graben on lines AA through D. However, the prominent topographic signature of the trough is missing on line E, indicating that the Adare Trough does not continue directly from line D to line E and may be truncated, reduced in amplitude, or offset. The signature of the trough seen in the satellite gravity also disappears south of line D suggesting that the trough is not simply buried by deep sediment south of this line.

Elevated topography on the flanks of the Adare Trough decreases smoothly to an average depth of 2500 m at approximately 50 km from the bounding faults of the central graben. This decrease in topography is greater than would be expected for a typical extinct spreading center [*Jonas et al.*, 1991] and is most likely caused by flexural uplift of the flanks of the trough in response to mechanical unloading of the lithosphere along its bounding faults. This flexural signature is similar to what is seen in oceanic rifts such as the Broken Ridge in the eastern Indian Ocean, Sorol Trough in the Western Equatorial Pacific, and the Coriolis Trough behind the New Hebrides arc [*Weissel and Karner*, 1989; *Hegarty and Weissel*, 1988; *Altis*, 1999]. The background depth of 2500 meters is shallower than the expected depth of greater than 4500 meters for seafloor of this age assuming a standard oceanic plate cooling model. This discrepancy may be somehow related to close proximity to the continental shelf or continued thermal activity after cessation of seafloor spreading in the Adare Basin.

Multibeam bathymetry data collected in the Adare Basin aboard the R/VIB Nathaniel B. Palmer is shown in Figure 4.4, and satellite derived topography data is plotted for reference [*Smith and Sandwell*, 1997]. Dashed boxes in Figure 4.4 show the locations of Figure 4.5 and Figure 4.6. The multibeam data was collected on

---

[1]The labeling scheme for the data lines in this study follows that of *Cande et al.* [2000].
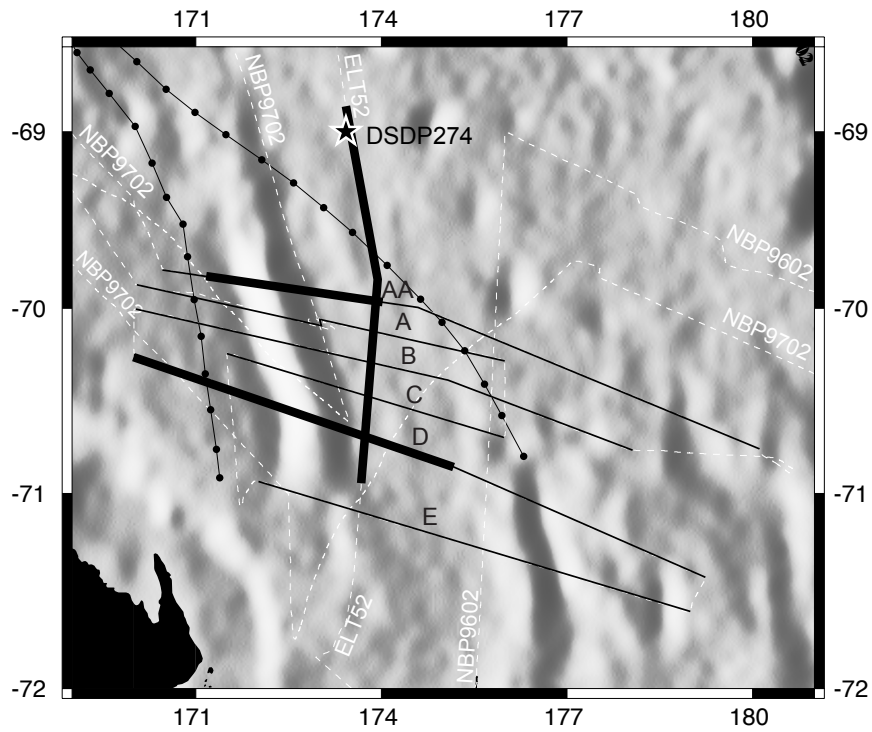
Figure 4.2: Single beam bathymetry lines AA-E collected on cruise NBP9702 aboard the R/VIB Nathaniel Palmer are shown by the thin black lines. Seismic lines for cruises NBP9702 and ELT 52 are shown with thick black lines. Shiptracks are shown by dashed white lines, and the edges of the Adare Basin are shown with black dots connected by lines as in *Cande et al.* [2000].
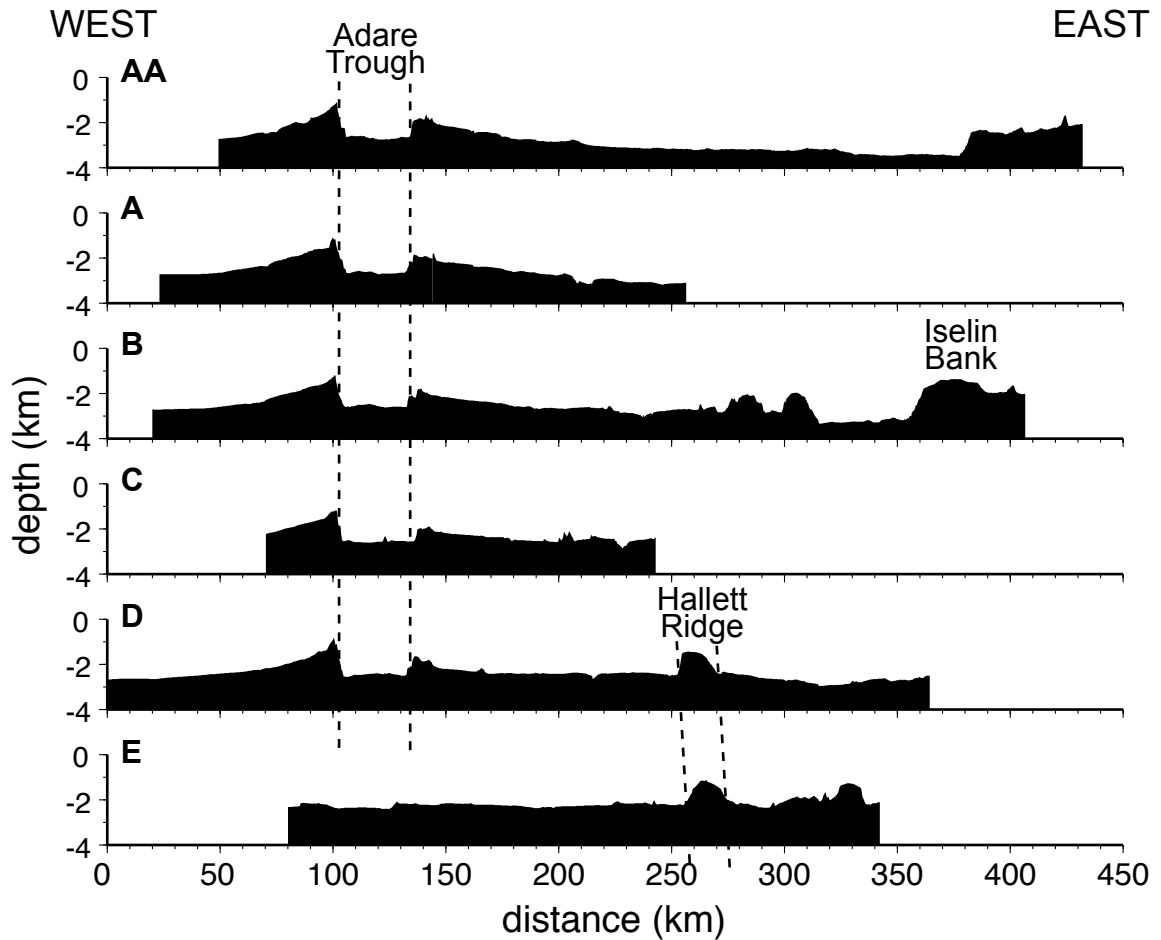
Figure 4.3: The Adare Trough is a NW trending, 40 km wide graben that is bounded by normal faults. The trough is asymmetric, with approximately 1 km of relief on the east flank and approximately 1.5 km of relief on the west flank. The Adare Trough is truncated, reduced in amplitude, or offset at approximately 71S, and there is virtually no topographic expression of the trough south of this point (the very subtle depression seen on line E may be the southernmost expression of the trough). The Hallett Ridge is a linear feature that is roughly parallel to the Adare Trough and is bounded by a prominent normal fault on its western side.

cruises NBP9602 and NBP9702 using a hull mounted SeaBeam 2100 system, and the data quality is thus highly dependent on sea state and accuracy of sea temperature profiles. Analysis of the multibeam data reveals that the western bounding fault of the central graben of the Adare Trough exhibits a very simple structure with a single, well-defined fault trace. The eastern bounding fault zone is substantially more complex, comprising 2-3 faults that progressively step down from the flank of the trough to the central graben in most areas. The crest of the eastern flank of the trough is marked by numerous small volcanic centers of unknown age. Scattered small volcanic centers are also found in the eastern half of the Adare Basin, including a cluster of them on line C at roughly 70.5° S, 175° E. The Hallett Ridge is a north trending linear feature in the SE corner of Figure 4.4 that is located at 177° E and extends south of approximately 71° 45' S. The Hallett Ridge is bounded by a large normal fault on its western side.

NW-trending faults and lineations parallel to the axis of the Adare Trough are clearly visible in several areas within the Adare Basin (Figure 4.5). We interpret these features to be abyssal hill fabric related to seafloor spreading along the Adare Trough. Thick sediment cover obscures features on the seafloor in the deeper parts of the western side of the basin at distances more than approximately 100 km from the central graben. However, features are much more easily identified in the eastern half of the basin where the sediments are thinner.

A roughly NW-trending break in slope can be seen in lines AA, A, and B at roughly 174.5-175.5° longitude and is shown by the easternmost line of black dots in Figure 4.6. The seafloor is significantly deeper to the east of this break in slope than to the west, and seafloor spreading fabric east of this boundary is NE-trending as opposed to the NW trending fabric seen in the Adare Basin. NE-trending abyssal hill fabric is clearly visible on the two north trending tracklines near the eastern end of lines A and B and is denoted by the black arrows in Figure 4.6. The NE orientation of abyssal hill fabric is consistent with that of surrounding seafloor created along the Southeast Indian Ridge (SEIR). We therefore suggest that this change in slope of the seafloor coupled with a change in spreading direction marks the boundary between seafloor
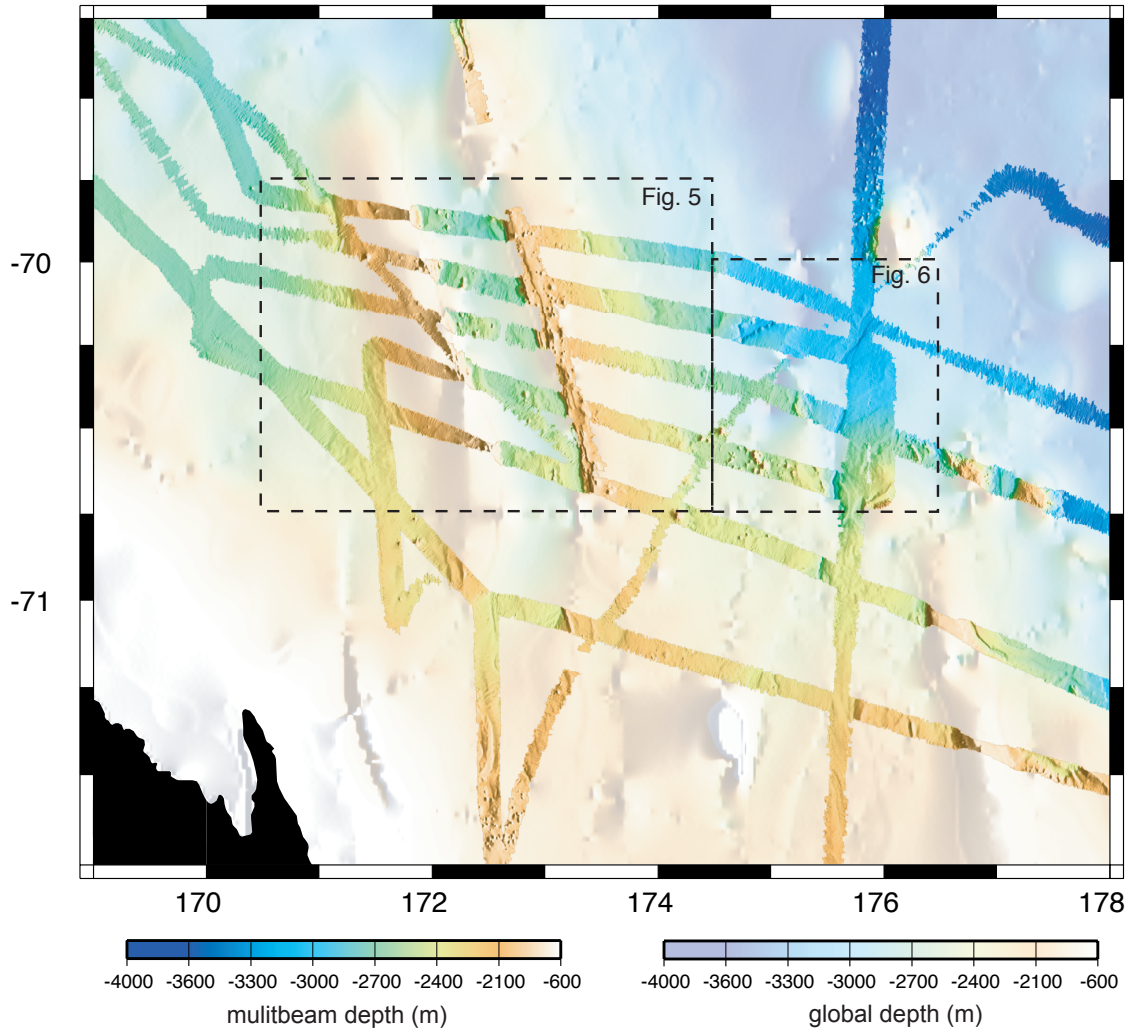
Figure 4.4: Multibeam bathymetry in the Adare Basin reveals seafloor spreading fabric aligned parallel to the central graben of the Adare Trough. The Hallett Ridge is a north trending linear feature in the SE corner of the figure that is located at 177° E and extends south of approximately 71° 45' S. The Hallett Ridge is bounded by a large normal fault on its western side. Dashed boxes show the locations of Figure 4.5 and Figure 4.6. Note that the map covers a smaller area than in Figure 4.2.
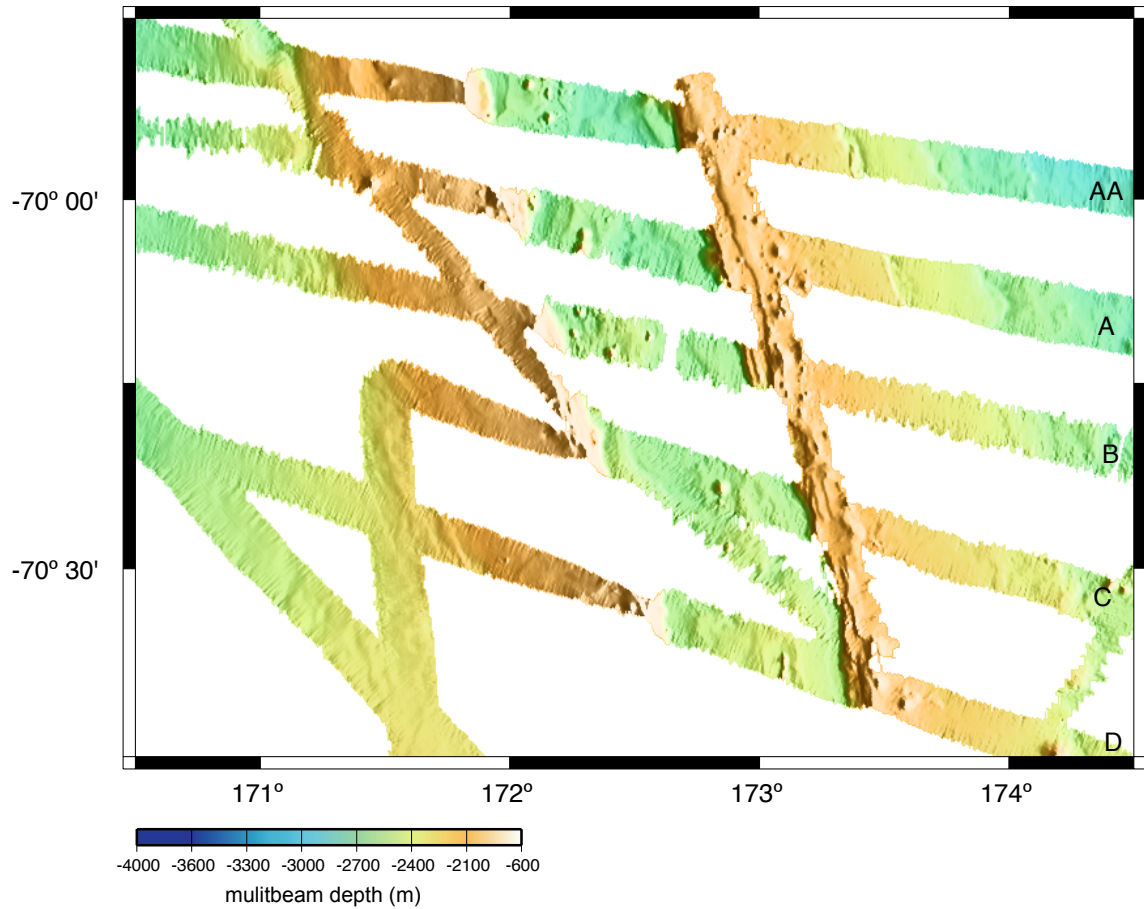
Figure 4.5: This detailed map of the Adare Basin clearly shows abyssal hill faults and lineations aligned parallel to the central graben of the Adare Trough. The western bounding fault of the central graben exhibits a very simple structure with a single, well-defined fault trace, whereas the eastern bounding fault is substantially more complex and consists of 2-3 faults that progressively step down from the flank of the trough to the central graben in most areas. Illumination is from the east.
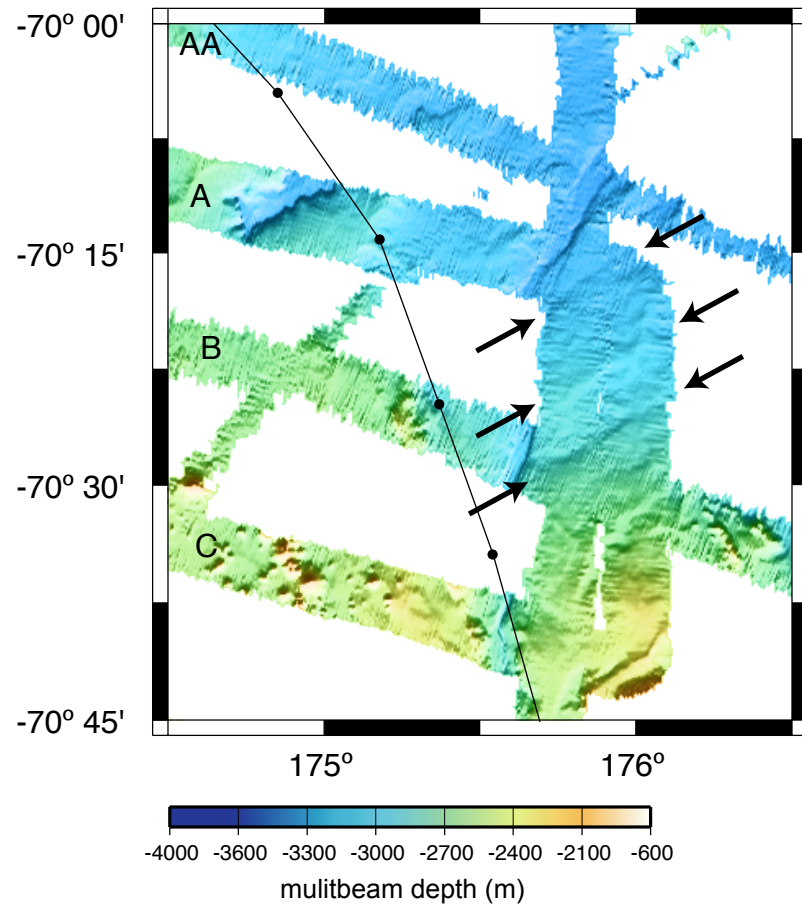
Figure 4.6: This detailed map of the eastern boundary of the Adare Basin shows NE-trending abyssal hill fabric on crust formed at the Southeast Indian Ridge (prominent lineations are denoted by black arrows). The eastern boundary of the Adare Basin is marked by a break in slope from the shallow Adare Basin crust to the west to the deeper Southeast Indian Ridge crust to the east. The location of the boundary is again shown with black dots connected by lines. Illumination is from the south.

created by spreading along the Adare Trough to the west and seafloor that was created along the SEIR to the east (i.e. it marks the trace of the triple junction between the plates of Australia, East Antarctica, and West Antarctica). The southern extent of this triple junction trace is obscured south of line C by sediment that becomes thicker close to the continental shelf to the south.

A large north-trending channel is clearly visible on lines AA, A, C ,and D at approximately 175.5-176° longitude indicating that there is significant northward movement of cold bottom water from the Ross Ice Shelf. This channel cuts across the grain of the NE-trending abyssal hill fabric east of the Adare Basin. There is also some evidence of northward movement of bottom water along the central graben of the Adare Trough. The best example of this is a small depression that currents have scoured around a small basement ridge within the central graben on line D. There are numerous small volcanic centers scattered throughout the central graben of the trough and on its flanks; however, this scouring effect is not well pronounced in these areas.

The results of a statistical analysis of the seafloor spreading fabric direction in the Adare Basin and surrounding region are shown in Figure 4.7. The gradient direction for each grid cell in each hourly data file was calculated and then summed up as unit vectors to obtain hourly gradient direction. Cells with slope values less than 0.05 were excluded from these calculations to avoid input from regional slopes that span several hours of data. Azimuthal markers are plotted perpendicular to the gradient direction for each hour of data and thus indicate the strike of bathymetric features on the seafloor. The length of the markers is proportional to the strength factor, a statistical measure of the azimuthal coherence of features on the seafloor. The value of the strength factor varies from 0 to 1. An hourly data file in which each grid cell contained the same slope direction would yield a strength factor of 1, whereas the strength factor would approach zero with a completely random distribution of slope directions. Azimuth markers are colored black in Figure 4.7 for hours in which the slopes are interpreted to be primarily controlled by abyssal hill fabric. Azimuth markers for hours with slopes that are controlled by other factors such as noisy data,

tilted pings, seamounts, thick sediment cover, channels, etc. are plotted in gray. The results of this analysis show very coherent NW trending abyssal hill fabric on the flanks of the Adare Trough and a change to NE-trending abyssal hill fabric to the east of the Adare Basin.

4.3   Stratigraphy: DSDP hole 274

DSDP hole 274 is located at 69.0°S, 173.4°E, roughly 250 km northwest of Cape Adare (Figure 4.1). The drill hole penetrated 415 meters of largely terrigenous sediments as well as the upper few meters of basalt in this location (Figure 4.8) [*Hayes et al.*, 1975; *Frakes*, 1975]. The oldest dated sediments within the drill hole are the Early Oligocene diatom rich detrital silty clays at the base of Unit 4 [*Hayes et al.*, 1975]. Based on regional magnetic models at the time [*Weissel and Hayes*, 1972] and extrapolation of sedimentation rates below the base of Unit 4, *Hayes et al.* [1975] suggest that the oldest sediments in the drill hole are likely Early Oligocene or older. More recent magnetic data collected in the Adare Basin and in the Balleny Corridor NE of the Adare Basin [*Cande et al.*, 2000] constrains the age of the ocean crust at DSDP 274 to be no older than Early Oligocene (chron 13).

The sedimentary section at DSDP 274 can be subdivided into 5 lithostratigraphic units on the basis of color, ratio of biogenic to clastic components, presence of silt layers, chert, or manganese nodules. The following descriptions of the stratigraphic and seismic units at DSDP hole 274 are summarized from *Piper and Brisco* [1975] and *Frakes* [1975].

4.3.1   Unit 6 (Seismic Unit SU6)

Unit 6 consists of dense, aphyritic basalt of which 3.6 meters was recovered. The basalt is cut by numerous white to green veins of calcite and chlorite, and volcanic breccia of unknown origin was recovered in part of the core. The boundary between this unit and the overlying sediment is marked by a sharp change in velocity and density which corresponds with a prominent subbottom reflector at 0.50 sec two-way
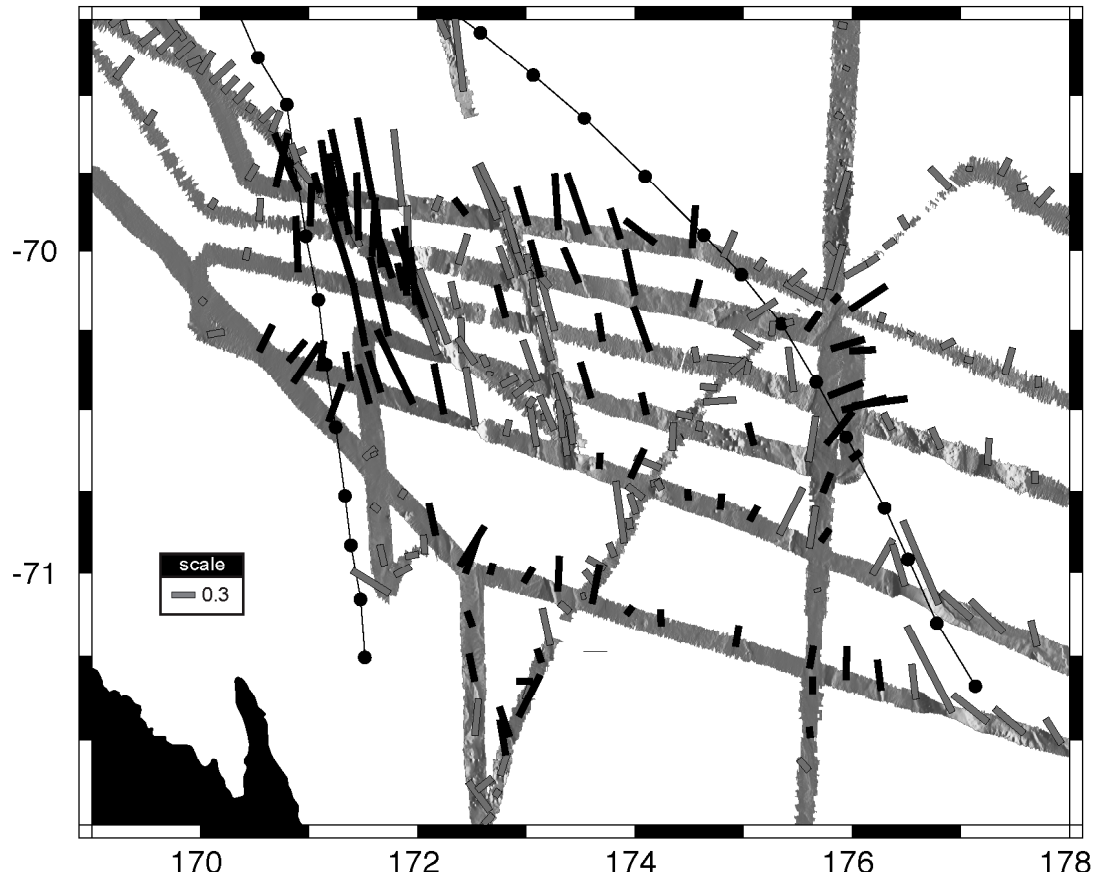
Figure 4.7: Results of a mathematical analysis of the multibeam data in which the gradient is calculated for every hour of data collected, and the resultant slope strength and directions are then plotted as azimuthal bars. The direction of the bars indicates the strike of features on the seafloor while the length of the bars indicates the slope strength values for a given hour of data. Slope strength is a statistical measure of the coherence of slope directions for a given hour of data. Black bars indicate that the slopes are controlled by abyssal hill fabric, and grey bars indicate that the slopes are controlled by other factors such as seamounts, channels, tilted pings, and noisy data.
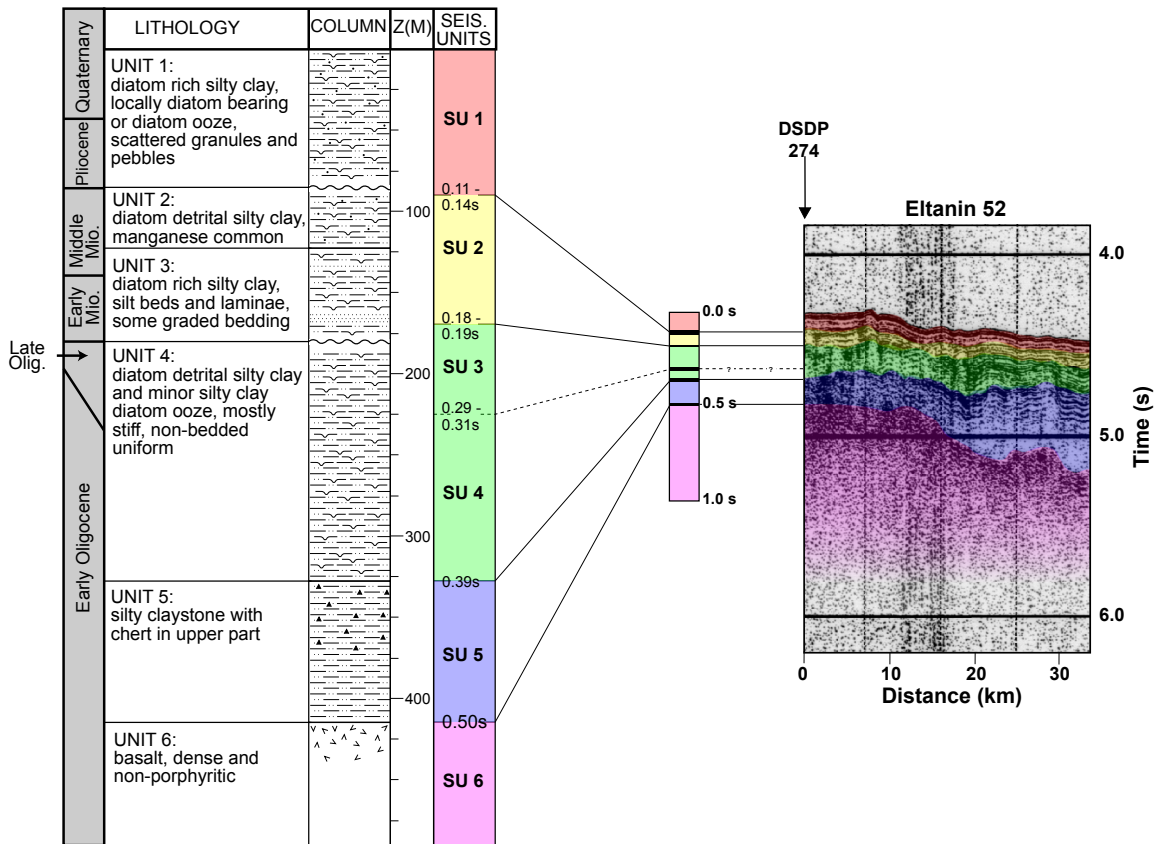
Figure 4.8: DSDP 274 stratigraphic column and correlation to ELT52 seismic line. Stratigraphic column after *Frakes* [1975] and *Hayes et al.* [1975]. Important seismostratigraphic markers include the package of reverberations off of chert layers at the top of SU5 as well as unconformities at the base of SU1 and SU2.

travel time in downhole velocity measurements as well as on the Eltanin 52 seismic profiler record.

4.3.2   Unit 5 (Seismic Unit SU5)

Unit 5 is comprised of an 87 meter thick sequence of semilithified to lithified silty claystone that contains only trace amounts of diatoms. Porcellaneous chert is common in the upper part of the unit, and these cherty layers correspond to a very distinct package of reflectors at approximately 0.39 sec two-way travel time. This series of reflectors is sandwiched between seismically transparent layers, so it is very easily identifiable in seismic section and one of the most important regional seismic markers.

4.3.3   Unit 4 (Seismic Unit SU3/SU4)

Unit 4 is the thickest sedimentary unit in the sequence at 148 meters and is a highly uniform package of diatomaceous detrital silty clays to silty clay diatom oozes. The unit is very rich in diatoms throughout. Unit 4 exhibited a very high degree of drilling deformation, but the rare undisturbed sections of core show very indistinct bedding. The sediments are semilithified in places, but are mainly stiff throughout. Unit 4 is unconformably overlain by the sediments of Unit 3, and this unconformity corresponds to a subbottom reflector at 0.18-0.19 sec two-way travel time. Another subbottom reflector which likely correlates to a zone of lithification within Unit 4 is seen at 0.29-0.31 sec two-way travel time in downhole velocity measurements. This reflection is not regionally significant, so SU3 and SU4 are treated as a single seismic unit that is hereafter referred to as SU3/4. Unit 4 corresponds to Seismic Unit SU3/4.

4.3.4   Unit 3 - Unit 2 (Seismic Unit SU2)

Unit 3 consists of diatom rich silty clay and claystone. Silt layers between 2 and 10 cm thick are common in the lower half of the unit while minor silt lenses and disrupted laminae are more common in the upper half. Some of the silt bodies show graded bedding. The contact between Unit 3 and Unit 2 is characterized by a color

gradation from the greenish gray sediments of Unit 3 to the moderate yellowish-brown sediments of Unit 2. Unit 2 is comprised of diatomaceous detrital silty clay and is virtually devoid of bedding or color layering. Unit 2 is characterized by its yellowish-brown color, which is caused by the presence of ferromanganese oxides, and ferromanganese-coated pebbles and granules are present throughout the unit. The top of Unit 2 is marked by a minor unconformity which corresponds to a subbottom reflection at 0.11-0.14 sec two-way travel time. There is no reflection associated with the boundary between Unit 2 and Unit 3, so these units together correspond to Seismic Unit SU2.

4.3.5 Unit 1 (Seismic Unit SU1)

Unit 1 is composed of greenish-gray diatom-rich silty clay. Diatom content within Unit 1 varies greatly but is highest near the base of the unit. Ice rafted granules and pebbles are also common. Unit 1 corresponds to Seismic Unit SU1.

4.4 Seismic Data

4.4.1 Eltanin 52 Seismic Data

The ELT52 seismic line is an analog seismic profiler record that was collected in 1972 aboard the R/V Eltanin (Figure 4.9). The location of seismic line ELT52 is shown as a thick black line in Figure 4.2. Seismic line ELT52 intersects DSDP 274 on its northern end and rises up onto the flank of the Adare Trough to the south where it intersects multichannel seismic lines that were collected during the NBP9702 cruise aboard the R/VIB Nathaniel Palmer.

Figure 4.9B shows that SU1-SU3/4 are laterally continuous from DSDP 274 to the intersection of ELT52 with NBP9702 Line D. SU5 is the most readily identifiable unit in this seismic section. The contact between SU5 and SU3/4 is clearly defined by the transition between the characteristic reverberations from the chert in the upper part of SU5 and the relatively transparent package of diatom rich silty clays at the base

of SU4. The sediment/basalt contact at the base of SU5 is also readily identifiable throughout the seismic section.

4.4.2 NBP9702 Seismic Data

48-channel seismic data was collected during the NBP9702 cruise at speeds of 5-6 knots with a 1200 m long streamer and six 210 cubic inch GI air guns. Migrated sections along NBP9702 seismic lines AA and D are shown in Figure 4.12 and 4.10. The velocity model used for the migrations was generated by semblance velocity analysis every 100 CMP. The signal-to-noise ratio on NBP9702 seismic line D is significantly higher than that of line AA due to factors related to rough seas and bad weather.

On NBP9702 seismic line D, penetration is typically 1-1.5 seconds maximum due to the high frequency of the GI air gun source. However, the sediment/basement contact is easily identifiable in most locations and detailed relationships between the seismic units on this line are clearly visible. The intersection of ELT52 with NBP9702 seismic line D is shown in Figure 4.10B by the red vertical dashed line at approximately 100 km. Seismic units at this location can be correlated from ELT52 to NBP9702 seismic line D, and the identification of unconformities within the section provides good stratigraphic control on the location of seismic units.

Figure 4.11 parts A-C show some details in selected locations along NBP9702 seismic line D which correspond to the dashed boxes shown in Figure 4.10. The unconformity between seismic units SU1 and SU2 is revealed at roughly 106 km on Figure 4.11C where reflectors within SU2 are truncated at the base of SU1. At approximately 100-105 km reflectors within SU3/4 onlap onto SU5 indicating that there was topography on the flanks of the Adare Trough at the time when the sediments of SU3/4 were deposited (Figures 4.10 and 4.11).

Although seismic units outside of the central graben of the Adare Trough can not be continuously traced across the bounding faults, the character of the seismic units and the locations of the unconformities are easily identifiable on either side
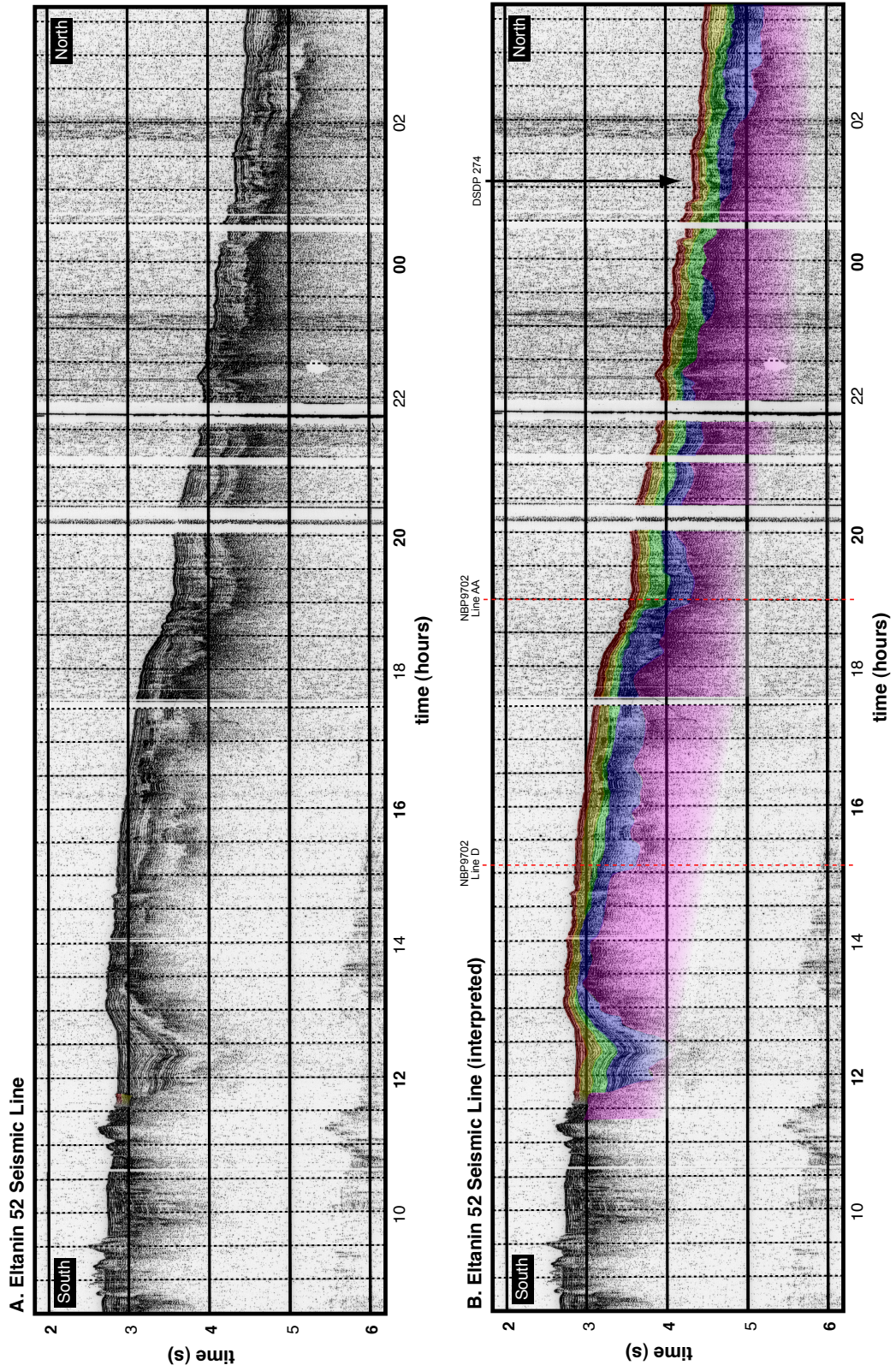
Figure 4.9: (caption on following page)

of the boundary. The characteristic package of reflections from the chert layers at the top of Unit 5 are visible in the lower part of the sedimentary section within the trough. In the western part of the central graben, only the upper part of Unit 5 is present. At roughly 73-74 km (Figure 4.11B), reflectors within SU3/4 are truncated at the base of SU2 and reflectors within SU1 onlap onto SU2, thus revealing the same unconformities that are found on the east flank of the Adare Trough.

Between 65 and 70 km on NBP9702 seismic line D, there is a series of minor normal faults that step down towards the west. These faults clearly offset seismic units SU6-SU2; however SU1 appears to be relatively undisturbed. At 50-53 km (Figure 4.11A), drag folding of SU5-SU2 is visible along the west bounding fault of the central graben of the trough. Again, the reflectors within SU1 are flat-lying, suggesting that motion along the bounding faults and minor faults within the trough ceased before the sediments of SU1 were deposited.

On NBP9702 seismic line AA (Figure 4.12), the data are much lower quality than on NBP9702 seismic line D largely due to complications with the air guns and problems with the streamer due to bad weather conditions. Penetration along NBP9702 seismic line AA is typically 0.5-1 second, and the sediment-basement contact can not be clearly distinguished within the central graben of the Adare Trough. A detailed interpretation of seismic units along this line was not possible due to these complications; however this seismic line still provides some useful information. Along the eastern bounding fault, the uppermost seismic reflectors are flat lying while reflectors deeper in the section are drag folded along the fault. Deeper reflectors on the west bounding fault are also drag folded, but the uppermost layers are truncated at the seafloor near the west bounding fault. This is likely the result of local scouring by bottom water currents.

Figure 4.9: ELT52 analog seismic profiler record. This line shallows to the south as it rises up onto the flank of the Adare Trough. Seismic units correlated to DSDP hole 274 can be traced to the intersection with NBP9702 lines AA and D (shown by the red dashed lines).
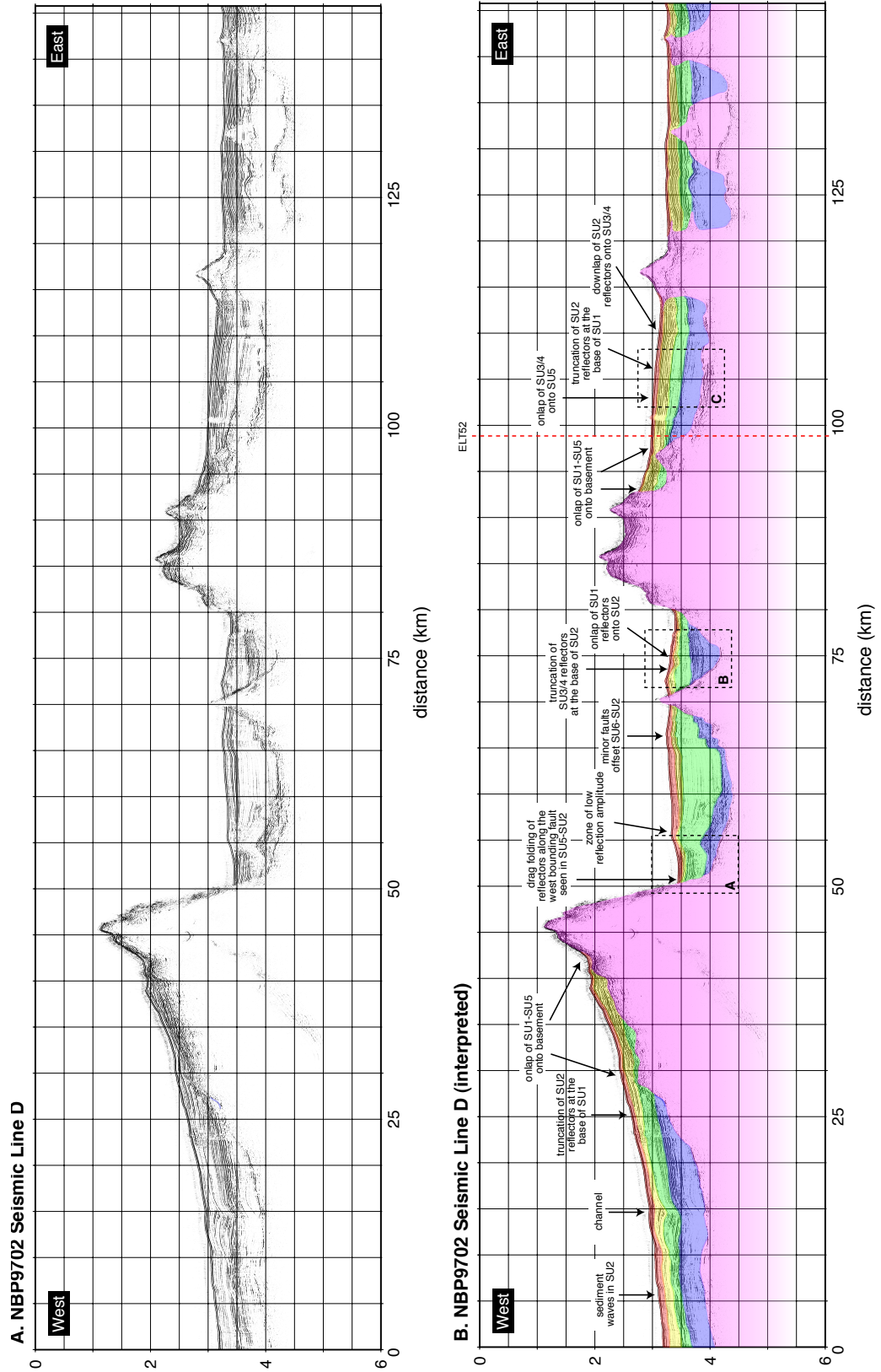
Figure 4.10: (caption on following page)

4.5   Discussion

Bathymetry data collected during the NBP9702 cruise shows that the Adare Trough is a NW trending structure with a 40 km wide central graben that is bounded by normal faults. The Adare Trough is asymmetric with 1.5 km relief on the west flank and 1 km of relief on the east flank. The prominent topographic signature of the trough is missing on line E, the southernmost line of our survey, thus indicating that the Adare Trough does not continue directly from line D to line E and may be truncated, reduced in amplitude, or offset. Multibeam bathymetry reveals seafloor spreading morphology on the flanks of the Adare Trough that is parallel to the trend of its axis. This provides evidence in support of *Cande et al.* [2000] who model the Adare Trough as an active spreading center during the Cenozoic until approximately 28 Ma (chron 9). NE-trending abyssal hill fabric is visible in some areas on the east side of the Adare Basin boundary, and this helps map the eastern boundary of the Adare Basin crust.

We have tied the multichannel seismic data collected during the NBP9702 cruise to DSDP hole 274 via the Eltanin 52 seismic line, and this reveals important information about the timing and extent of tectonic activity related to the formation of the Adare Trough. The oldest dated sediments in DSDP 274 are Early Oligocene diatom rich, silty clays at the base of Unit 4 (seismic unit SU3/4) [*Hayes et al.*, 1975]. Biostratigraphic control is insufficient to determine an accurate age for Unit 5 (seismic unit SU5); however, magnetic anomalies recently identified in the Balleny Corridor indicate that DSDP 274 is located on Early Oligocene crust (chron 13). This indicates that Unit 5 is also Early Oligocene in age. The upper part of SU5 is identified within the central graben of the Adare Trough based on correlations with ELT52, suggesting that the crust underlying the central graben of the trough formed during Early Oligocene time. This age is in agreement with the magnetic model of *Cande*

Figure 4.10: NBP9702 line D 48-channel migrated section. The vertical red dashed line indicates the intersection with the ELT52 seismic line. Dashed boxes indicate the location of detailed insets that are shown in Figure 4.11A-4.11C.
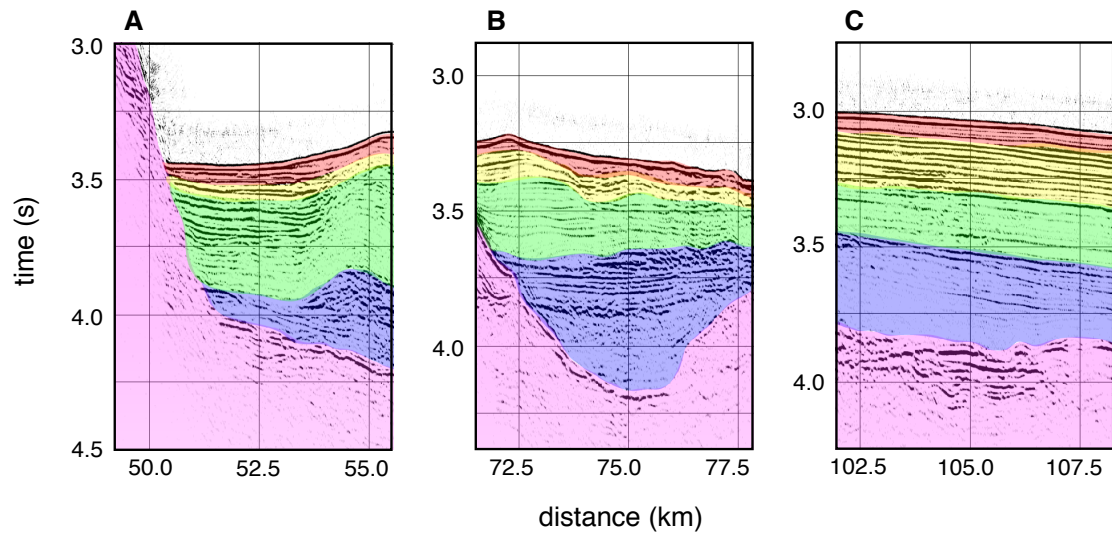
Figure 4.11: NBP9702 Seismic Line D insets showing details of selected areas along NBP9702 seismic line D.

et al. [2000].

SU2 (middle Miocene, 12-15 Ma) is the youngest faulted unit within the Adare Trough indicating that the trough is no longer active. SU2 is unconformably overlain by the flat lying Pliocene (5 Ma) sediments of SU1. The analysis of our seismic data suggests that after the cessation of seafloor spreading in the Adare Basin at approximately 28 Ma (chron 9), some amount of faulting continued within the Adare Trough until at least 12-15 Ma and may have continued until as late as 5 Ma. Although the Adare Trough acted as a spreading center from Eocene time until approximately 28 Ma, its morphology is very similar to that of known oceanic rifts such as the Broken Ridge in the eastern Indian Ocean, Sorol Trough in the western Pacific, and the Coriolis Trough behind the New Hebrides arc. *Weissel and Karner* [1989] showed that flexural rebound is a viable explanation for the uplift of oceanic rift flanks even when the lithosphere is thermally very young. They found that in the case of the Coriolis Trough, they were able to fit the topography (over 2 km of relief) with an effective elastic thickness of less than 5 km. The Sorol Trough also appears to have formed on thermally young lithosphere. *Altis* [1999] suggests that the Caroline Ridge
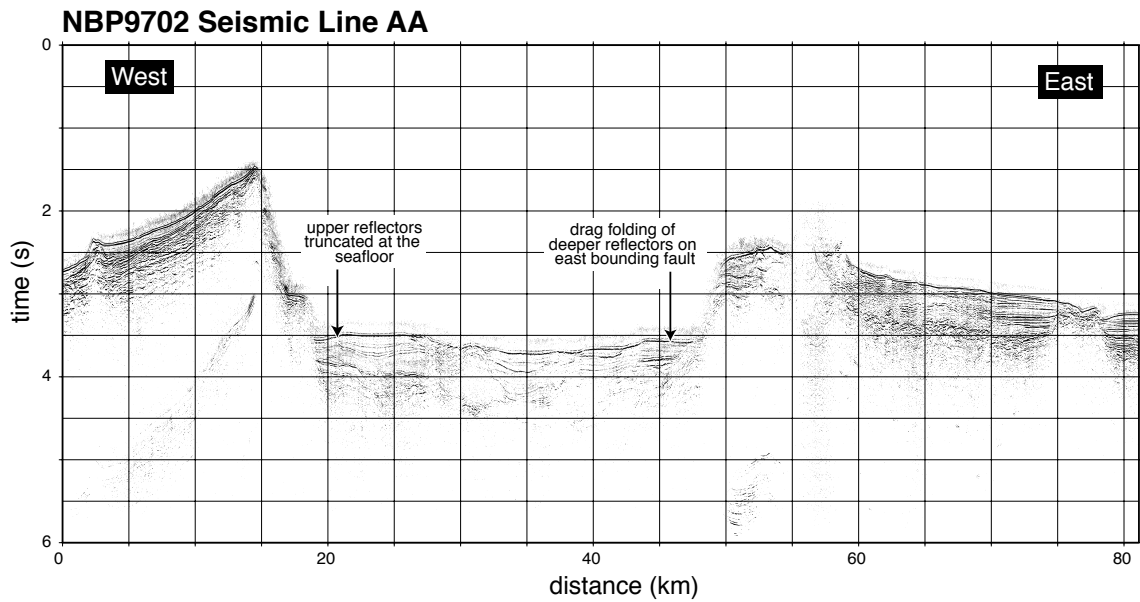
Figure 4.12: NBP9702 seismic line AA. Detailed correlation of seismic units with the ELT 52 seismic line was not possible due to data quality issues related to rough seas and poor weather conditions. Along the east bounding fault, the uppermost reflectors are flat lying while reflectors deeper in the section are drag folded along the fault. Deeper reflectors along the western bounding fault are also drag folded. However the uppermost layers are truncated at the seafloor near the fault indicating local scouring due to bottom water current activity.

was formed in the Late Oligocene by hot spot volcanism on top of Oligocene seafloor. They also suggest that the Caroline Ridge was subsequently rifted apart by the Sorol Trough in the 17-7 Ma time interval. Taking into account these results, the flexural uplift of the flanks of the Adare Trough may have occured in the 28 Ma to 15-5 Ma time interval after the cessation of seafloor spreading.

Appendix A

The table on the following pages includes all the magnetic and fracture zone picks used to calculate the Australia-Pacific finite rotations presented in this study. Segment numbers indicate ridge/fracture zone great circle segments used in the reconstructions. Points not used in the reconstructions were assigned a segment number of 100. Fracture zone picks digitized from satellite-derived gravity [*Sandwell and Smith*, 1997] are assigned to cruise ID "grav." Magnetic anomaly picks extrapolated from abyssal hill fabric orientation on multibeam data are assigned to cruise IDs ending in "mb." PLT=plate, SEG=great circle segment number, LAT=latitude, LON=longitude, UNC=combined navigation and picking uncertainty, PICK=magnetic anomaly or fracture zone ID, FZ AGE=age range during which the fracture zone was an active transform fault between ridge segments, CRUISE=geophysical cruise ID.

Table A.1: Magnetic anomaly and fracture zone picks used to calculate Australia-Pacific finite rotations.

PLT	SEG	LAT	LON	UNC	PICK	FZ AGE	CRUISE
aus	9	-47.0415	162.1710	2.3994	18o		PU9301
aus	100	-50.2885	157.2057	0.9704	18o		ew9513
aus	2	-49.5595	157.7795	0.8599	18o		ew9513
aus	4	-49.1010	158.1765	1.0702	18o		ew9513
aus	100	-48.7500	158.6700	0.9524	18o		ew9513
aus	100	-50.1748	157.5001	0.9454	18o		ew9513
aus	100	-50.3924	156.3657	1.0793	18o		ew9513
aus	100	-50.3728	156.5134	5.8145	18o		ggl29
aus	100	-48.4701	159.3196	5.2537	18o		rs124
aus	100	-47.7711	161.1410	5.0728	18o		rs124
aus	100	-48.3813	160.1524	5.2140	18o		elt34
aus	6	-48.1896	160.7123	5.1143	18o		elt53
aus	100	-47.7976	161.1200	5.0515	18o		elt44
aus	100	-47.7321	161.1670	5.0444	18o		elt44
aus	100	-48.7326	158.7223	3.0017	18o		ew9513mb
aus	100	-48.7695	158.6223	3.0017	18o		ew9513mb
aus	4	-49.0778	158.2205	3.0017	18o		ew9513mb
aus	4	-49.1282	158.1350	3.0017	18o		ew9513mb
aus	2	-49.5411	157.8184	3.0017	18o		ew9513mb
aus	2	-49.5866	157.7247	3.0017	18o		ew9513mb
aus	100	-50.1578	157.5464	3.0017	18o		ew9513mb
aus	100	-50.1910	157.4491	3.0017	18o		ew9513mb
aus	100	-50.3248	157.1539	5.0010	18o		ew9513mb
aus	100	-50.2830	157.2547	5.0010	18o		ew9513mb
aus	100	-48.4489	159.3708	3.0017	18o		rigsismb
aus	100	-48.4972	159.2527	3.0017	18o		rigsismb

Table A.1: continued

PLT	SEG	LAT	LON	UNC	PICK	FZ AGE	CRUISE
aus	1	-49.6340	157.6338	7.0000	FZ1	18o-20o	grav
aus	1	-49.7350	157.7385	7.0000	FZ1	18o-20y	grav
aus	1	-49.8397	157.8413	7.0000	FZ1	18y-19	grav
aus	1	-49.9127	157.9116	7.0000	FZ1	18y-18o	grav
aus	1	-49.9750	157.9744	7.0000	FZ1	17o-18o	grav
aus	3	-49.2447	157.9375	7.0000	FZ2	18o-	grav
aus	3	-49.3134	158.0119	7.0000	FZ2	18o-18o	grav
aus	3	-49.3852	158.0674	7.0000	FZ2	18y-18o	grav
aus	5	-48.8492	158.4742	7.0000	FZ3	18o-18o	grav
aus	5	-48.8754	158.5080	7.0000	FZ3	18o-18o	grav
aus	5	-48.9076	158.5376	7.0000	FZ3	18o-18o	grav
aus	7	-47.8841	160.9237	7.0000	FZ6	18o-	grav
aus	7	-47.9234	160.9612	7.0000	FZ6	18o-	grav
aus	7	-47.9569	160.9853	7.0000	FZ6	18o-	grav
aus	8	-47.4774	161.6044	7.0000	FZ7	-18o	grav
aus	8	-47.5064	161.6328	7.0000	FZ7	-18o	grav
aus	8	-47.5349	161.6654	7.0000	FZ7	-18o	grav
pac	9	-55.8789	162.4350	5.6211	18o		th91b
pac	9	-56.3640	162.3541	1.5094	18o		ew9513
pac	9	-56.3272	162.3566	3.0017	18o		ew9513mb
pac	9	-56.4072	162.3568	3.0017	18o		ew9513mb
pac	4	-59.2754	161.3528	0.8419	18o		ew9513
pac	100	-59.6450	161.7395	0.9722	18o		ew9513
pac	2	-59.4615	161.5285	1.0366	18o		ew9513
pac	6	-57.4951	161.9496	1.0470	18o		ew9513
pac	6	-57.6481	161.8670	5.0911	18o		th92b
pac	100	-55.3006	162.7760	5.6528	18o		th91b

Table A.1: continued

PLT	SEG	LAT	LON	UNC	PICK	FZ AGE	CRUISE
pac	1	-59.7647	161.5920	7.0000	FZ1	-18o	grav
pac	1	-59.7672	161.6552	7.0000	FZ1	-18o	grav
pac	1	-59.7714	161.7153	7.0000	FZ1	-18o	grav
pac	1	-59.7657	161.7734	7.0000	FZ1	-18o	grav
pac	3	-59.3603	161.3742	7.0000	FZ2	18y-18o	grav
pac	3	-59.3673	161.4318	7.0000	FZ2	18o-18o	grav
pac	3	-59.3750	161.4944	7.0000	FZ2	18o-18o	grav
pac	3	-59.3814	161.5386	7.0000	FZ2	18o-18o	grav
pac	3	-59.3897	161.5890	7.0000	FZ2	18o-18o	grav
pac	5	-58.8700	161.2431	7.0000	FZ3	18o-	grav
pac	5	-58.8783	161.3241	7.0000	FZ3	18o-	grav
pac	5	-58.8867	161.3990	7.0000	FZ3	18o-	grav
pac	7	-57.0192	161.9441	7.0000	FZ6	18y-18o	grav
pac	7	-57.0395	162.0822	7.0000	FZ6	18o-18o	grav
pac	7	-57.0695	162.1978	7.0000	FZ6	18o-18o	grav
pac	7	-57.0833	162.2610	7.0000	FZ6	18o-18o	grav
pac	8	-56.4310	162.3428	7.0000	FZ7	18o-18o	grav
pac	8	-56.4400	162.3895	7.0000	FZ7	18o-18o	grav
pac	8	-56.4490	162.4380	7.0000	FZ7	18o-18o	grav
aus	100	-50.5975	157.4975	1.4513	17o		ew9513
aus	2	-49.8974	158.0974	1.1027	17o		ew9513
aus	100	-49.4210	158.5366	1.1882	17o		ew9513
aus	100	-50.5256	157.7772	1.8828	17o		ew9513
aus	100	-50.8020	156.7499	2.0326	17o		ew9513
aus	100	-50.5371	157.4729	5.3076	17o		ggl29
aus	100	-48.8491	159.6489	5.0928	17o		rs124
aus	100	-48.0157	161.3350	5.0467	17o		rs124

Table A.1: continued

PLT	SEG	LAT	LON	UNC	PICK	FZ AGE	CRUISE
aus	100	-48.6955	160.1433	5.2140	17o		elt34
aus	100	-48.6251	160.5437	5.1775	17o		elt53
aus	100	-47.9694	161.4300	5.0379	17o		elt44
aus	6	-46.7745	163.5980	5.0398	17o		EL40A
aus	6	-46.8981	163.1950	0.9093	17o		NBP0007B
aus	6	-46.7685	163.6730	0.6245	17o		PU9301
aus	6	-47.1350	162.4950	1.8521	17o		PU9301
aus	6	-46.7761	163.4950	1.2370	17o		PU9301
aus	100	-49.4009	158.5793	3.0017	17o		ew9513mb
aus	100	-49.4454	158.4885	3.0017	17o		ew9513mb
aus	2	-49.8822	158.1291	3.0017	17o		ew9513mb
aus	2	-49.9193	158.0484	3.0017	17o		ew9513mb
aus	100	-50.5162	157.8252	3.0017	17o		ew9513mb
aus	100	-50.5361	157.7262	3.0017	17o		ew9513mb
aus	100	-50.6297	157.4601	5.0010	17o		ew9513mb
aus	100	-50.5948	157.5530	5.0010	17o		ew9513mb
aus	100	-48.8268	159.6974	3.0017	17o		rigsismb
aus	100	-48.8818	159.5837	3.0017	17o		rigsismb
aus	6	-46.7633	163.6716	5.0010	17o		gnzmb
aus	6	-46.7206	163.8847	5.0010	17o		gnzmb
aus	6	-46.9310	163.1443	5.0010	17o		np0007mb
aus	6	-46.8871	163.2342	5.0010	17o		np0007mb
aus	1	-49.9750	157.9744	7.0000	FZ1	17o-18o	grav
aus	1	-50.0847	158.0754	7.0000	FZ1	17y-18y	grav
aus	1	-50.1585	158.1474	7.0000	FZ1	16o-18y	grav
aus	1	-50.2556	158.2447	7.0000	FZ1	16y-17o	grav
aus	1	-50.3198	158.2996	7.0000	FZ1	15o-17o	grav

Table A.1: continued

PLT	SEG	LAT	LON	UNC	PICK	FZ AGE	CRUISE
aus	3	-49.5784	158.2914	7.0000	FZ2	17o-18y	grav
aus	3	-49.6185	158.3327	7.0000	FZ2	17o-17o	grav
aus	3	-49.6764	158.3936	7.0000	FZ2	17y-17o	grav
aus	3	-49.7286	158.4502	7.0000	FZ2	16o-17o	grav
aus	4	-48.1145	161.1359	7.0000	FZ6	17o-	grav
aus	4	-48.1425	161.1595	7.0000	FZ6	17o-	grav
aus	4	-48.1615	161.1776	7.0000	FZ6	17o-	grav
aus	5	-47.6353	161.7542	7.0000	FZ7	-17o	grav
aus	5	-47.6798	161.7985	7.0000	FZ7	-17o	grav
aus	5	-47.7337	161.8619	7.0000	FZ7	-17o	grav
pac	100	-57.4438	161.5510	7.1358	17o		th92b
pac	2	-59.6180	160.9759	1.5747	17o		ew9513
pac	2	-59.4176	161.0197	1.3528	17o		ew9513
pac	100	-57.3481	161.6037	1.1623	17o		ew9513
pac	100	-57.4438	161.5510	5.0911	17o		th92b
pac	6	-55.0150	162.3720	5.1417	17o		th91b
pac	6	-55.4025	162.1090	5.5450	17o		th91b
pac	1	-59.7052	160.9308	7.0000	FZ1	15y-17o	grav
pac	1	-59.7246	161.0462	7.0000	FZ1	15o-17o	grav
pac	1	-59.7281	161.1038	7.0000	FZ1	15o-17a	grav
pac	1	-59.7417	161.2118	7.0000	FZ1	16y-17a	grav
pac	1	-59.7478	161.3332	7.0000	FZ1	16y-18y	grav
pac	3	-59.2511	160.6878	7.0000	FZ2	16o-17o	grav
pac	3	-59.2779	160.8401	7.0000	FZ2	16o-17a	grav
pac	3	-59.3042	160.9623	7.0000	FZ2	17y-17a	grav
pac	3	-59.3211	161.0814	7.0000	FZ2	17o-18y	grav
pac	4	-56.9649	161.7567	7.0000	FZ6	17y-17o	grav

Table A.1: continued

PLT	SEG	LAT	LON	UNC	PICK	FZ AGE	CRUISE
pac	4	-56.9812	161.8089	7.0000	FZ6	17o-18y	grav
pac	4	-56.9957	161.8722	7.0000	FZ6	17o-18y	grav
pac	5	-56.3028	161.8978	7.0000	FZ7	17y-17o	grav
pac	5	-56.3197	161.9629	7.0000	FZ7	17y-17o	grav
aus	100	-50.8258	157.7258	0.6115	16o		ew9513
aus	2	-50.0511	158.2411	0.9812	16o		ew9513
aus	4	-49.5645	158.6645	0.8348	16o		ew9513
aus	100	-49.1717	159.0578	1.4243	16o		ew9513
aus	100	-50.7363	157.9995	1.0623	16o		ew9513
aus	100	-51.1121	157.0427	2.3904	16o		ew9513
aus	100	-49.0136	159.7924	5.3616	16o		rs124
aus	8	-48.1134	161.4140	5.0263	16o		rs124
aus	100	-48.9711	160.1387	5.1775	16o		elt34
aus	100	-48.8493	160.4524	5.0878	16o		elt53
aus	10	-47.7139	162.0530	5.0503	16o		elt34
aus	8	-48.0374	161.5540	5.0848	16o		elt44
aus	11	-46.8899	163.8270	5.0130	16o		EL40A
aus	11	-47.0062	163.3010	0.8097	16o		NBP0007B
aus	11	-46.8761	163.8370	0.4229	16o		PU9301
aus	11	-47.2119	162.8580	1.4418	16o		PU9301
aus	10	-47.6727	162.1410	0.8280	16o		PU9301
aus	11	-46.9712	163.5560	0.8280	16o		PU9301
aus	100	-49.1535	159.0983	3.0017	16o		ew9513mb
aus	100	-49.1925	159.0051	3.0017	16o		ew9513mb
aus	4	-49.5469	158.7095	3.0017	16o		ew9513mb
aus	4	-49.5864	158.6125	3.0017	16o		ew9513mb
aus	2	-50.0362	158.2783	3.0017	16o		ew9513mb

Table A.1: continued

PLT	SEG	LAT	LON	UNC	PICK	FZ AGE	CRUISE
aus	2	-50.0713	158.1908	3.0017	16o		ew9513mb
aus	100	-50.7247	158.0437	3.0017	16o		ew9513mb
aus	100	-50.7528	157.9520	3.0017	16o		ew9513mb
aus	100	-50.8539	157.6807	5.0010	16o		ew9513mb
aus	100	-50.8211	157.7693	5.0010	16o		ew9513mb
aus	100	-48.9950	159.8396	3.0017	16o		rigsismb
aus	100	-49.0385	159.7173	3.0017	16o		rigsismb
aus	11	-46.9593	163.6861	5.0010	16o		gnzmb
aus	11	-47.0433	163.2625	5.0010	16o		np0007mb
aus	11	-47.0000	163.3438	5.0010	16o		np0007mb
aus	1	-50.1353	158.1247	7.0000	FZ1	16o-18y	grav
aus	1	-50.2556	158.2447	7.0000	FZ1	16y-17o	grav
aus	1	-50.3631	158.3384	7.0000	FZ1	15y-17y	grav
aus	1	-50.4599	158.4075	7.0000	FZ1	15y-17y	grav
aus	1	-50.5448	158.4870	7.0000	FZ1	13o-16o	grav
aus	3	-49.6986	158.4194	7.0000	FZ2	16o-17o	grav
aus	3	-49.7504	158.4724	7.0000	FZ2	16o-17y	grav
aus	3	-49.8037	158.5302	7.0000	FZ2	16o-17y	grav
aus	3	-49.8712	158.6035	7.0000	FZ2	16y-16o	grav
aus	5	-49.2801	158.9225	7.0000	FZ3	16o-17y	grav
aus	5	-49.3097	158.9551	7.0000	FZ3	16o-17y	grav
aus	5	-49.3448	158.9846	7.0000	FZ3	16o-16o	grav
aus	5	-49.3795	159.0228	7.0000	FZ3	16o-16o	grav
aus	6	-48.8784	160.1349	7.0000	FZ4	16o-16o	grav
aus	6	-48.9162	160.1828	7.0000	FZ4	16o-16o	grav
aus	6	-48.9500	160.2075	7.0000	FZ4	16o-16o	grav
aus	7	-48.2248	161.2292	7.0000	FZ6	16o-	grav

Table A.1: continued

PLT	SEG	LAT	LON	UNC	PICK	FZ AGE	CRUISE
aus	7	-48.2464	161.2477	7.0000	FZ6	16o-	grav
aus	9	-47.7901	161.9308	7.0000	FZ7	16o-17y	grav
aus	9	-47.8115	161.9524	7.0000	FZ7	16o-17y	grav
aus	9	-47.8337	161.9776	7.0000	FZ7	16o-16o	grav
aus	9	-47.8563	161.9973	7.0000	FZ7	16y-16o	grav
pac	4	-59.1200	160.3982	1.1985	16o		ew9513
pac	2	-59.5431	160.6893	0.6127	16o		ew9513
pac	2	-59.3582	160.7537	0.7997	16o		ew9513
pac	10	-56.1353	161.5446	1.0492	16o		ew9513
pac	8	-56.6551	161.4418	0.9338	16o		ew9513
pac	100	-57.2147	161.2980	1.0470	16o		ew9513
pac	100	-57.6747	161.3372	10.0899	16o		elt16
pac	11	-54.8955	162.2030	5.0699	16o		th91b
pac	11	-55.0910	161.9330	5.1417	16o		th91b
pac	10	-56.0954	161.5420	3.0017	16o		ew9513mb
pac	10	-56.1793	161.5436	3.0017	16o		ew9513mb
pac	2	-59.5736	160.6634	3.0017	16o		ew9513mb
pac	2	-59.5144	160.7241	3.0017	16o		ew9513mb
pac	1	-59.6322	160.6015	7.0000	FZ1	13o-16o	grav
pac	1	-59.6851	160.8227	7.0000	FZ1	15y-17y	grav
pac	1	-59.7149	160.9854	7.0000	FZ1	15y-17o	grav
pac	1	-59.7281	161.1038	7.0000	FZ1	15o-17a	grav
pac	1	-59.7478	161.3332	7.0000	FZ1	16y-18y	grav
pac	3	-59.1864	160.3611	7.0000	FZ2	15o-16o	grav
pac	3	-59.2332	160.6024	7.0000	FZ2	16y-17y	grav
pac	3	-59.2631	160.7554	7.0000	FZ2	16o-17o	grav
pac	3	-59.2779	160.8401	7.0000	FZ2	16o-17a	grav

Table A.1: continued

PLT	SEG	LAT	LON	UNC	PICK	FZ AGE	CRUISE
pac	5	-58.7403	160.6203	7.0000	FZ3	16o-	grav
pac	5	-58.7576	160.6818	7.0000	FZ3	16o-	grav
pac	5	-58.7742	160.7561	7.0000	FZ3	16o-	grav
pac	6	-57.8071	160.9161	7.0000	FZ4	16o-	grav
pac	6	-57.8395	161.0071	7.0000	FZ4	16o-	grav
pac	6	-57.8624	161.0950	7.0000	FZ4	16o-	grav
pac	7	-56.8301	161.2374	7.0000	FZ6	16y-16o	grav
pac	7	-56.8653	161.3689	7.0000	FZ6	16o-16o	grav
pac	7	-56.9017	161.5145	7.0000	FZ6	16o-17y	grav
pac	9	-56.2039	161.4947	7.0000	FZ7	16y-16o	grav
pac	9	-56.2351	161.6464	7.0000	FZ7	16o-16o	grav
pac	9	-56.2743	161.7559	7.0000	FZ7	16o-17y	grav
aus	1	-51.0680	157.9680	0.7308	15o		ew9513
aus	3	-50.2243	158.4062	0.9812	15o		ew9513
aus	5	-49.8113	158.8714	0.6004	15o		ew9513
aus	100	-49.4449	159.3066	1.0702	15o		ew9513
aus	1	-50.9614	158.2371	0.8287	15o		ew9513
aus	100	-51.3555	157.2749	0.9605	15o		ew9513
aus	1	-50.9993	158.1174	5.2965	15o		elt44
aus	100	-49.2752	160.0218	5.0414	15o		rs124
aus	100	-48.3084	161.5670	5.0117	15o		rs124
aus	100	-49.2854	160.1346	5.1775	15o		elt34
aus	100	-49.1545	160.3780	5.0646	15o		elt53
aus	100	-47.7962	162.2530	5.0126	15o		elt34
aus	100	-48.1658	161.7900	5.0263	15o		elt44
aus	100	-48.0277	162.1020	5.0169	15o		elt44
aus	10	-47.0029	164.0420	5.0293	15o		EL40A

Table A.1: continued

PLT	SEG	LAT	LON	UNC	PICK	FZ AGE	CRUISE
aus	10	-47.1351	163.4280	0.5121	15o		NBP0007B
aus	10	-47.0628	163.8260	0.6680	15o		GEODYNZ2
aus	10	-46.9970	164.0260	0.8280	15o		PU9301
aus	10	-47.2707	163.1390	1.0322	15o		PU9301
aus	100	-47.8112	162.2170	1.0323	15o		PU9301
aus	10	-47.0869	163.5920	1.0322	15o		PU9301
aus	100	-49.4284	159.3523	3.0017	15o		ew9513mb
aus	100	-49.4720	159.2521	3.0017	15o		ew9513mb
aus	5	-49.7891	158.9135	3.0017	15o		ew9513mb
aus	5	-49.8364	158.8287	3.0017	15o		ew9513mb
aus	3	-50.2084	158.4452	3.0017	15o		ew9513mb
aus	3	-50.2423	158.3603	3.0017	15o		ew9513mb
aus	1	-50.9456	158.2791	3.0017	15o		ew9513mb
aus	1	-50.9781	158.1871	3.0017	15o		ew9513mb
aus	1	-51.0885	157.9130	5.0010	15o		ew9513mb
aus	1	-51.0551	158.0053	5.0010	15o		ew9513mb
aus	100	-49.2517	160.0623	3.0017	15o		rigsismb
aus	100	-49.3040	159.9513	3.0017	15o		rigsismb
aus	100	-48.3483	161.4786	5.0010	15o		rigsismb
aus	100	-48.2908	161.6296	5.0010	15o		rigsismb
aus	10	-47.1177	163.7402	5.0010	15o		gnzmb
aus	10	-47.0332	163.9255	5.0010	15o		gnzmb
aus	10	-47.1655	163.3796	5.0010	15o		np0007mb
aus	10	-47.1285	163.4615	5.0010	15o		np0007mb
aus	2	-50.2967	158.2817	7.0000	FZ1	15o-17o	grav
aus	2	-50.4295	158.3829	7.0000	FZ1	15y-17y	grav
aus	2	-50.5448	158.4870	7.0000	FZ1	13o-16o	grav

Table A.1: continued

PLT	SEG	LAT	LON	UNC	PICK	FZ AGE	CRUISE
aus	2	-50.6618	158.5746	7.0000	FZ1	13y-16y	grav
aus	2	-50.7831	158.6744	7.0000	FZ1	13y-15o	grav
aus	4	-49.9327	158.6742	7.0000	FZ2	15o-16y	grav
aus	4	-49.9827	158.7296	7.0000	FZ2	15y-16y	grav
aus	4	-50.0264	158.7831	7.0000	FZ2	15y-15o	grav
aus	4	-50.0535	158.8115	7.0000	FZ2	15y-15o	grav
aus	6	-49.5223	159.1790	7.0000	FZ3	15o-16y	grav
aus	6	-49.5553	159.2122	7.0000	FZ3	15o-16y	grav
aus	6	-49.5854	159.2516	7.0000	FZ3	15y-15o	grav
aus	6	-49.6148	159.2780	7.0000	FZ3	15y-15o	grav
aus	7	-49.1499	160.3948	7.0000	FZ4	15o-	grav
aus	7	-49.1777	160.4190	7.0000	FZ4	15o-	grav
aus	7	-49.2003	160.4408	7.0000	FZ4	15o-	grav
aus	8	-48.3873	161.3581	7.0000	FZ6	15o-	grav
aus	8	-48.4195	161.3834	7.0000	FZ6	15o-	grav
aus	8	-48.4479	161.4093	7.0000	FZ6	15o-	grav
aus	9	-47.9166	162.0632	7.0000	FZ7	15o-15o	grav
aus	9	-47.9593	162.1094	7.0000	FZ7	15y-15o	grav
aus	9	-47.9851	162.1395	7.0000	FZ7	15y-15o	grav
aus	9	-48.0129	162.1697	7.0000	FZ7	15y-15o	grav
pac	100	-57.0341	160.9130	7.2026	15o		th92b
pac	5	-59.0108	160.0101	0.4881	15o		ew9513
pac	3	-59.3875	160.1744	0.7322	15o		ew9513
pac	1	-59.8628	161.0038	1.3333	15o		ew9513
pac	3	-59.2510	160.2905	1.2737	15o		ew9513
pac	100	-57.0306	160.8818	0.7020	15o		ew9513
pac	100	-57.5382	161.0443	10.0899	15o		elt16

Table A.1: continued

PLT	SEG	LAT	LON	UNC	PICK	FZ AGE	CRUISE
pac	100	-57.0341	160.9130	5.1843	15o		th92b
pac	10	-54.7284	161.9770	5.0699	15o		th91b
pac	10	-54.8528	161.8060	5.0728	15o		th91b
pac	1	-59.8870	160.9769	3.0017	15o		ew9513mb
pac	1	-59.8371	161.0306	3.0017	15o		ew9513mb
pac	3	-59.4176	160.1446	3.0017	15o		ew9513mb
pac	3	-59.3607	160.1983	3.0017	15o		ew9513mb
pac	5	-58.9858	160.0316	3.0017	15o		ew9513mb
pac	5	-59.0347	159.9797	3.0017	15o		ew9513mb
pac	2	-59.4963	160.0921	7.0000	FZ1	-15o	grav
pac	2	-59.5884	160.4454	7.0000	FZ1	13y-16y	grav
pac	2	-59.6497	160.6556	7.0000	FZ1	15y-16o	grav
pac	2	-59.6924	160.8724	7.0000	FZ1	15y-17y	grav
pac	2	-59.7281	161.1038	7.0000	FZ1	15o-17a	grav
pac	4	-59.0903	159.9648	7.0000	FZ2	15y-15o	grav
pac	4	-59.1298	160.1074	7.0000	FZ2	15y-16y	grav
pac	4	-59.1532	160.2179	7.0000	FZ2	15y-16y	grav
pac	4	-59.1864	160.3611	7.0000	FZ2	15o-16o	grav
pac	6	-58.6556	160.3516	7.0000	FZ3	15o-	grav
pac	6	-58.6765	160.4033	7.0000	FZ3	15o-	grav
pac	7	-57.7023	160.6288	7.0000	FZ4	15o-	grav
pac	7	-57.7295	160.7057	7.0000	FZ4	15o-	grav
pac	8	-56.7555	161.0350	7.0000	FZ6	15y-16y	grav
pac	8	-56.7778	161.0849	7.0000	FZ6	15o-16y	grav
pac	8	-56.7975	161.1544	7.0000	FZ6	15o-16y	grav
pac	9	-56.0601	161.0925	7.0000	FZ7	13o-15o	grav
pac	9	-56.0812	161.1528	7.0000	FZ7	13o-15o	grav

Table A.1: continued

PLT	SEG	LAT	LON	UNC	PICK	FZ AGE	CRUISE
aus	100	-49.5455	160.1212	7.0741	13o		elt34
aus	100	-49.4841	160.2626	7.0875	13o		elt53
aus	1	-51.2820	158.1820	0.6115	13o		ew9513
aus	3	-50.4315	158.6115	0.8599	13o		ew9513
aus	5	-50.0156	159.0471	1.0702	13o		ew9513
aus	100	-49.6525	159.4925	0.6004	13o		ew9513
aus	1	-51.1719	158.4618	1.1793	13o		ew9513
aus	1	-51.1531	158.4955	5.1917	13o		elt44
aus	100	-49.4746	160.2046	5.2536	13o		rs124
aus	9	-48.5291	161.7520	5.0263	13o		rs124
aus	3	-50.4614	158.5270	5.0263	13o		th91b
aus	11	-47.9123	162.5420	5.0350	13o		elt34
aus	12	-47.1039	164.2570	5.0293	13o		EL40A
aus	9	-48.4445	162.0110	10.0071	13o		ELT16
aus	12	-47.3186	163.6080	0.8094	13o		NBP0007B
aus	12	-47.1548	164.0490	1.1603	13o		GEODYNZ2
aus	12	-47.0632	164.2940	0.6682	13o		GEODYNZ2
aus	12	-47.0930	164.1770	1.0323	13o		PU9301
aus	12	-47.3518	163.5350	1.4418	13o		PU9301
aus	11	-47.9841	162.3140	1.2369	13o		PU9301
aus	12	-47.2894	163.6550	1.2369	13o		PU9301
aus	100	-49.6323	159.5389	3.0017	13o		ew9513mb
aus	100	-49.6730	159.4476	3.0017	13o		ew9513mb
aus	5	-49.9988	159.0864	3.0017	13o		ew9513mb
aus	5	-50.0358	159.0031	3.0017	13o		ew9513mb
aus	3	-50.4177	158.6453	3.0017	13o		ew9513mb
aus	3	-50.4522	158.5621	3.0017	13o		ew9513mb

Table A.1: continued

PLT	SEG	LAT	LON	UNC	PICK	FZ AGE	CRUISE
aus	1	-51.1536	158.5018	3.0017	13o		ew9513mb
aus	1	-51.1903	158.4167	3.0017	13o		ew9513mb
aus	1	-51.3028	158.1182	3.0010	13o		ew9513mb
aus	1	-51.2654	158.2221	3.0010	13o		ew9513mb
aus	100	-49.4508	160.2503	3.0017	13o		rigsismb
aus	100	-49.5031	160.1326	3.0017	13o		rigsismb
aus	9	-48.5766	161.6575	3.0010	13o		rigsismb
aus	9	-48.5144	161.8079	3.0010	13o		rigsismb
aus	12	-47.2208	163.9240	3.0010	13o		gnzmb
aus	12	-47.3446	163.5508	3.0010	13o		np0007mb
aus	12	-47.3152	163.6463	3.0010	13o		np0007mb
aus	2	-50.5203	158.4648	7.0000	FZ1	13o-16o	grav
aus	2	-50.6311	158.5511	7.0000	FZ1	13y-16y	grav
aus	2	-50.7556	158.6571	7.0000	FZ1	13y-15o	grav
aus	2	-50.8620	158.7508	7.0000	FZ1	13y-13o	grav
aus	2	-50.9805	158.8494	7.0000	FZ1	12y-13o	grav
aus	4	-50.1077	158.8546	7.0000	FZ2	13o-15y	grav
aus	4	-50.1713	158.9070	7.0000	FZ2	13o-13o	grav
aus	4	-50.2438	158.9717	7.0000	FZ2	13y-13o	grav
aus	4	-50.2732	158.9945	7.0000	FZ2	13y-13o	grav
aus	6	-49.7123	159.3747	7.0000	FZ3	13o-13o	grav
aus	6	-49.7491	159.4110	7.0000	FZ3	13o-13o	grav
aus	6	-49.7764	159.4351	7.0000	FZ3	13o-13o	grav
aus	6	-49.8009	159.4579	7.0000	FZ3	13y-13o	grav
aus	6	-49.8254	159.4794	7.0000	FZ3	13y-13o	grav
aus	7	-49.3625	160.6004	7.0000	FZ4	13o-	grav
aus	7	-49.3986	160.6226	7.0000	FZ4	13o-	grav

Table A.1: continued

PLT	SEG	LAT	LON	UNC	PICK	FZ AGE	CRUISE
aus	7	-49.4287	160.6473	7.0000	FZ4	13o-	grav
aus	8	-48.6328	161.5469	7.0000	FZ6	13o-	grav
aus	8	-48.6599	161.5710	7.0000	FZ6	13o-	grav
aus	8	-48.6814	161.5827	7.0000	FZ6	13o-	grav
aus	10	-48.0669	162.2355	7.0000	FZ7	13o-13o	grav
aus	10	-48.1094	162.2817	7.0000	FZ7	13o-13o	grav
aus	10	-48.1531	162.3334	7.0000	FZ7	13y-13o	grav
aus	10	-48.1997	162.3790	7.0000	FZ7	13y-13o	grav
aus	10	-48.2405	162.4264	7.0000	FZ7	13y-13o	grav
pac	100	-56.8493	160.6190	7.1555	13o		th92b
pac	5	-58.8678	159.5078	1.5557	13o		ew9513
pac	3	-59.2171	159.6100	1.4541	13o		ew9513
pac	1	-59.7397	160.5392	1.3336	13o		ew9513
pac	3	-59.1238	159.8618	0.8788	13o		ew9513
pac	5	-58.6286	159.7655	0.7428	13o		ew9513
pac	100	-58.5261	160.5104	0.6216	13o		ew9513
pac	11	-55.8227	160.7612	1.6276	13o		ew9513
pac	9	-56.4192	160.8266	0.5886	13o		ew9513
pac	100	-56.8827	160.5413	1.1623	13o		ew9513
pac	100	-57.3676	160.6774	10.0729	13o		elt16
pac	100	-56.8493	160.6190	5.1187	13o		th92b
pac	12	-54.5275	161.6910	5.0515	13o		th91b
pac	12	-54.5459	161.6380	5.0263	13o		th91b
pac	11	-55.7952	160.7924	3.0017	13o		ew9513mb
pac	11	-55.8495	160.7313	3.0017	13o		ew9513mb
pac	1	-59.7607	160.4975	3.0017	13o		ew9513mb
pac	1	-59.7162	160.5778	3.0017	13o		ew9513mb

Table A.1: continued

PLT	SEG	LAT	LON	UNC	PICK	FZ AGE	CRUISE
pac	3	-59.2477	159.5888	3.0017	13o		ew9513mb
pac	3	-59.1921	159.6486	3.0017	13o		ew9513mb
pac	5	-58.8906	159.4802	3.0017	13o		ew9513mb
pac	5	-58.8453	159.5335	3.0017	13o		ew9513mb
pac	100	-58.5015	160.5380	3.0017	13o		ew9513mb
pac	100	-58.5543	160.4757	3.0017	13o		ew9513mb
pac	2	-59.3289	159.5449	7.0000	FZ1	-13o	grav
pac	2	-59.4306	159.8732	7.0000	FZ1	-13o	grav
pac	2	-59.4963	160.0921	7.0000	FZ1	-15o	
pac	2	-59.5884	160.4454	7.0000	FZ1	13y-16y	grav
pac	2	-59.6322	160.6015	7.0000	FZ1	13o-16o	grav
pac	4	-58.9424	159.4362	7.0000	FZ2	13y-13o	grav
pac	4	-58.9833	159.5825	7.0000	FZ2	13y-13o	grav
pac	4	-59.0336	159.7430	7.0000	FZ2	13o-13o	grav
pac	4	-59.0598	159.8450	7.0000	FZ2	13o-15y	grav
pac	6	-58.4528	159.7974	7.0000	FZ3	13o-	grav
pac	6	-58.4725	159.8472	7.0000	FZ3	13o-	grav
pac	6	-58.4945	159.8922	7.0000	FZ3	13o-	grav
pac	7	-57.5371	160.2588	7.0000	FZ4	13o-	grav
pac	7	-57.5689	160.3266	7.0000	FZ4	13o-	grav
pac	8	-56.6020	160.6401	7.0000	FZ6	13y-13o	grav
pac	8	-56.6392	160.7078	7.0000	FZ6	13o-13o	grav
pac	8	-56.6593	160.7522	7.0000	FZ6	13o-13o	grav
pac	8	-56.6811	160.7990	7.0000	FZ6	13o-13o	grav
pac	10	-55.9017	160.6932	7.0000	FZ7	13y-13o	grav
pac	10	0 -55.9307	160.7597	7.0000	FZ7	13y-13o	grav
pac	10	-55.9600	160.8403	7.0000	FZ7	13y-13o	grav

Table A.1: continued

PLT	SEG	LAT	LON	UNC	PICK	FZ AGE	CRUISE
pac	10	0 -55.9979	160.9227	7.0000	FZ7	13y-15y	grav
pac	10	-56.0227	160.9947	7.0000	FZ7	13y-15y	grav
pac	10	0 -56.0601	161.0925	7.0000	FZ7	13o-15o	grav
pac	10	-56.0812	161.1528	7.0000	FZ7	13o-15o	grav
aus	100	-50.1593	160.0685	7.0833	12o		elt34
aus	100	-50.1668	160.2705	7.0815	12o		elt53
aus	100	-50.7925	158.9325	0.7389	12o		ew9513
aus	100	-50.3896	159.3696	0.8348	12o		ew9513
aus	100	-50.2000	159.6650	0.7174	12o		ew9513
aus	100	-50.7834	159.2355	5.4531	12o		ggl29
aus	100	-50.1094	160.3326	5.1917	12o		rs124
aus	1	-48.8618	162.0160	5.0467	12o		rs124
aus	100	-50.1457	160.0775	5.1143	12o		elt34
aus	100	-50.1424	160.2489	5.0878	12o		elt53
aus	100	-50.7794	159.0110	5.0467	12o		th91b
aus	100	-48.1156	163.0510	5.0350	12o		elt34
aus	100	-48.5907	162.6450	5.0042	12o		elt44
aus	3	-48.3132	162.8900	5.0671	12o		elt44
aus	4	-47.6398	163.9260	0.7100	12o		NBP0007B
aus	4	-47.3366	164.6160	3.4946	12o		PU9301
aus	4	-47.4840	164.1940	0.8280	12o		PU9301
aus	100	-48.2603	162.8470	1.0323	12o		PU9301
aus	4	-47.7014	163.7850	1.2369	12o		PU9301
aus	100	-50.3763	159.4127	3.0017	12o		ew9513mb
aus	100	-50.4101	159.3167	3.0017	12o		ew9513mb
aus	100	-50.7763	158.9710	3.0017	12o		ew9513mb
aus	100	-50.8089	158.8874	3.0017	12o		ew9513mb

Table A.1: continued

PLT	SEG	LAT	LON	UNC	PICK	FZ AGE	CRUISE
aus	100	-50.0834	160.3982	3.0017	12o		rigsismb
aus	100	-50.1371	160.2418	3.0017	12o		rigsismb
aus	1	-48.9073	161.9246	5.0010	12o		rigsismb
aus	1	-48.8468	162.0768	5.0010	12o		rigsismb
aus	4	-47.5719	164.0887	5.0010	12o		gnzmb
aus	4	-47.6639	163.8754	5.0010	12o		np0007mb
aus	4	-47.6315	163.9598	5.0010	12o		np0007mb
aus	2	-48.4362	162.6155	7.0000	FZ7	12o-12o	grav
aus	2	-48.4606	162.6309	7.0000	FZ7	12o-12o	grav
aus	2	-48.5073	162.6441	7.0000	FZ7	12y-12o	grav
aus	2	-48.5479	162.6933	7.0000	FZ7	12y-12o	grav
pac	100	-56.4052	159.9380	7.0979	12o		th92b
pac	3	-55.6023	160.2123	1.0490	12o		ew9513
pac	1	-56.1328	160.1665	1.2803	12o		ew9513
pac	100	-56.4218	159.5342	1.2778	12o		ew9513
pac	100	-57.1060	160.1148	10.0442	12o		elt16
pac	100	-56.4052	159.9380	5.0379	12o		th92b
pac	4	-54.0854	161.0800	5.0699	12o		th91b
pac	100	-54.0039	161.3620	5.0263	12o		th91b
pac	100	-56.4024	159.5704	3.0017	12o		ew9513mb
pac	100	-56.4507	159.4979	3.0017	12o		ew9513mb
pac	1	-56.1032	160.1932	3.0017	12o		ew9513mb
pac	1	-56.1575	160.1314	3.0017	12o		ew9513mb
pac	3	-55.5744	160.2402	3.0017	12o		ew9513mb
pac	3	-55.6337	160.1835	3.0017	12o		ew9513mb
pac	2	-55.6576	160.1742	7.0000	FZ7	11y-12o	grav
pac	2	-55.7085	160.2869	7.0000	FZ7	11o-12o	grav

Table A.1: continued

PLT	SEG	LAT	LON	UNC	PICK	FZ AGE	CRUISE
pac	2	-55.7693	160.3996	7.0000	FZ7	12y-12o	grav
pac	2	-55.8186	160.5036	7.0000	FZ7	12o-12o	grav
aus	3	-47.4166	164.7670	2.0572	11o		PU9301
aus	3	-47.5331	164.4460	1.2369	11o		PU9301
aus	3	-47.8531	163.8340	1.0323	11o		PU9301
aus	100	-50.2828	160.3746	7.0875	11o		elt53
aus	100	-50.9573	159.0682	0.7389	11o		ew9513
aus	100	-50.2563	160.3334	5.1380	11o		rs124
aus	1	-48.9868	162.1170	5.0117	11o		rs124
aus	100	-50.3075	160.0650	5.0646	11o		elt34
aus	100	-50.2769	160.3685	5.0878	11o		elt53
aus	100	-50.9015	159.2020	5.0467	11o		th91b
aus	100	-48.1885	163.2310	5.0350	11o		elt34
aus	3	-47.7571	164.0420	0.8097	11o		NBP0007B
aus	100	-50.9429	159.1015	3.0017	11o		ew9513mb
aus	100	-50.9744	159.0202	3.0017	11o		ew9513mb
aus	100	-50.2317	160.3935	3.0017	11o		rigsismb
aus	100	-50.2863	160.2538	3.0017	11o		rigsismb
aus	1	-49.0464	162.0276	5.0010	11o		rigsismb
aus	1	-48.9844	162.1939	5.0010	11o		rigsismb
aus	3	-47.7797	163.9905	5.0010	11o		np0007mb
aus	3	-47.7489	164.0762	5.0010	11o		np0007mb
aus	2	-48.6641	162.7815	7.0000	FZ7	11o-	grav
aus	2	-48.6961	162.7927	7.0000	FZ7	11o-	grav
aus	2	-48.7277	162.7935	7.0000	FZ7	11o-	grav
pac	100	-56.2846	159.7400	7.0922	11o		th92b
pac	1	-56.0361	160.0126	0.7034	11o		ew9513

Table A.1: continued

PLT	SEG	LAT	LON	UNC	PICK	FZ AGE	CRUISE
pac	100	-56.9708	159.8241	10.0144	11o		elt16
pac	100	-56.2846	159.7400	5.0299	11o		th92b
pac	3	-53.9700	160.9150	5.0229	11o		th91b
pac	3	-53.7660	161.2140	5.0263	11o		th91b
pac	1	-56.0155	160.0475	3.0017	11o		ew9513mb
pac	1	-56.0635	159.9854	3.0017	11o		ew9513mb
pac	2	-55.6576	160.1742	7.0000	FZ7	11y-12o	grav
pac	2	-55.6851	160.2321	7.0000	FZ7	11y-12o	grav
pac	2	-55.7085	160.2869	7.0000	FZ7	11o-12o	grav
pac	2	-55.7404	160.3509	7.0000	FZ7	11o-12o	grav

Bibliography

Altis, S., Origin and tectonic evolution of the Caroline Ridge and the Sorol Trough, western tropical Pacific, from admittance and tectonic modeling analysis, *Tectonophysics*, *313*, 271–292, 1999.

Behrendt, J. C., and A. K. Cooper, Evidence of rapid Cenozoic uplift of the shoulder escarpment of the Cenozoic West Antarctica Rift System and speculation on possible climate forcing, *Geology*, *19*, 315–319, 1991.

Behrendt, J. C., W. E. LeMasurier, A. K. Cooper, et al., Geophysical studies of the West Antarctic Rift System, *Tectonics*, *10*, 1257–1273, 1991.

Brancolini, G., A. K. Cooper, and F. Coren, Seismic facies and glacial history in the Western Ross Sea (Antarctica), in *Geology and seismic stratigraphy of the Antarctic Margin, Antarctic Res. Ser.*, vol. 68, pp. 209–233, AGU, Washington, D. C., 1995.

Cande, S. C., and D. V. Kent, Revised calibration of the geomagnetic polarity timescale for the Late Cretaceous and Cenozoic, *J. Geophys. Res.*, *100*, 6093–6095, 1995.

Cande, S. C., J. M. Stock, R. D. Müller, and T. Ishihara, Cenozoic motion between East and West Antarctica, *Nature*, *404*, 145–150, 2000.

Caress, D. W., and D. N. Chayes, Improved processing of Hydrosweep DS multibeam data on the R/V Maurice Ewing, *Mar. Geophys. Res.*, *18*, 631–650, 1996.

Carter, L., and I. N. McCave, The sedimentary regime beneath the Deep Western Boundary Current inflow to the Southwest Pacific Ocean, *J. Sediment. Res.*, *67*, 1005–1017, 1997.

Carter, L., and J. Wilkin, Abyssal circulation around New Zealand - a comparison between observations and a global circulation model, *Mar. Geol.*, *159*, 221–239, 1999.

Carter, R. M., and R. J. Norris, Cenozoic history of southern New Zealand: An accord between geological observations and plate-tectonic predictions, *Earth Planet. Sci. Lett.*, *31*, 85–94, 1976.

Chang, T., On the statistical properties of estimated rotations, *J. Geophys. Res.*, *87*, 6319–6329, 1987.

Chang, T., J. Stock, and P. Molnar, The rotation group in plate tectonics and the representation of uncertainties of plate reconstructions, *Geophys. J. Int.*, *101*, 649–661, 1990.

Collot, J.-Y., G. Lamarche, R. A. Wood, et al., Morphostructure of an incipient subduction zone along a transform plate boundary: Puysegur Ridge and Trench, *Geology*, *23*, 519–522, 1995.

Coombs, D. S., et al., The Dun Mountain ophiolite belt, New Zealand, its tectonic setting, constitution, and origin, with special reference to the southern portion, *American Journal of Science*, *276*, 561–603, 1976.

Cooper, A. K., and F. J. Davey, Episodic rifting of the Phanerozoic rocks of the Victoria Land Basin, western Ross Sea, Antarctica, *Science*, *229*, 1085–1087, 1985.

Dalziel, I. W., and D. H. Elliot, West Antarctica: problem child of Gondwana, *Tectonics*, *1*, 3–19, 1982.

Davey, F. J., Geophysical studies in the Ross Sea region, *J. R. Soc. N. Z.*, *11*, 465–479, 1981.

Davey, F. J., and G. Brancolini, The Late Mesozoic and Cenozoic structural setting of the Ross Sea region, in *Geology and seismic stratigraphy of the Antarctic Margin,*

Antarctic Res. Ser., edited by A. K. Cooper, P. R. Barker, and G. Brancolini, vol. 68, pp. 167–182, AGU, Washington, D. C., 1995.

Delteil, J., J.-Y. Collot, R. Wood, R. Herzer, et al., From strike-slip faulting to oblique subduction: a survey of the Alpine Fault-Puysegur Trench transition, New Zealand, results of cruise Geodynz-sud Leg 2, *Mar. Geophys. Res.*, *18*, 383–399, 1996.

Ewing, M. R., R. Houtz, and J. Ewing, South Pacific sediment distribution, *J. Geophys. Res.*, *74*, 2477–2493, 1969.

Faugères, J.-C., M. L. Mézerias, and D. A. V. Stow, Contourite drift types and their distribution in the north and south Atlantic Ocean basins, *Sediment. Geol.*, *82*, 1898–203, 1993.

Faugères, J.-C., D. A. V. Stow, P. Imbert, and A. Viana, Seismic features diagnostic of contourite drifts, *Mar. Geol.*, *162*, 1–38, 1999.

Fitzgerald, P. G., The Transantarctic Mountains of the Southern Victoria Land: the application of apatite fission track analysis to a rift shoulder uplift, *Tectonics*, *11*, 634–662, 1992.

Fitzgerald, P. G., Thermochonologic constraints on post-Paleozoic tectonic evolution of the central Transantarctic Mountains, Antarctica, *Tectonics*, *13*, 818–836, 1994.

Fitzgerald, P. G., M. Sandiford, P. J. Barrett, and A. J. W. Gleadow, Asymmetric extension associated with uplift and subsidence in the Transantarctic Mountains and the Ross Sea Embayment, *Earth Planet. Sci. Lett.*, *81*, 67–78, 1986.

Fox, P. J., and D. G. Gallo, The geology of the North Atlantic transform plate boundaries and their aseismic extensions, in *The Geology of North America, vol M., The Western North Atlantic Region*, edited by R. Vogt and B. E. Tucholke, pp. 157–172, Geol. Soc. of Am., 1986.

Frakes, L. A., Paleoclimatic significance of some sedimentary components at Site 274,

in *Initial Reports of the Deep Sea Drilling Project*, vol. 28, pp. 785–787, Washington (U.S. Government Printing Office), 1975.

Gaina, C., et al., The tectonic history of the Tasman Sea: A puzzle with 13 pieces, *J. Geophys. Res.*, *103*, 12,413–12,433, 1998.

Hamilton, R. J., B. P. Luyendyk, C. C. Sorlien, and L. R. Bartek, Cenozoic tectonics of the Cape Roberts Rift Basin and Transantarctic Mountains Front, Southwestern Ross Sea, Antarctica, *Tectonics*, *20*, 325–342, 2001.

Hayes, D. E., and J. Ringis, Seafloor spreading in the Tasman Sea, *Nature*, *243*, 454–458, 1973.

Hayes, D. E., et al., Site 274, in *Initial Reports of the Deep Sea Drilling Project*, vol. 28, pp. 369–433, Washington (U.S. Government Printing Office), 1975.

Hegarty, K. A., and J. K. Weissel, Complexities in the development of the Caroline Plate Region, Western Equatorial Pacific, in *The Ocean Basins and Margins, Volume 7B: The Pacific Ocean*, chap. 6, pp. 277–301, 1988.

Hellinger, S. J., The uncertainties of finite rotations in plate tectonics, *J. Geophys. Res.*, *86*, 9312–9318, 1981.

Houtz, R., and F. J. Davey, Seismic profiler and sonobuoy measurements in the Ross Sea, Antarctica, *J. Geophys. Res.*, *78*, 3448–3468, 1973.

Hunt, T., Stokes magnetic anomaly system, *N.Z. J. Geol. Geophys.*, *21*, 595–606, 1978.

Jonas, J., S. Hall, and J. F. Casey, Gravity anomalies over extinct spreading centers: a test of gravity models of active centers, *J Geophys. Res.*, *96*, 11,759–11,777, 1991.

Kamp, P. J. J., The mid-Cenozoic Challenger Rift System of western New Zealand and its implications for the age of Alpine Fault inception, *Geol. Soc. Am. Bull.*, *97*, 255–281, 1986.

Kennett, J. P., et al., *Initial Reports of the Deep Sea Drilling Project, vol 29*, U.S. Gov. Print. Off., Washington, D. C., 1973.

King, P. R., Tectonic reconstructions of New Zealand: 40 Ma to the present, *N.Z. J. Geol. Geophys.*, *43*, 611–638, 2000.

Lamarche, G., and J.-F. Lebrun, Transition from strike-slip faulting to oblique subduction: active tectonics at the Puysegur Margin, South New Zealand, *Tectonophysics*, *316*, 67–89, 2000.

Lamarche, G., J.-Y. Collot, R. A. Wood, et al., The Oligocene-Miocene Pacific-Australia plate boundary, south of New Zealand: Evolution from oceanic spreading to strike-slip faulting, *Earth Planet. Sci. Lett.*, *148*, 129–139, 1997.

LeMasurier, W. E., Late Cenozoic volcanism on the Antarctic Plate, in *Volcanoes of the Antarctic Plate and Southern Ocean*, edited by W. E. Lemasurier and J. W. Thomson, pp. 1–17, AGU, Washington, D. C., 1990.

Macdonald, K. C., K. Kastens, F. N. Spiess, and S. P. Miller, Deep tow studies of the Tamayo transform fault, *Mar. Geophys. Res.*, *4*, 37–70, 1996.

Massell, C., et al., Neotectonics of the Macquarie Ridge Complex, Australia-Pacific plate boundary, *J. Geophys. Res.*, *105*, 13,457–13,480, 2000.

McAdoo, D., and S. Laxon, Antarctic Tectonics: Constraints from an ERS-1 satelite marine gravity field, *Science*, *276*, 556–560, 1997.

Molnar, P., T. Atwater, J. Mammerickx, and S. M. Smith, Magnetic anomalies, bathymetry, and the tectonic evolution of the South Pacific since the late Cretaceous, *Geophys. J. R. Astron. Soc.*, *40*, 383–420, 1975.

Pezard, P. A., R. N. Anderson, W. B. F. Ryan, et al., Accretion, structure, and hydrology of intermediate spreading-rate oceanic-crust from drillhole experiments and sea-floor observations, *Marine Geophys. Res.*, *14*, 93–123, 1992.

Piper, D. J. W., and C. B. Brisco, Deep-water continental-margin sedimentation, DSDP Leg 28, Antarctica, in *Initial Reports of the Deep Sea Drilling Project*, vol. 28, pp. 727–755, Washington (U.S. Government Printing Office), 1975.

Royer, J.-Y., and T. C. Chang, Evidence for relative motions between the Indian and Austalian plates during the last 20 My from plate tectonic reconstructions - implications for the deformation of the Indo-Australian plate, *J. Geophys. Res.*, *96*, 11,779–11,802, 1991.

Royer, J. Y., and D. T. Sandwell, Evolution of the Eastern Indian Ocean since the Late Cretaceous: constraints from GEOSAT altimetry, *J. Geophys. Res.*, *94*, 12,755–13,782, 1989.

Sandwell, D. T., and W. Smith, Marine gravity-anomaly from Geosat and ERS-1 satellite altimetry, *J. Geophys. Res.*, *102*, 10,039–10,054, 1997.

Schuur, C. L., M. F. Coffin, C. Frohlich, et al., Sedimentary regimes at the Macquarie Ridge Complex: Interaction of Southern Ocean circulation and plate boundary bathymetry, *Paleoceanography*, *13*, 646–670, 1998.

Smith, W. H. F., and D. T. Sandwell, Global seafloor topography from satellite altimetry and ship depth soundings, *Science*, *277*, 1956–1962, 1997.

Stock, J., and P. Molnar, Some geometrical aspects of uncertainties in combined plate reconstructions, *Geology*, *11*, 697–701, 1983.

Stock, J. M., and P. Molnar, Uncertainties in the relative positions of the Australia, Antarctica, Lord Howe, and Pacific plates since the Late Cretaceous, *J. Geophys. Res.*, *87*, 4697–4714, 1982.

Stock, J. M., and P. Molnar, Revised early Tertiary history of plate motion in the Southwest Pacific, *Nature*, *325*, 495–499, 1987.

Sutherland, R., The Australia-Pacific boundary and Cenozoic plate motions in the SW Pacific: Some constraints from Geosat data, *Tectonics*, *14*, 819–831, 1995.

Sutherland, R., Cenozoic bending of New Zealand basement terranes and Alpine Fault displacement: a brief review, *N.Z. J. Geol. Geophys.*, *42*, 295–301, 1999.

Sutherland, R., F. Davey, and J. Beavan, Plate boundary deformation in South Island, New Zealand, is related to inherited lithospheric structure, *Earth Planet. Sci. Lett.*, *177*, 141–151, 2000.

Tanahashi, M., T. Ishihara, M. Yuasa, et al., Preliminary report of the TH95 geologican and geophysical survey results in the Ross Sea and Dumont D'Urville Sea, *Proc. NIPR Symp. Antarct. Geosci.*, *10*, 36–58, 1997.

Van Andel, T. H., Fracture zones, comments on earth sciences, *Geophysics*, pp. 159–166, 1971.

Walcott, R. I., Rectonstructoins of the New Zealand region for the Neogene, *Palaeogeography, Palaeoclimatology, and Palaeoecology*, *46*, 217–231, 1984.

Weissel, J. K., and D. E. Hayes, Evolution of the Tasman Sea reappraised, *Earth Planet. Sci. Lett.*, *36*, 77–84, 1972.

Weissel, J. K., and G. D. Karner, Flexural uplift of rift flanks due to mechanical unloading of the lithosphere during extension, *J. Geophys. Res.*, *94*, 13,919–13,950, 1989.

Weissel, J. K., D. E. Hayes, and E. M. Herron, Plate tectonic synthesis: the displacements between Australia, New Zealand, and Antarctica since the Late Cretaceous, *Mar. Geol*, *25*, 231–277, 1977.

Wood, R., G. Lamarche, R. Herzer, J. Delteil, and B. Davy, Paleogene seafloor spreading in the southeast Tasman Sea, *Tectonics*, *15*, 966–975, 1996.

Wood, R., et al., Cretaceous-Tertiary tectonic history of the Fiordland margin, New Zealand, *N.Z. J. Geol. Geophys.*, *43*, 289–302, 2000.